



National Library
of Canada

Bibliothèque nationale
du Canada

Canadian Theses Service

Services des thèses canadiennes

Ottawa, Canada
K1A 0N4

CANADIAN THESES

THÈSES CANADIENNES

NOTICE

The quality of this microfiche is heavily dependent upon the quality of the original thesis submitted for microfilming. Every effort has been made to ensure the highest quality of reproduction possible.

If pages are missing, contact the university which granted the degree.

Some pages may have indistinct print especially if the original pages were typed with a poor typewriter ribbon or if the university sent us an inferior photocopy.

Previously copyrighted materials (journal articles, published tests, etc.) are not filmed.

Reproduction in full or in part of this film is governed by the Canadian Copyright Act, R.S.C. 1970, c. C-30.

**THIS DISSERTATION
HAS BEEN MICROFILMED
EXACTLY AS RECEIVED**

AVIS

La qualité de cette microfiche dépend grandement de la qualité de la thèse soumise au microfilmage. Nous avons tout fait pour assurer une qualité supérieure de reproduction.

S'il manque des pages, veuillez communiquer avec l'université qui a conféré le grade.

La qualité d'impression de certaines pages peut laisser à désirer, surtout si les pages originales ont été dactylographiées à l'aide d'un ruban usé ou si l'université nous a fait parvenir une photocopie de qualité inférieure.

Les documents qui font déjà l'objet d'un droit d'auteur (articles de revue, examens publiés, etc.) ne sont pas microfilmés.

La reproduction, même partielle, de ce microfilm est soumise à la Loi canadienne sur le droit d'auteur, SRC 1970, c. C-30.

**LA THÈSE A ÉTÉ
MICROFILMÉE TELLE QUE
NOUS L'AVONS REÇUE**

THE UNIVERSITY OF ALBERTA

CONTINUOUS OXYGEN DETERMINATION IN METALLURGICAL PROCESSES

by

DEWEI ZHU

(C)

A THESIS

SUBMITTED TO THE FACULTY OF GRADUATE STUDIES AND RESEARCH
IN PARTIAL FULFILMENT OF THE REQUIREMENTS FOR THE DEGREE
OF MASTER OF SCIENCE

IN
METALLURGICAL ENGINEERING

DEPARTMENT OF MINING, METALLURGICAL, PETROLEUM ENGINEERING

EDMONTON, ALBERTA

FALL, 1986

Permission has been granted to the National Library of Canada to microfilm this thesis and to lend or sell copies of the film.

The author (copyright owner) has reserved other publication rights, and neither the thesis nor extensive extracts from it may be printed or otherwise reproduced without his/her written permission.

L'autorisation a été accordée à la Bibliothèque nationale du Canada de microfilmer cette thèse et de prêter ou de vendre des exemplaires du film.

L'auteur (titulaire du droit d'auteur) se réserve les autres droits de publication; ni la thèse ni de longs extraits de celle-ci ne doivent être imprimés ou autrement reproduits sans son autorisation écrite.

ISBN 0-315-32330-2

THE UNIVERSITY OF ALBERTA
RELEASE FORM

NAME OF AUTHOR DEWEI ZHU
TITLE OF THESIS CONTINUOUS OXYGEN DETERMINATION IN
METALLURGICAL PROCESSES
DEGREE FOR WHICH THESIS WAS PRESENTED MASTER OF SCIENCE
YEAR THIS DEGREE GRANTED FALL, 1986

Permission is hereby granted to THE UNIVERSITY OF ALBERTA LIBRARY to reproduce single copies of this thesis and to lend or sell such copies for private, scholarly or scientific research purposes only.

The author reserves other publication rights, and neither the thesis nor extensive extracts from it may be printed or otherwise reproduced without the author's written permission.

(SIGNED) ... *Dewei Zhu* ...

PERMANENT ADDRESS:

... *Gaochun Jiangsu Prov.* ...
... *P. R. C.* ...
...

DATED ... *Sept. 15th* ... 1986

THE UNIVERSITY OF ALBERTA
FACULTY OF GRADUATE STUDIES AND RESEARCH

The undersigned certify that they have read, and recommend to the Faculty of Graduate Studies and Research, for acceptance, a thesis entitled CONTINUOUS OXYGEN DETERMINATION IN METALLURGICAL PROCESSES submitted by DEWEI ZHU in partial fulfilment of the requirements for the degree of MASTER OF SCIENCE in METALLURGICAL ENGINEERING.

T. H. Ewell
.....

Supervisor

B. M. Marshall
.....

Con. Secretary
.....

Date *Sept. 17, 1986*
.....

Abstract

Existing papers on various applications of $ZrO_2(+CaO)$ solid electrolytes in metallurgy are too numerous to be reviewed in this thesis. However, major and representative works are covered to provide a historic perspective to the subject.

Theoretical principles of the study are carefully developed. The cell voltage of a nonisothermal oxygen concentration cell with a $ZrO_2(+CaO)$ solid electrolyte is derived for the first time by irreversible thermodynamics. The derivations confirmed earlier results obtained by viewing the cell as an isothermal nonisobaric cell in series with an nonisothermal isobaric cell. Furthermore, electronic conduction problems in a $ZrO_2(+CaO)$ solid electrolyte under nonisothermal conditions are considered. The effective ionic transport number of the $ZrO_2(+CaO)$ electrolyte under nonisothermal conditions is calculated by numerical integration to compare with that of the $ZrO_2(+CaO)$ electrolyte under isothermal conditions.

The theoretical background of aluminum electrolysis is briefly presented. The thermodynamic significance of oxygen pressure measured in the $Na_3AlF_6-Al_2O_3-Al$ system is pointed out. One hundred years after the invention of the Hall-Heroult process it may now be possible to measure the activity of alumina in cryolite.

Experimental set-ups and measuring devices are described. Methods of constructing the nonisothermal oxygen

cells are developed. Certain experimental procedures have to be followed in order to obtain reliable and consistent results. By measuring the EMF of the nonisothermal oxygen probe, which is immersed in molten steel, the oxygen level in steel is determined continuously.

Results of oxygen levels in molten steel characterized the probe. They confirmed that the nonisothermal oxygen probe can work well continuously under steelmaking conditions. Oxygen levels of 1-2 ppm at about 1510°C are measured in molten steel by the nonisothermal oxygen probe for extended periods of time.

The air reference oxygen probe was, as expected, stable and reliable for continuous oxygen measurements in molten steel. While the Ni-NiO reference oxygen probe behaved reasonably well, the Mo-MoO₂ probe did not behave as well as the Ni-NiO probe. The electrochemical determination of oxygen by oxygen probes is compared with that by acid-soluble aluminum analysis and inert gas fusion analysis.

Oxygen pressure was measured for Na₃AlF₆-Al₂O₃ melts with different alumina concentrations. A relationship between measured oxygen activity and alumina concentration is yet to be established. The performance of the oxygen probe is satisfactory in terms of resistance to chemical attack.

Finally, some suggestions for future work are made.

Acknowledgements

The author wishes to express his thanks to Stelco Inc. for their supply of some experimental materials and steel sample analyses, in particular to Mr. Steve Wilson for his helpful assistance.

The author also wishes to express his sincere appreciation for the assistance and cooperation received from all the technical staff of the Department of Mining, Metallurgical, and Petroleum Engineering, in particular, Ms. Tina Barker, Mr. Bob Konzuk, Mr. Shiraz Merali, and Mr. Rob Stefaniuk.

The author also wishes to express thanks to his fellow graduate students, in particular, Mr. Stan Backs, and Mr. Jonathon Brown for their proof-reading of this thesis and their helpful comments.

Finally, the author is deeply indebted to his advisor Dr. T. H. Etsell for his knowledgeable guidance and kind encouragement.

Chapter	Table of Contents	Page
I.	Introduction	1
	A. $ZrO_2(+CaO)$ solid electrolyte	1
	B. Review of the applications of $ZrO_2(+CaO)$ solid electrolytes in metallurgical processes	2
	Disposable oxygen probes for determining oxygen activity in steelmaking processes	3
	Continuous oxygen measurements in molten steel	7
	Applications of galvanic cells with $ZrO_2(+CaO)$ solid electrolytes in molten slags and salts	10
	C. Applying the oxygen probe to the $Na_3AlF_6-Al_2O_3$ system	11
II.	Theoretical Considerations	16
	A. Ionic transport in solid conductors	16
	B. Oxygen ion conductors	21
	C. Principles of the oxygen concentration cell with a $ZrO_2(+CaO)$ solid electrolyte	24
	D. Mixed conduction in $ZrO_2(+CaO)$	27
	E. Principles of the nonisothermal oxygen concentration cell with a $ZrO_2(+CaO)$ solid electrolyte	32
	Derivation of the Seebeck coefficient of a $ZrO_2(+CaO)$ solid electrolyte from irreversible thermodynamics	35
	Derivation of the EMF expression for a nonisothermal and nonisobaric cell with a $ZrO_2(+CaO)$ solid electrolyte from irreversible thermodynamics	41
	Considerations of electronic conduction in a nonisothermal cell with a $ZrO_2(+CaO)$ solid electrolyte	47
	Further considerations of effective ionic transport number	54

F.	Calculation of dissolved oxygen in molten steel from the EMF measured by nonisothermal oxygen probes	56
	Thermoelectric EMF caused by different leads to an oxygen concentration cell	59
	Oxygen partial pressure and temperature dependence of the Seebeck coefficient	62
	Calculation of the oxygen activity in steel from the measured EMF	63
G.	Fundamentals of the $\text{Na}_3\text{AlF}_6\text{-Al}_2\text{O}_3$ system	66
	Properties of the $\text{Na}_3\text{AlF}_6\text{-Al}_2\text{O}_3$ electrolyte	67
	Anode Effect	69
H.	Oxygen pressure determination in a molten $\text{Na}_3\text{AlF}_6\text{-Al}_2\text{O}_3$ system	71
III.	Experimental	74
	A. Experimental set-up	74
	B. Construction of the nonisothermal oxygen probe	77
	Oxygen probe with an air reference electrode	77
	Oxygen probe with solid metal-metal oxide reference electrodes	81
	C. Measuring equipment	86
	D. Steel deoxidation and reoxidation	87
	E. Oxygen measurement in cryolite	88
	F. Sampling and sample analysis	90
	Steel samples	90
	$\text{Na}_3\text{AlF}_6\text{-Al}_2\text{O}_3$ samples	96
IV.	Results and Discussion	97
	A. Experimental data processing with a computer program	97
	B. Performance of the air reference oxygen probe	99
	Resistance against chemical attack	99

Measurement of dissolved oxygen in molten steel	106
Probe response to varying oxygen content ...	116
C. Performance of solid metal-metal oxide reference oxygen probes	119
Measurement of dissolved oxygen in steel ...	121
Advantages of the solid reference electrode oxygen probe over the air reference electrode probe when used under very low oxygen conditions	128
D. Oxygen pressure measurement by the air reference oxygen probe in the $\text{Na}_3\text{AlF}_6\text{-Al}_2\text{O}_3$ system	130
E. Possible industrial applications	141
Continuous oxygen-measurement in steelmaking processes	141
Control of deoxidation with Al, Si and Mn by oxygen activity measurements in steelmaking	142
Oxygen activity measurements in LD-convertor processes	144
Oxygen probes in aluminum electrolysis cells	144
F. Suggestions for future work	145
Experimental conditions for oxygen measurements in steel	145
Thermodynamic study on the $\text{Na}_3\text{AlF}_6\text{-Al}_2\text{O}_3$ system by using galvanic cells with $\text{ZrO}_2(+\text{CaO})$ solid electrolytes	145
Determination of $(\bar{S}_2+\bar{Q}_2/T)$ and $(\bar{S}_3+\bar{Q}_3/T)$ in $\text{ZrO}_2(+\text{CaO})$ solid electrolytes by Seebeck coefficient measurements	146
Conclusions	148
Bibliography	149
Appendix I	154
Appendix II	156

Appendix III157

Appendix IV158

List of Tables

Table		Page
1	Table of P_0 by Scaife et al.	30
2	P_0 obtained by Iwase	31
3	E_{ion} values for typical nonisothermal conditions	57
4	Quantitative analysis of the rods by EDXA	101
5	Results of a run on very low oxygen level	113
6	$K(Al_2O_3)$ by various researchers	117
7	[O] level determined by the air reference probe	125
8	[O] level determined by the Mo-MoO ₂ probe	126
9	Results of the emf obtained on the Na ₃ AlF ₆ -Al ₂ O ₃ system by the air reference probe	133
10	Results of the emf obtained on the Na ₃ AlF ₆ -Al ₂ O ₃ system by the Ni-NiO reference probe	135
11	Results of the emf obtained on the Na ₃ AlF ₆ -Al ₂ O ₃ system by the Cr-Cr ₂ O ₃ reference probe	137

List of Figures

Figure	Page
1 Oxygen probes with $ZrO_2(+CaO)$ -based solid electrolytes	5
2 Chronopotentiometric curve	13
3 Mechanism of ionic transport	18
4 Effect of temperature on ionic conductivity	25
5 Effect of aliovalent doping on ionic conductivity	26
6 Figurative representation of the laboratory-made cell	58
7 Isothermal cell with different leads	60
6 Nonisothermal cell with different leads	60
9 Experimental set-up for tests on molten steel	75
10 Design of the air reference electrode probe	78
11 Design of solid metal-metal oxide reference probes	83
12 Experimental set-up for tests on the $Na_3AlF_6-Al_2O_3$ system	91
13 Cell voltage vs. time at 5 ppm [O]	105
14 Cell voltage vs. time at 7 ppm [O]	106
15 Cell voltage vs. time at 15 ppm [O]	107
16 Cell voltage vs. time at 30 ppm [O]	108
17 Cell voltage vs. time at 55 ppm [O]	109
18 Cell voltage vs. time at 100 ppm [O]	110
19 Cell voltage vs. time at 155 ppm [O]	111
20 [O] level determined by the air reference probe vs. that by inert gas fusion analysis	114
21 [O] level determined by the oxygen probe vs. that calculated from acid-soluble Al analysis	118

Figure	Page
22 The probe response to varying oxygen content	120
23 [O] in steel determined by the Ni-NiO probe vs. that by the acid-soluble Al analysis	122
24 [O] in steel determined by the Ni-NiO reference probe	123
25 [O] determined by the air reference probe vs. that by the Ni-NiO reference probe	127
26 EMF response of a air reference probe on the $\text{Na}_3\text{AlF}_6\text{-Al}_2\text{O}_3$ system	139
27 EMF reponse of a Ni-NiO reference probe on the $\text{Na}_3\text{AlF}_6\text{-Al}_2\text{O}_3$ system	140

List of Plates

Plate	Page
1	Photograph of a typical air reference probe79
2	Photograph of a typical solid reference probe84
3	Sampling gun used for taking steel samples92
4	Devices used for taking steel samples94
5	Micrograph of an unused $ZrO_2(+CaO)$ rod102
6	Micrograph of a used $ZrO_2(+CaO)$ rod103
7	Micrograph of a $ZrO_2(+CaO)$ rod after use in $Na_3AlF_6-Al_2O_3$131

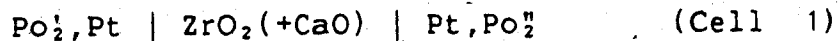
I. Introduction

A. $ZrO_2(+CaO)$ solid electrolyte

Eighty six years ago in 1900, after he discovered electrolytic conduction in ZrO_2 at high temperature, Nernst⁽¹⁾ used it as a glower for incandescent lighting. It was Wagner⁽²⁾ who elucidated the defect structure of stabilized ZrO_2 in 1930 and later, together with Kiukkola⁽³⁾, determined its electrolytic structure. In that often-cited work Wagner and Kiukkola demonstrated the successful use of a $ZrO_2(+CaO)$ solid electrolyte in an oxygen concentration cell for thermodynamic measurements. Kingery et al.⁽⁴⁾ confirmed the oxygen ion conduction through diffusion and conductivity measurements in 1960.

Since those pioneering works, $ZrO_2(+CaO)$ solid electrolytes have received a great deal of attention from scientists in many areas, especially in metallurgy. CaO stabilized, or partially stabilized ZrO_2 oxygen ion conductors now are widely used for many physico-chemical experiments at high temperature. Usually the solid electrolyte is incorporated into an electrochemical oxygen concentration cell.

An oxygen concentration cell or probe with $ZrO_2(+CaO)$ as electrolyte can be represented as:



where P_{O_2} and $P_{O_2}^{\circ}$ are the oxygen pressures at the two electrodes. According to Nernst's equation the electromotive force generated by the oxygen gradient in the cell is:

$$E = \frac{RT}{4F} \ln (P_{O_2}^{\circ}/P_{O_2}) \quad (\text{Eq. 1})$$

if the ionic transference number of $ZrO_2(+CaO)$ is unity, where R is the gas constant, T is temperature and F is the Faraday constant.

The $ZrO_2(+CaO)$ solid electrolyte in Cell 1 has oxygen vacancies in its structure. At temperatures above $600^{\circ}C$ it can act as an ionic oxygen conductor. This unique property has made $ZrO_2(+CaO)$ suitable for many applications:

(a) Oxygen sensors for control of automotive emissions and combustion control of furnaces.

(b) Oxygen sensors for determining dissolved oxygen in liquid metals, especially molten steel, and even molten salts and slags.

(c) Electrochemical oxygen pumps.

(d) High temperature fuel cells.

B. Review of the applications of $ZrO_2(+CaO)$ solid electrolytes in metallurgical processes

Since it was first discovered, metallurgists have been trying to take advantage of the $ZrO_2(+CaO)$ solid electrolyte

3

in studying fundamentals of metallurgical processes as well as in developing practical applications. . For example, oxygen probes utilizing a $ZrO_2(+CaO)$ solid electrolyte have been developed for oxygen measurement in various metallurgical processes.

Disposable oxygen probes for determining oxygen activity in steelmaking processes

Dissolved oxygen content was first reported as being measured in liquid copper, lead and silver by using oxygen concentration cells with $ZrO_2(+CaO)$ -based solid electrolytes⁽⁵⁾⁽⁶⁾ about 25 years ago. A few years later, papers⁽⁷⁾⁽⁸⁾ on demonstrating possible applications of oxygen concentration cells for determining the oxygen content of molten steel began to appear in the literature. In 1966 after reviewing previous work by Matsushita and Goto⁽⁹⁾, Fitterer⁽¹⁰⁾ developed an oxygen probe with a small disc of $ZrO_2(+CaO)$ solid electrolyte fused into the end of a silica tube. An air reference electrode was used in that design which formed the basis for the commercialized oxygen probes commonly used in today's steel industry.

Oxygen occurs in different forms within liquid steel, i.e., either dissolved in steel or chemically combined in the form of suspended oxide particles. The content of dissolved oxygen determines the course of refining, deoxidation and reoxidation processes, while the precipitated and unremoved oxygen fraction determines the

oxide inclusion content of liquid steel.

Electrochemical measurement of dissolved oxygen in steel can give valuable information for controlling the progress of individual stages in steelmaking. Probes with $ZrO_2(+CaO)$ solid electrolytes are now commercially available for oxygen measurement in steelmaking processes.

Four basic types of sensors have been developed for single immersion measurement to determine dissolved oxygen in liquid steel. The structure of these probes is displayed in Fig. 1.⁽¹¹⁾

Basically, all of these sensors are oxygen concentration cells with $ZrO_2(+CaO)$ as the electrolyte, which can be represented by Cell 1. When the probes are immersed into steel, a voltage develops across the electrolyte because of the difference in oxygen pressure at the two electrodes. Thus by measuring the cell voltage, P_{O_2} , the unknown oxygen pressure in equilibrium with dissolved oxygen in steel can be determined according to Eq. 1 if P_{O_2} , the reference electrode oxygen pressure, is known.

According to their reference electrodes, all of these oxygen probes can be classified into two groups: (a) gaseous reference electrode oxygen probe, and (b) solid reference electrode oxygen probe.

With the gaseous reference electrode probe, the oxygen partial pressure of the reference electrode is determined by the oxygen partial pressure in the gaseous phase over the electrode. A typical gaseous phase used is simply air with

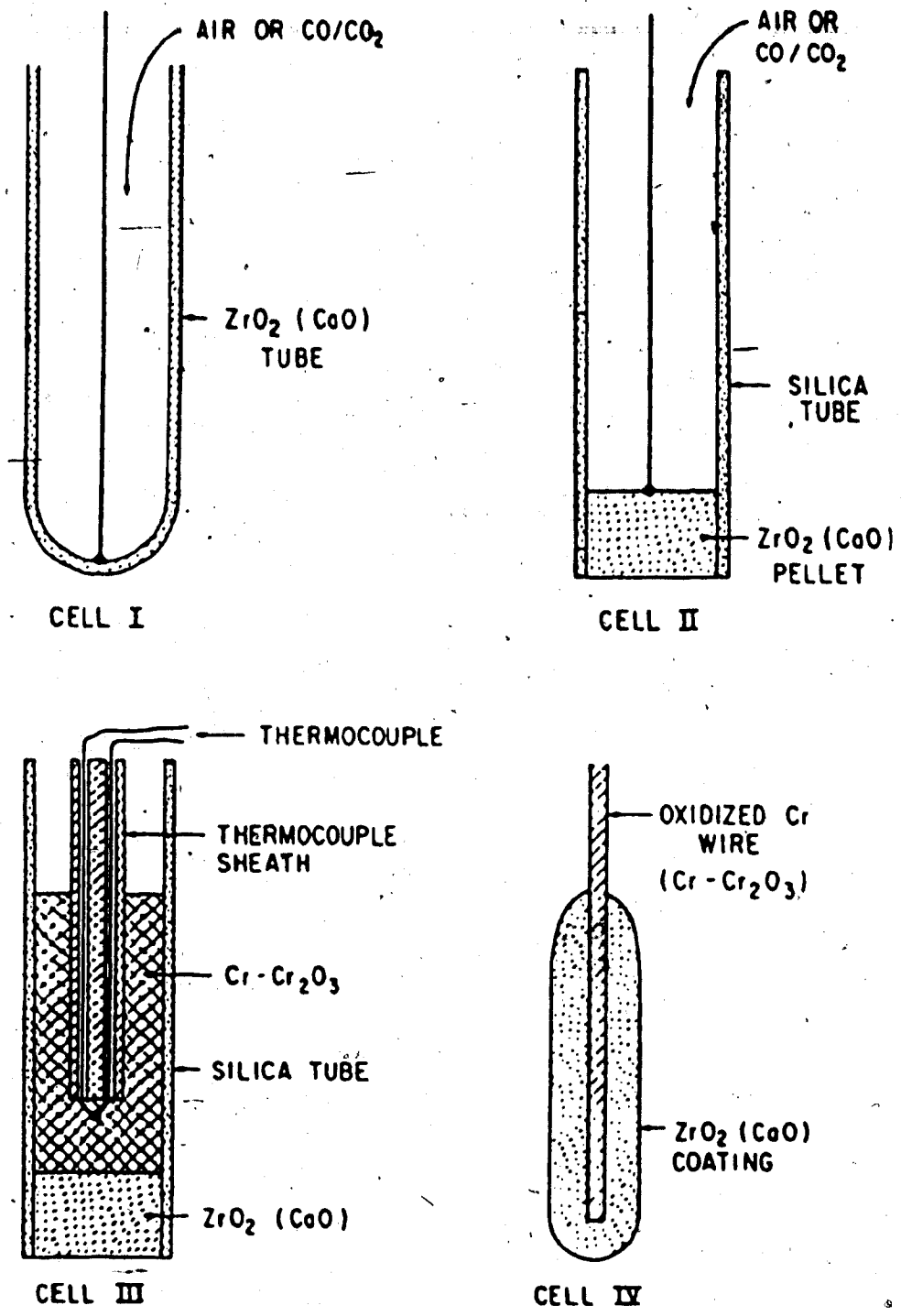


Fig. 1 Oxygen probes with $ZrO_2(+CaO)$ -based solid electrolyte

$P_{O_2} = 0.21$ atm. The solid reference electrode probe uses a solid metal-metal oxide mixture as its reference electrode. The oxygen partial pressure over the reference electrode is determined by the thermodynamic equilibrium between the metal and metal oxide. Typical metal-metal oxides used are Cr-Cr₂O₃ and Ni-NiO.

Single-reading oxygen probes (or disposable oxygen probes as they are sometimes called) have achieved a high industrial standard and are regularly used in steelmaking operations throughout the world, especially in Japan and West Germany.

While conventional chemical analysis for oxygen can only give total oxygen content in steel, an oxygen probe can measure the activity of oxygen in molten steel. Oxygen activity is far more meaningful in terms of dynamic process control in the steelmaking industry. The electrochemical measurement of oxygen by oxygen probes also has the advantage of being virtually instantaneous in contrast to the 8-10 minutes required for sampling and analysis by the conventional inert gas fusion method. In a process as rapid as steelmaking this represents a very valuable economic gain. Furthermore, electrochemical measurement is simple and inexpensive compared with most other choices.

For the reasons mentioned above oxygen probes are now applied in steelmaking to:

- (a) Establish working instructions for apportionment

of after-blow and for the charging of deoxidizers in the LD-converter process.

(b) Adjust the optimum oxygen activity in effervescent steel to prevent formation of a skin layer of blowholes.

(c) Adjust oxygen activity in semi-killed steel.

(d) Directly determine the aluminum content in killed steel.

(e) Measure the degree of oxidation of iron in metallurgical slags.

Continuous oxygen measurements in molten steel

It is naturally a logical extension to attempt continuous oxygen measurements in liquid steel after disposable oxygen probes have achieved such wide success. However, suitable probes for continuous oxygen measurements are not commercially available and their use has, to date, been mainly confined to laboratory investigations⁽¹²⁾, with the exception of a few pilot plant studies.⁽¹³⁾⁽¹⁴⁾

There is a considerable interest in the steel industry in the use of continuously-measuring oxygen sensors in the area of continuous casting. Continuous monitoring of dissolved oxygen fluctuations in liquid steel throughout the casting process would allow control of reoxidation of steel due to oxygen in the atmosphere or in the entrained slag. A number of attempts have been made to use electrolyte tubes coated with a porous ceramic layer⁽¹⁵⁾⁽¹⁶⁾, unprotected electrolyte tubes⁽¹⁷⁾, unprotected electrolyte pellets sealed

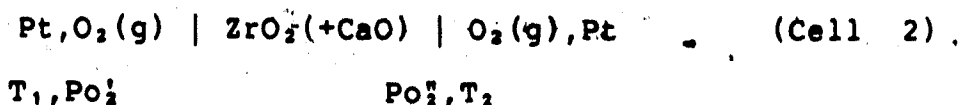
into refractory tubes⁽¹⁸⁾ or a stabilized zirconia brick⁽¹⁹⁾ to make a continuously-measuring oxygen probe.

All oxygen probes mentioned above are called isothermal probes since the two electrodes in the probes work at the same temperature. Several sources of error limit the accuracy and reliability of these isothermal oxygen probes under the conditions of continuous oxygen measurement. These include chemical attack of cell components, inadequate mechanical strength, thermal shock sensitivity, and electronic conductivity in the electrolyte and the consequential oxygen permeability. Perhaps the most serious problem facing continuous oxygen measurement by isothermal oxygen probes is oxygen transfer induced by electronic conduction and by diffusion of molecular oxygen through the fine pores and microcracks in the electrolyte from the reference electrode to liquid steel.

To overcome these problems Etsell and Alcock⁽²⁰⁾ introduced a nonisothermal oxygen probe which consisted of a partially stabilized zirconia electrolyte rod and a cermet rod. It is called a nonisothermal probe because its reference electrode and working electrode operate at different temperatures. The Pt, air reference electrode at a lower temperature is attached to the electrolyte rod 5-15 cm from the end while molten steel serves as the working electrode. Both the electrolyte and the cermet rod tips are immersed into molten steel during the measurement. The Mo-ZrO₂ cermet rod serves the purpose of maintaining

continuous electrical contact with liquid steel.

The above mentioned nonisothermal cell can be represented as:



Initial experimental results indicate that this nonisothermal probe has the advantage of being more rugged, and more resistant to chemical attack and thermal shock. It is also less susceptible to polarization due to reduced oxygen permeability through the electrolyte. This advantage is very important for determining dissolved oxygen in strongly deoxidized steels.

There is a current trend in the steelmaking industry to try to produce strongly deoxidized steels, which require final oxygen levels of 5 ppm or less. Isothermal probes used for measuring dissolved oxygen at steelmaking temperatures (generally above 1550°C) under this low oxygen activity encounter serious polarization problems. This is because the ionic transference number of the electrolyte under such conditions can be as low as 0.84⁽²¹⁾. If the probe is used for an extended period of time, oxygen will transfer through the electrolyte and cause an increase in oxygen activity in the vicinity of the electrode with the lower oxygen activity. However, with a nonisothermal oxygen probe the electrode polarization problem will be much less

severe due to the longer current path and lower average temperature. Hence it was apparent that a nonisothermal probe would be more promising for continuous oxygen measurements in strongly deoxidized steel.

Applications of galvanic cells with $ZrO_2(+CaO)$ solid electrolytes in molten slags and salts

As early as 1961 Renz and Schmalzried⁽²²⁾ reported measurements of free enthalpies of formation of solid phases in $PbO-SiO_2$ with a galvanic cell using a $ZrO_2(+CaO)$ solid electrolyte. The cell, of the type



was set up and the activity of PbO was measured. While papers on the above mentioned $PbO-SiO_2$ system, which is the most important slag system in lead smelting and some glass production procedures, continued to appear,⁽²³⁾⁽²⁴⁾⁽²⁵⁾ works on other molten metal oxides, chlorides, and sulphates, such as $NaCl-KCl$ ⁽²⁶⁾, $Na_2O-B_2O_3$ ⁽²⁷⁾, $Na_2O-NaCl$ ⁽²⁸⁾ and $Na_2O-Na_2SO_4$ ⁽²⁹⁾ also appeared in the literature.

More recently, in 1980, Goto⁽³⁰⁾ et al. measured stable oxygen pressures in steelmaking slags by using solid electrolyte oxygen sensors. An empirical relationship was obtained between oxygen pressure and the ratio of ferric to total iron content in the slag. This could provide very important information for the dynamic control of steelmaking

operations. Later Wanbe et al.⁽³¹⁾ and Iwase⁽³²⁾⁽³³⁾⁽³⁴⁾ measured activities of Fe_2O_3 in complex slags such as $\text{CaO-Fe}_2\text{O}_3$, $\text{SrO-Fe}_2\text{O}_3$, $\text{FeO-SiO}_2\text{-MnO}$, and $\text{CaO-MgO-MnO-Fe}_2\text{O}_3\text{-SiO}_2\text{-P}_2\text{O}_5$, using disposable electrochemical oxygen sensors. Their results seemed to indicate that a stable EMF can be obtained and that chemical attack of the $\text{ZrO}_2(+\text{CaO})$ solid electrolyte by FeO -containing slags would not affect cell potentials.

C. Applying the oxygen probe to the $\text{Na}_2\text{AlF}_6\text{-Al}_2\text{O}_3$ system

Because the author of this thesis was closely associated with the aluminum industry, he is strongly aware of the immense importance of any instrumental method for determining alumina content in molten cryolite. Generally in aluminum electrowinning, alumina is added to molten cryolite at a temperature of about 960°C . Alumina is then dissolved and reduced to aluminum liquid forming at the cathode, while a CO-CO_2 mixture is released at the carbon anode. As the electrolysis process progresses, alumina has to be added continually to maintain a certain level of alumina concentration in the melt. Otherwise the alumina level can drop gradually to such a low level that the anode effect occurs.

When this anode effect happens, the cell voltage can rise to 50 to 100 V, while the current passing through the cell remains the same or decreases slightly. As a result a considerable amount of electricity is wasted. Considering

the magnitude of direct current used for an aluminum electrolytic cell is usually anywhere from 50,000 to 200,000 A, even if the anode effect lasts only a few minutes the drop in energy efficiency is substantial. Therefore there is great interest in the aluminum industry to be able to monitor alumina content in aluminum electrolytic melts.

Aluminum researchers have been trying to measure alumina concentration in molten cryolite by various means. One is called the chronopotentiometric method. In this method a constant current pulse is imposed on a graphite anode dipping into the aluminum bath while the cell voltage is recorded. By a suitable choice of anodic current density, i , a curve as shown in Fig. 2 can be obtained.

Transition time, τ , is a measure of the time needed to deplete the melt at the surface of the graphite electrode with respect to oxygen-containing ions and thereby induce an anode effect. Within the range of alumina concentrations normally encountered in aluminum cells and at sufficiently short transition times, the Sand equation was found to be obeyed by Richards⁽³⁵⁾ and Thonstad⁽³⁶⁾⁽³⁷⁾

$$i\tau^{1/2} = K[\%Al_2O_3] \quad (\text{Eq. } -2)$$

where K is a constant related to the diffusion coefficient of the oxygen-containing species in the $Na_3AlF_6-Al_2O_3$ melt and $[\%Al_2O_3]$ is the weight per cent of alumina in the melt. From Eq. 2 we can see that by measuring $\tau^{1/2}$, the

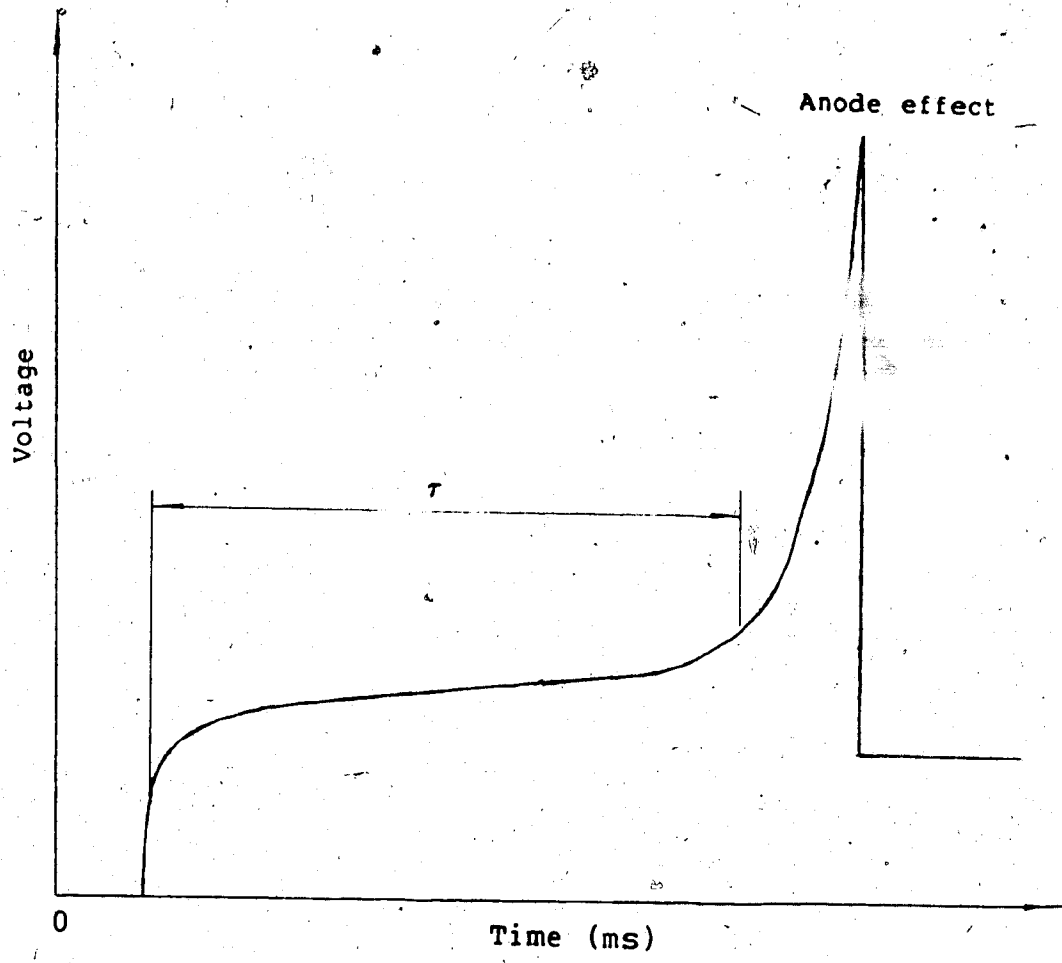


Fig. 2 Chronopotentiometric curve

concentration of alumina in cryolite can be followed continuously.

Though Richards and Thonstad seemed to have obtained good results with graphite anodes, Dewing⁽³⁸⁾ pointed out that graphite, as an anode material, has its problems. First its surface is liable to be rough and/or porous. Secondly it is subject to air oxidation during the measurement. Above all, it is difficult to get a small and reproducible surface area. Therefore Dewing experimented with precious metal anodes. The consequent chronopotentiometric measurements showed that transition time is diffusion controlled only up to 0.7% Al_2O_3 on gold and up to 1.6% Al_2O_3 on platinum. This result contradicts the claim by Thonstad⁽³⁹⁾ that transition time is diffusion controlled within the range of usual alumina concentrations in aluminum electrolytic cells.

Encouraged by the performance of $\text{ZrO}_2(+\text{CaO})$ solid electrolytes in molten oxides and salts as reported in recent studies, and aware of the dilemma in measuring alumina concentration in cryolite by the chronopotentiometric method, the author of this thesis first proposed employing oxygen concentration cells with $\text{ZrO}_2(+\text{CaO})$ solid electrolytes in the $\text{Na}_3\text{AlF}_6-\text{Al}_2\text{O}_3$ system. Regardless of the species in which oxygen ions exist in the melt, there will be only one oxygen partial pressure in equilibrium with dissolved alumina in an given $\text{Na}_3\text{AlF}_6-\text{Al}_2\text{O}_3$ melt in contact with aluminum. That oxygen pressure may be

able to be measured by an oxygen probe. Alumina activity in the melt can then be thermodynamically calculated from the measured oxygen pressure. Being able to monitor alumina activity will provide the aluminum industry with a powerful tool for dynamic process control. Therefore, efforts were made to develop a possible relationship between alumina and the oxygen pressure in molten cryolite.

Oxygen pressure or alumina activity measurements in molten cryolite could also provide valuable information about thermodynamics of the $\text{Al}_2\text{O}_3\text{-Na}_3\text{AlF}_6$ system, which is still relatively unstudied due to the highly corrosive nature of the melt. Though the present study on using a $\text{ZrO}_2(+\text{CaO})$ solid electrolyte oxygen probe in the alumina-cryolite system is preliminary, the prospects for future studies are very exciting.

II. Theoretical Considerations

A. Ionic transport in solid conductors

Until the turn of the century, classical chemistry and crystallography had an idealized picture of the composition and crystal structure of inorganic compounds. It was believed inorganic compounds had definite, unvarying compositions. In addition, it was assumed that the atoms at lattice sites were arranged in an ideal structure where all the lattice sites were occupied.

From the early 1900's this picture began to change as many inorganic compounds were found to be non-stoichiometric. Later, theoretical considerations showed that all inorganic compounds may, in principle, have a variable composition. In fact, the very exact stoichiometric composition is an exception rather than the rule and can only be achieved at definite sets of temperature and partial pressures of the species in a crystal.

It has become clear that no crystals are perfect. At any temperature crystals contain different structural imperfections or defects which can be classified mainly into three groups: (a) point defects, (b) line defects, (c) plane defects. In addition to the structural defects, crystals also contain electronic imperfections, i.e., electrons and holes, which are often relatively free to move in the crystal.

Assuming that ionic conductivity is the result of a direct exchange of positions between neighbouring cations and anions in an ionic crystal without any structural or electronic defects, the energy required to effect such an exchange is nearly 15 eV, making it virtually impossible for the exchange to occur. However, the energy required to effect an exchange of positions between an ion and a neighbouring defect is much smaller. Therefore, it is the structural defects, especially point defects, that make ionic conduction possible.

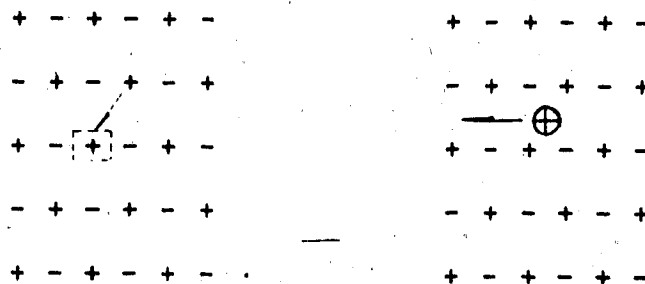
During ionic conduction ions move through the lattice by some jumping process which is mediated through defects. The two types of defects mostly responsible for ion transport are:

- (1) Schottky defects,
- (2) Frenkel defects.

In Schottky defects positive and negative ions leave their normal sites to create vacancies while in Frenkel defects an ion moves to an interstitial position leaving a vacancy at its lattice site. Some possible transport mechanisms involving these defects are illustrated in Fig. 3.

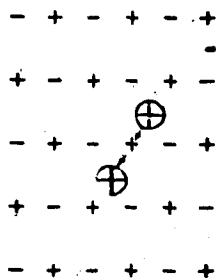
Ionic transport, in general, is governed by the jump probability of an ion into a defect. This in turn is proportional to:

- (a) The probability for the ion to jump into the defect in a given direction per unit time, which is the jump frequency ω ;



(a) Vacancy mechanism

(b) Interstitial mechanism



(c) Interstitialcy mechanism

Fig. 3 Mechanism of ionic transport

(b) The probability that a given site has a defect at a nearest neighbour site, that is, the mole fraction of defects multiplied by the number of nearest neighbour sites.

The jump frequency depends upon the potential barrier seen by ions on normal sites. Assuming the Einstein model to be true and that the ions are vibrating harmonically around their equilibrium positions with a vibrational frequency ν_0 , the expression for the jump frequency for a point defect in ionic solids has been derived as:

$$\omega = \nu_0 \exp(-\Delta G_m/kT) \quad (\text{Eq. 3})$$

where ΔG_m is the difference between the free energy of the ion at the saddle-point position and that at the lattice site position. In other words, ΔG_m is the free energy barrier that opposes the migration of ions and is termed the "free energy of migration". ΔG_m can be written as

$$\Delta G_m = \Delta H_m - T\Delta S_m \quad (\text{Eq. 4})$$

where ΔH_m is the "enthalpy of migration", and ΔS_m is the "entropy of migration". Then,

$$\omega = \nu_0 \exp(\Delta S_m/k) \exp(-\Delta H_m/kT) \quad (\text{Eq. 5})$$

Assuming a to be the interionic distance, n to be the number of interstitial ions per unit volume, and q to be the electrical charge of the ion, the ionic conductivity, σ , is given by:

$$\sigma = na^2q^2\omega/kT$$

or

$$\sigma = nq\mu \quad (\text{Eq. 6})$$

where the mobility, μ , is given by,

$$\mu = a^2 q \omega/kT \quad (\text{Eq. 7})$$

If the charge carrier can jump into more than one forward position, then the ionic conductivity expression has to be multiplied by an additional numerical factor. This is 4 for the NaCl structure, for example. A similar expression holds true for the vacancy or interstitialcy mechanism. If x is the mole fraction of defects then $n = Nx$, where N is the total number of ions per unit volume, and σ can be written as

$$\sigma = N x a^2q^2\omega/kT \quad (\text{Eq. 8})$$

If there is more than one type of charge carrier, this has to be summed for all the different mechanisms,

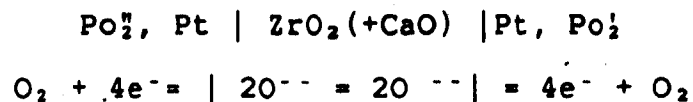
$$\sigma = \sum n_i q_i \mu_i \quad (\text{Eq. 9})$$

where subscript i indicates different mechanisms of ionic conduction.

B. Oxygen ion conductors

Most of the oxygen ion conductors, such as, ZrO_2 , ThO_2 , CeO_2 , and Bi_2O_3 , have the cubic fluorite structure. They can become oxygen ion conductors at relatively high temperatures due to the presence of oxygen vacancies. In the current study only CaO partially stabilized ZrO_2 is employed.

The $ZrO_2(+CaO)$ oxygen ion conductors conduct oxygen by the vacancy mechanism. Oxygen transport through the electrolyte can be illustrated schematically

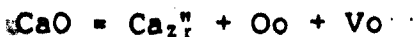


The basic process involved in the $ZrO_2(+CaO)$ electrolyte is that an oxygen molecule from the gas phase acquires four electrons from the cathode and diffuses through the electrolyte to the anode where it donates the electrons and thus is released to the ambient atmosphere. The exact mechanism of the electrode reaction is very complicated and involves a number of intermediate steps. In spite of considerable efforts made in this area, it is still difficult to draw an unambiguous picture of the process.

The addition of CaO to ZrO_2 , known as aliovalent doping, helps in developing a highly conducting phase in two ways:

- (a) The fluorite phase is stabilized.
- (b) More oxygen ion vacancies are created in the lattice.

The addition of CaO would result in the following reaction:

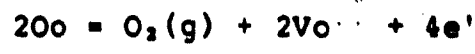


Here Kroger and Vink's notation is adopted. The substitution of zirconium (valence 4) sites by calcium (valence 2) results in two positive "effective charges". This is balanced by the creation of an oxygen ion vacancy. Thus, addition of one mole of CaO creates one mole of oxygen ion vacancies.

The conductivity of $ZrO_2(+CaO)$ depends on temperature and doping concentration of aliovalent oxides. In addition, as for all oxygen ion conductors, calcia stabilized zirconia's conductivity depends on the ambient oxygen pressure or activity. If the ambient oxygen pressure is low, the oxygen ions (O_o) leave the solid electrolyte according to the following mechanism:

 In Kroger and Vink's notation the type of imperfection is indicated by a major symbol and a subscript. In an oxide MO the metal ions on the regular lattice positions are written M_m , where the subscript describes the type of the lattice sites. For example, oxygen on regular lattice site are written O_o . Vacancies are written V with subscript M or O referring to vacant metal or oxygen sites respectively. Interstitial ions or sites are described with a subscript i.

The charge carried by a site is indicated by a superior dot and a superior prime for effective positive and effective negative charge, respectively. The effective charge is different from the actual charge. It is the charge with respect to the perfect crystal. Thus for an oxygen ion on its normal site, the effective charge is zero, whereas a doubly ionized oxygen vacancy has two effective positive charges and is written as V_o .

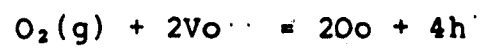


From the above reaction we have:

$$n = K_1^{1/4} [V_o]^{1/2} P_{O_2}^{-1/4} \quad (\text{Eq. 10})$$

where n is the concentration of excess electrons, K₁ is the equilibrium constant for the reaction, and P_{O₂} is the ambient oxygen pressure. Thus the above mechanism gives rise to additional oxygen ion vacancies and excess electrons.

For high ambient oxygen pressure or activity, the defect equilibrium can be expressed as:



Hence

$$p = K_2^{1/2} [V_o]^{1/2} P_{O_2}^{-1/4} \quad (\text{Eq. 11})$$

where p is the concentration of electron holes, K₂ is the equilibrium constant of the reaction, and P_{O₂} is the ambient oxygen pressure. This reaction gives rise to fewer oxygen ion vacancies and more electron holes.

Therefore at high oxygen pressure the conductivity would be predominantly hole conductivity while at low oxygen pressures excess electron conduction would dominate. It is only in the intermediate ambient oxygen pressure range that

the conductivity is ionic and virtually independent of oxygen pressure.

The level and range of ionic or electronic conductivity are controlled by temperature and aliovalent doping. The higher the temperature, the narrower the range of oxygen pressure over which ionic conductivity exists. This temperature effect on ionic conductivity range appear in Fig. 4. The effect of the concentration of the aliovalent dopant on the range of ionic conductivity is shown in Fig. 5. As can be seen from Fig. 5, increasing dopant concentration broadens the range of ionic conductivity.

C. Principles of the oxygen concentration cell with a $ZrO_2(+CaO)$ solid electrolyte

The simplest oxygen galvanic cell is represented as in Cell 1. Since oxygen can transport through $ZrO_2(+CaO)$, when there is a difference in oxygen concentration or chemical potential between two electrodes, oxygen at the higher chemical potential will tend to transport through the electrolyte. Under open-circuit conditions, the electromotive force generated is given by the Nernst equation (Eq. 1):

$$E = \frac{RT}{4F} \ln(P_{O_2}^{\text{high}}/P_{O_2}^{\text{low}})$$

if the ionic transference number of $ZrO_2(+CaO)$ is unity, where E is electromotive force, n is the number of electrons

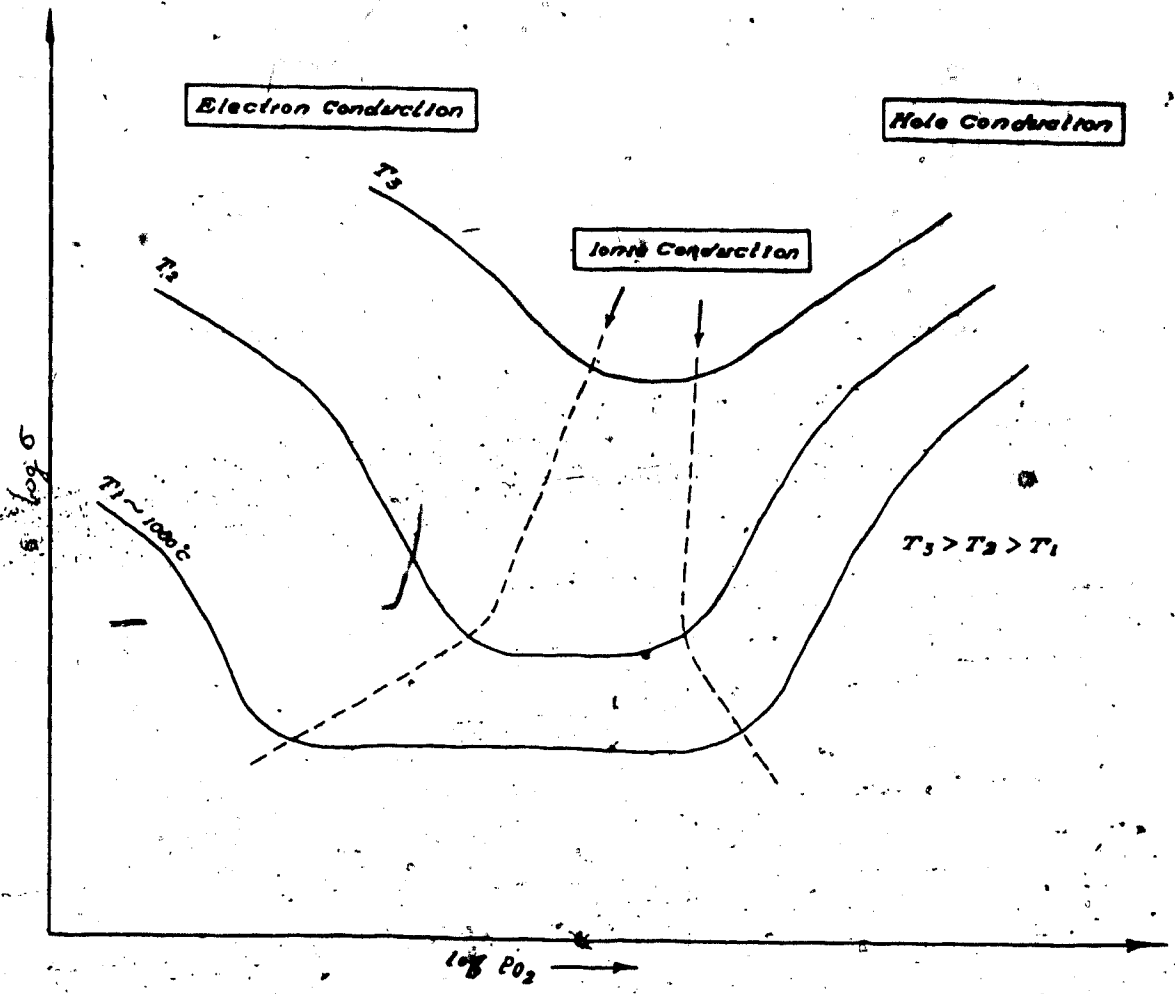


Fig. 4 Effect of temperature on ionic conductivity

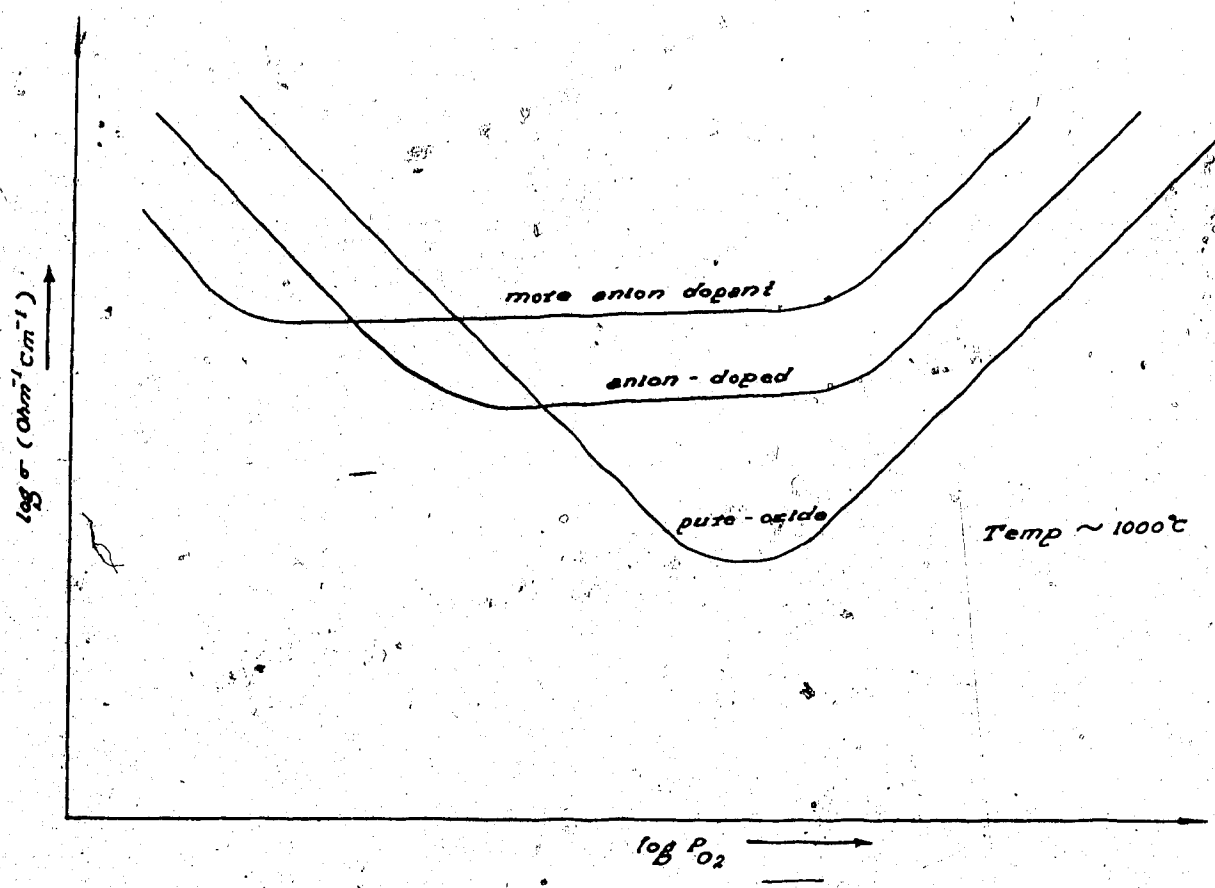
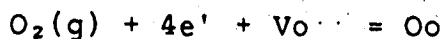


Fig. 5 Effect of aliovalent doping on ionic conductivity

involved in the electrode reaction, F is the Faraday constant, R is the gas constant, T is temperature, and $P_{O_2}^1$ and $P_{O_2}^2$ are the oxygen pressures at the electrodes.

The cathodic process may be represented by the simple reaction



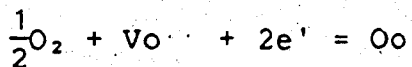
The reverse reaction takes place at the anode. When the temperature is high and ambient oxygen pressure is low, $ZrO_2(+CaO)$ may exhibit substantial electronic conductivity. Then the general formula for the EMF of Cell 1 is:

$$E = \frac{1}{4F} \int_{\mu_{O_2}^2}^{\mu_{O_2}^1} t_{ion} d\mu_{O_2} \quad (\text{Eq. 12})$$

where $\mu_{O_2}^1$ and $\mu_{O_2}^2$ are the chemical potentials of oxygen at the electrodes, and t_{ion} is the ionic transference number of the $ZrO_2(+CaO)$ solid electrolyte.

D. Mixed conduction in $ZrO_2(+CaO)$

In a $ZrO_2(+CaO)$ solid electrolyte, there is a useful range of oxygen pressure in which the electrolyte is predominantly ionic at a given temperature. Outside this range, positive hole conduction occurs at high oxygen pressures and electron conduction at low oxygen pressures. The oxygen pressure dependence of positive hole conduction and electron conduction is based on the following equilibria:



and

$$\frac{1}{2}O_2 + V_o = O_o + 2h$$

The relative magnitude of the ionic and electronic contribution establishes the ionic transference number for the electrolyte. The partial conductivity for each of the ionic and electronic defect species is given by

$$\sigma_i = C_i q_i \mu_i \quad (\text{Eq. 13})$$

where C_i is the concentration of the species, q_i its charge, and μ_i its mobility. Then the ionic transference number, t_{ion} is defined by

$$t_{ion} = \frac{\sigma_{m_i} + \sigma_{v_m}}{\sigma_{m_i} + \sigma_{v_m} + \sigma_e + \sigma_h} \quad (\text{Eq. 14})$$

where the subscripts h and e refer to positive holes and electrons, m_i refers to metal interstitials, and v_m refers to metal vacancies.

Schmalzried⁽⁴⁰⁾ assumed a PO_2 -independent σ_{ion} , and

$$\sigma_h \propto PO_2 \quad \text{and} \quad \sigma_e \propto PO_2^{-1/n}$$

Eq. 14 would then be reduced to

$$t_{ion} = [1 + \left(\frac{PO_2}{P_e}\right)^{-1/n} + \left(\frac{PO_2}{P_h}\right)^{1/n}]^{-1} \quad (\text{Eq. 15})$$

where P_e , P_h and n are constants, P_h equals the high P_{O_2} , where $t_{ion} = 0.5$ ($\sigma_{ion} = \sigma_h$), and P_e equals the low P_{O_2} , where $t_{ion} = 0.5$ ($\sigma_{ion} = \sigma_e$). Schmalzried substituted Eq. 15 into Eq. 12 and integrated to obtain

$$E = \frac{RT}{F} \left(\ln \frac{P_{O_2}^{n/4} + P_e^{1/4}}{P_{O_2}^{1/4} + P_e^{n/4}} + \ln \frac{P_{O_2}^{1/4} + P_h^{1/4}}{P_{O_2}^{n/4} + P_h^{1/4}} \right) \quad (\text{Eq. 16})$$

where $P_{O_2}^1$ and $P_{O_2}^n$ are the oxygen partial pressures at each electrode, respectively, and $n=4$ (cf. Eq. 10 and 11).

To date there is no way to predict P_e from structural knowledge of the solid electrolyte. Yet numerous attempts have been made to determine P_e experimentally. There are mainly three techniques: the permeability flux method, the coulometric titration technique, and open-circuit EMF measurements.

Although there are wide discrepancies among values of P_e determined experimentally, they all have the same form of temperature dependence:

$$\log P_e = -\frac{B}{T} + A \quad (\text{Eq. 17})$$

where A and B are experimental constants. Some of the earlier data, reviewed by Scaife et al. ⁽⁴¹⁾ are shown in Table 1. The discrepancies were explained as the result of different techniques and materials used in each researcher's lab. More recently Iwase ⁽⁴²⁾ summarized his results obtained by a coulometric titration technique in Table 2. Because

Table 1 Table of P_0 by Scaife et al.

Material	A	B	P_0 , atm(1600°C)
CSIRO CSZ	16.7	-62,300	$10^{-16.5}$
CSIRO YSZ	16.0	-60,100	$10^{-16.1}$
PD 327M CSZ	17.8	-63,100	$10^{-15.9}$
MET 201 CSZ	17.5	-61,800	$10^{-15.5}$
MET XP1115 CSZ	15.8	-57,700	$10^{-15.0}$

Table 2 P₀ obtained by Iwase

Sample code	Temperature range (K)	A	B
ZR-11, ZR-11C	1273-1494	12.76	-5.33×10^4
	1494-1873	18.69	-6.21×10^4
ZR-15	1273-1588	11.94	-5.14×10^4
	1588-1873	17.67	-6.05×10^4
ZR-15C	1273-1588	11.44	-5.14×10^4
	1588-1873	17.17	-6.05×10^4

the electrolyte rod used in present study has a composition that is similar to that of the material used by Etsell and Flengas⁽⁴³⁾, the formula

$$\log P_0 = -\frac{5.45 \times 10^4}{T} + 14.0 \quad (\text{Eq. 18})$$

derived from their measurements is employed. When a galvanic cell with a $\text{ZrO}_2(+\text{CaO})$ solid electrolyte is used under high temperature and low oxygen pressure conditions, P_0 should be calculated according Eq. 17 and substituted into Eq. 16 to obtain the correct cell voltage.

E. Principles of the nonisothermal oxygen concentration cell with a $\text{ZrO}_2(+\text{CaO})$ solid electrolyte

For a nonisothermal cell with a $\text{ZrO}_2(+\text{CaO})$ solid electrolyte, the two electrodes work at different temperatures. Therefore, in addition to a concentration gradient, there is also a temperature gradient across the solid electrolyte. Consequently the EMF of the cell will include a thermal electromotive force contribution.

When an ionic conductor such as $\text{ZrO}_2(+\text{CaO})$ is placed in a temperature gradient, a force will be exerted on the ionic species causing them to drift and giving rise to an electric current in the electrolyte. Under steady-state conditions the electric current has to be zero in order to maintain electrical neutrality. This is achieved because there is an exact balance between the driving force exerted on an ionic

species by the temperature gradient, ΔT , and that by the electric field, $\Delta\phi$, which is built up by the preferential drift of ionic species in the temperature gradient. The coefficient of proportionality between these two quantities is called the homogeneous thermoemf,

$$\Delta\phi_{(\text{hom})} = \alpha_{(\text{hom})}\Delta T \quad (\text{Eq. 19})$$

In a real experiment, the measured thermoemf is not accounted for by $\Delta\phi_{(\text{hom})}$ alone since a contact potential exists between the metallic electrodes and the ionic conductor. Because this contact potential is dependent on temperature, its values at the two electrodes will not cancel. This gives rise to the so-called heterogeneous contribution $\Delta\phi_{(\text{het})}$ to the measured thermoemf $\Delta\phi$. The third part of the measured thermoemf is the homogeneous potential difference $\Delta\phi_n$ due to the temperature gradient in the contact wires. All of these three parts combine to give the measured thermoemf $\Delta\phi$. The thermoemf per degree temperature is termed the Seebeck coefficient, which can be expressed as follows:

$$\alpha = -\Delta\phi/\Delta T = -(\Delta\phi_{(\text{hom})}/\Delta T) - (\Delta\phi_{(\text{het})}/\Delta T) - (\Delta\phi_n/\Delta T) \quad (\text{Eq. 20})$$

The thermoemf in turn consists of three individual potentials as given by the relationship:

$$\Delta\phi = \Delta\phi(O^{2-}, E) - \Delta\phi(e^-, Pt) + \Delta\phi(c) \quad (\text{Eq. 21})$$

where $\Delta\phi(O^{2-}, E)$ is the EMF across the electrolyte which has resulted from the thermally induced flow of O^{2-} ions, $\Delta\phi(e^-, Pt)$ is an EMF across the platinum metal electrodes and lead due to the thermally induced flow of electrons, and $\Delta\phi(c)$ is the difference between contact potentials of the electrolyte-electrode interfaces at the two different temperatures.

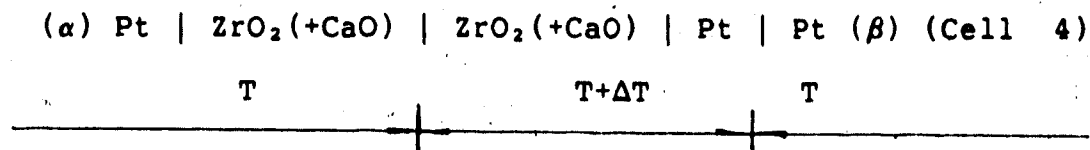
The thermoemf phenomena in $ZrO_2(+CaO)$ -based solid electrolytes was studied by Fisher⁽⁴⁴⁾, Ruka⁽⁴⁵⁾ and Pizzini et al.⁽⁴⁶⁾. Though the actual Seebeck coefficient values found by different researchers did not always agree, they all indicated that α is dependent on oxygen partial pressure, but not on temperature. The general expression for the Seebeck coefficient of $ZrO_2(+CaO)$ -based solid electrolytes can be given as

$$\Delta\alpha = \frac{1}{2F} \left(-\frac{1}{2} S_{O_2}^\circ + \frac{1}{2} R \ln P_{O_2} + \bar{S}_{O_2} + \frac{Q_{O_2}^\circ}{T} \right) - \alpha^{(Pt)} \quad (\text{Eq. 22})$$

where $S_{O_2}^\circ$ is the standard molar entropy of oxygen, \bar{S}_{O_2} is the partial molar entropy of oxygen ions, P_{O_2} is the uniform ambient oxygen pressure, $Q_{O_2}^\circ$ is the heat of transport of oxygen ions, $\alpha^{(Pt)}$ is the Seebeck coefficient for platinum, and R , F and T have the same meaning as used previously.

Derivation of the Seebeck coefficient of a $ZrO_2(+CaO)$ solid electrolyte from irreversible thermodynamics

A thermocell involving $ZrO_2(+CaO)$ with inert metallic leads, such as Pt, is represented by the scheme



The thermoelectromotive force $E(T, T+\Delta T)$ may be determined for the condition of a uniform partial pressure of oxygen in a gas phase over $ZrO_2(+CaO)$. The thermoelectromotive force per degree, α , is defined as⁽⁴⁷⁾

$$\alpha = \lim_{\Delta T \rightarrow 0} \frac{E(T, T+\Delta T)}{\Delta T} = \frac{dE}{dT} = \frac{d(\phi^{(\alpha)} - \phi^{(\beta)})}{dT} \quad (\text{Eq. 23})$$

where $\phi^{(\alpha)}$ and $\phi^{(\beta)}$ are the electric potentials in the Pt leads at the terminals α and β .

The following derivation is confined to isotropic crystals without local stresses. Thus transport properties such as partial conductivities and heats of transfer are presumed to be independent of crystallographic direction.

Although it is possible to formulate equations in a more general manner, the following equations are derived for conditions where anions are much more mobile than cations. In this case, one may formulate transport equations of anions and electrons (species 2 and 3) with respect to cations (species 1) as the reference system. Thus, the

equations for the flux of anions and electrons, J_2 and J_3 , respectively, in moles per unit area per unit time for one dimensional gradients of composition and temperature are

$$J_2 = -\frac{\sigma_2}{4F^2} \left[\frac{d\eta_2}{dx} + \left(\bar{S}_2 + \frac{Q_2^\circ}{T} \right) \frac{dT}{dx} \right] \quad (\text{Eq. 24})$$

$$J_3 = -\frac{\sigma_3}{F^2} \left[\frac{d\eta_3}{dx} + \left(\bar{S}_3 + \frac{Q_3^\circ}{T} \right) \frac{dT}{dx} \right] \quad (\text{Eq. 25})$$

where σ_2 and σ_3 are the partial electric conductivities for anions and electrons, η_2 and η_3 are the electrochemical potentials, \bar{S}_2 and \bar{S}_3 are the partial molar entropies, Q_2° and Q_3° are the heats of transfer, F is the Faraday constant, and x is distance.

The electrochemical potentials are related to the respective chemical potentials μ_2 and μ_3 by

$$\eta_2 = \mu_2 - 2F\phi \quad (\text{Eq. 26})$$

$$\eta_3 = \mu_3 - F\phi \quad (\text{Eq. 27})$$

where ϕ is the local electric potential, and μ_i is the chemical potential of component i , which is defined by

$$\mu_i = \left(\frac{\partial G}{\partial n_i} \right)_{P, T, \phi=0, n_j, j \neq i} \quad (\text{Eq. 28})$$

Under steady-state conditions electrical neutrality is maintained, so the fluxes J_2 and J_3 must be equivalent,

i.e.,

$$-J_3 = 2J_2 \quad (\text{Eq. 29})$$

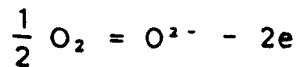
Substituting Eq. 24 and Eq. 25 into Eq. 29

$$\frac{\sigma_3}{F^2} \left[\frac{d\eta_3}{dx} + \left(\bar{S}_3 + \frac{Q_3}{T} \right) \frac{dT}{dx} \right] = -2 \times \frac{\sigma_2}{4F^2} \left[\frac{d\eta_2}{dx} + \left(\bar{S}_2 + \frac{Q_2}{T} \right) \frac{dT}{dx} \right] \quad (\text{Eq. 30})$$

Simplifying the above equation,

$$\sigma_3 \left[\frac{d\eta_3}{dx} + \left(\bar{S}_3 + \frac{Q_3}{T} \right) \frac{dT}{dx} \right] = -\frac{\sigma_2}{2} \left[\frac{d\eta_2}{dx} + \left(\bar{S}_2 + \frac{Q_2}{T} \right) \frac{dT}{dx} \right] \quad (\text{Eq. 31})$$

The term $\frac{d\eta_2}{dx}$ can be expressed in terms of $\frac{d\eta_3}{dx}$ starting writing the reaction



From the above reaction, we have

$$\frac{1}{2} \mu_{\text{O}_2} = \mu_2 - 2\mu_3 = \eta_2 - 2\eta_3 \quad (\text{Eq. 32})$$

Regrouping, the above equation,

$$\eta_2 = \frac{1}{2}\mu_{O_2} + 2\eta_3 \quad (\text{Eq. 33})$$

Differentiating Eq. 33, gives.

$$\frac{d\eta_2}{dx} = \frac{d\eta_2}{dT} \frac{dT}{dx} = \left(\frac{1}{2} \frac{d\mu_{O_2}}{dT} + 2 \frac{d\eta_3}{dT} \right) \frac{dT}{dx} \quad (\text{Eq. 34})$$

Also

$$\frac{d\eta_3}{dx} = \frac{d\eta_3}{dT} \frac{dT}{dx} \quad (\text{Eq. 35})$$

Substituting Eq. 34 and Eq. 35 into Eq. 31,

$$-\frac{\sigma_2}{2} \left[\left(\frac{1}{2} \frac{d\mu_{O_2}}{dT} + 2 \frac{d\eta_3}{dT} \right) \frac{dT}{dx} + \left(\bar{S}_2 + \frac{Q_2^\circ}{T} \right) \frac{dT}{dx} \right] = \sigma_3 \left[\frac{d\eta_3}{dT} \frac{dT}{dx} + \left(\bar{S}_3 + \frac{Q_3^\circ}{T} \right) \frac{dT}{dx} \right] \quad (\text{Eq. 36})$$

Regrouping the above equation and solving for $\frac{d\eta_3}{dT}$,

$$\frac{d\eta_3}{dT} = \frac{1}{2} \frac{\sigma_2}{\sigma_2 + \sigma_3} \left[-\frac{1}{2} \frac{d\mu_{O_2}}{dT} - \bar{S}_2 - \frac{Q_2^\circ}{T} \right] - \frac{\sigma_3}{\sigma_2 + \sigma_3} \left(\bar{S}_3 + \frac{Q_3^\circ}{T} \right) \quad (\text{Eq. 37})$$

Differentiating $\mu_{O_2} = \mu_{O_2}^\circ + RT \ln P_{O_2}$ gives:

$$\frac{d\mu_{O_2}}{dT} = -S_{O_2}^\circ + R \ln P_{O_2} \quad (\text{Eq. 38})$$

Substituting Eq. 38 into Eq. 37:

$$\frac{d\eta_3}{dT} = \frac{1}{2} \frac{\sigma_2}{\sigma_2 + \sigma_3} \left[\frac{1}{2} S_{O_2}^\circ - \frac{1}{2} R \ln P_{O_2} - \bar{S}_2 - \frac{Q_2^\circ}{T} \right] - \frac{\sigma_3}{\sigma_2 + \sigma_3} \left(\bar{S}_3 + \frac{Q_3^\circ}{T} \right) \quad (\text{Eq. 39})$$

The above equation will be used later but now the relationship between α and $\frac{d\eta_3}{dT}$ in the $ZrO_2(+CaO)$ and Pt phases in Cell 4 has to be developed in order to derive the general expression for α .

From the definition of the electrochemical potential of electrons in Eq. 27, and the fact the chemical potential of electrons at the two terminals of Cell 4 is equal, it follows that the potential difference between the terminals of Cell 4 equals

$$\phi^{(a)} - \phi^{(b)} = (\eta_3^{(Pt,a)} - \eta_3^{(Pt,b)}) / F \quad (\text{Eq. 40})$$

In the case of local equilibrium at a phase boundary, the electrochemical potential, η_3 , is the same on both sides of the interface. Thus the right-hand side of Eq. 40 is determined by the local difference of η_3 within the ZrO_2 and Pt phases involving temperature gradients. Hence, Eq. 23 may be applied:

$$\alpha = \frac{d(\phi^{(a)} - \phi^{(b)})}{dT} = \frac{1}{F} \left(\frac{d\eta_3^{(ZrO_2)}}{dT} - \frac{d\eta_3^{(Pt)}}{dT} \right) \quad (\text{Eq. 41})$$

According to Eq. 41 the total thermoelectric power is equal to the difference of two terms. The first term is characteristic of the ZrO_2 solid electrolyte, the second term of the Pt lead material. Let

$$-\frac{1}{F} \frac{d\eta_3^{(ZrO_2)}}{dT} \equiv \alpha^{(ZrO_2)} \quad (\text{Eq. 42})$$

and

$$-\frac{1}{F} \frac{d\eta_3^{(Pt)}}{dT} \equiv \alpha^{(Pt)} \quad (\text{Eq. 43})$$

Eq. 41 may be rewritten as:

$$\alpha = \alpha^{(ZrO_2)} - \alpha^{(Pt)} \quad (\text{Eq. 44})$$

The individual terms on the right-hand side of Eq. 44 are called the absolute thermoelectric powers of the respective phases. In an open circuit, the flux of electrons (J_3) in Pt is zero. Thus it follows from Eq. 25, for electrons in Pt,

$$\frac{d\eta_3}{dT} = -\left(\bar{S}_3 + \frac{Q_3^*}{T}\right) \quad (\text{Eq. 45})$$

Substituting Eq. 45 into Eq. 43, gives:

$$\alpha^{(Pt)} = \frac{1}{F} \left(\bar{S}_3^{(Pt)} + \frac{Q_3^*}{T} \right) \quad (\text{Eq. 46})$$

Similarly substituting Eq. 39 into Eq. 42, gives:

$$\begin{aligned} \alpha^{(ZrO_2)} &= \frac{1}{F} \frac{d\eta_3^{(ZrO_2)}}{dT} \\ &= \frac{t_{ion}}{2F} \left(-\frac{1}{2} S_{O_2} + \frac{1}{2} R \ln P_{O_2} + \left(\bar{S}_2 + \frac{Q_2^*}{T} \right) \right) - \frac{t_e}{F} \left(\bar{S}_3 + \frac{Q_3^*}{T} \right) \quad (\text{Eq. 47}) \end{aligned}$$

where $t_{ion} = \frac{\sigma_2}{\sigma_2 + \sigma_3}$, and $t_e = \frac{\sigma_3}{\sigma_2 + \sigma_3}$. Under predominant ionic conduction conditions

$$\alpha^{(ZrO_2)} = \frac{1}{2F} \left[-\frac{1}{2} S \dot{O}_2 + \frac{1}{2} R \ln P_{O_2} + \bar{S}_2 + \frac{Q_2^*}{T} \right] \quad (\text{Eq. 48})$$

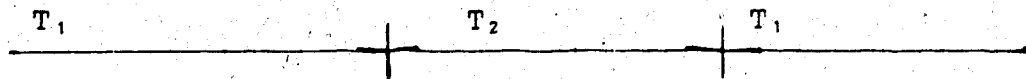
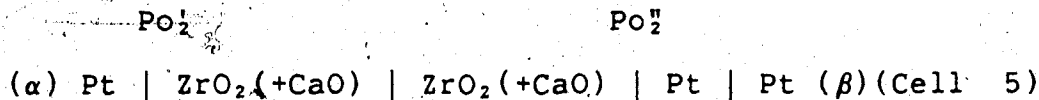
Substituting Eq. 47 and 46 into Eq. 44 gives the full expression of thermoelectric power for Cell 4:

$$\begin{aligned} \alpha &= \alpha^{(ZrO_2)} - \alpha^{(Pt)} \\ &= \frac{t_{ion}}{2F} \left[-\frac{1}{2} S \dot{O}_2 + \frac{1}{2} R \ln P_{O_2} + \bar{S}_2 + \frac{Q_2^*}{T} \right] - \frac{t_e}{F} \left(\bar{S}_3 + \frac{Q_3^*}{T} \right) - \frac{1}{F} \left(\bar{S}_3^{(Pt)} + \frac{Q_3^*}{T} \right) \end{aligned} \quad (\text{Eq. 49})$$

α can be experimentally measured and is termed the Seebeck coefficient.

Derivation of the EMF expression for a nonisothermal and nonisobaric cell with a $ZrO_2(+CaO)$ solid electrolyte from irreversible thermodynamics

A nonisothermal and nonisobaric cell with a $ZrO_2(+CaO)$ solid electrolyte can be represented as



In 1981 Etsell and Alcock⁽²⁰⁾ first reported using a nonisothermal cell like the one represented above. It was

proposed that the above cell could be visualized ~~as an~~ isothermal cell with an oxygen gradient at temperature T in series with an isobaric cell with a temperature gradient at a uniform oxygen pressure. The EMF of the cell is

$$E = E' + \frac{RT_2}{4F} \ln(Po_2^{\prime\prime}/Po_2^{\prime}) \quad (\text{Eq. 50})$$

if the ionic transference number of $ZrO_2(+CaO)$ is unity. The thermal contribution, E' , is the thermoemf of a thermal cell under oxygen pressure, Po_2^{\prime} .

Alternatively, the cell can be visualized as an isothermal cell with the same oxygen gradient at T_1 in series with an isobaric cell with the same temperature gradient at oxygen pressure, $Po_2^{\prime\prime}$. The EMF of the cell is

$$E = E'' + \frac{RT_1}{4F} \ln(Po_2^{\prime\prime}/Po_2^{\prime}) \quad (\text{Eq. 51})$$

where E'' is the thermoemf of a thermal cell under oxygen pressure Po_2^{\prime} .

In the current study the general EMF expression for the nonisothermal and nonisobaric cell was developed through principles of irreversible thermodynamics.

First of all, the EMF of Cell 5 can be simply written as

$$E = \phi^{(\alpha)} - \phi^{(\beta)} \quad (\text{Eq. 52})$$

where $\phi^{(\alpha)}$ and $\phi^{(\beta)}$ are the electric potentials of the α end and β end, respectively. From the definition of the electrochemical potential of electrons in Eq. 27 it follows that the potential difference between the terminals of Cell 5 is given by

$$\phi^{(\alpha)} - \phi^{(\beta)} = -\frac{1}{F} (\eta_3^{(\text{Pt}, \alpha)} - \eta_3^{(\text{Pt}, \beta)}) \quad (\text{Eq. 53})$$

In cases of local equilibrium at a phase boundary, the electrochemical potential, η_3 , is the same at the two sides of the interface, such as the Pt-ZrO₂ and ZrO₂-Pt interfaces. Thus, $\eta_3^{(\text{Pt}, \beta)} - \eta_3^{(\text{Pt}, \alpha)}$ is determined by the local differences of η_3 within the ZrO₂ and Pt phases involving temperature and oxygen gradients. This gives:

$$\phi^{(\alpha)} - \phi^{(\beta)} = -\frac{1}{F} (\eta_3^{(\text{ZrO}_2)} - \eta_3^{(\text{Pt})}) \quad (\text{Eq. 54})$$

Differentiating the above equation we get:

$$\frac{d(\phi^{(\alpha)} - \phi^{(\beta)})}{dx} = -\frac{1}{F} \left(\frac{d\eta_3^{(\text{ZrO}_2)}}{dx} - \frac{d\eta_3^{(\text{Pt})}}{dx} \right) \quad (\text{Eq. 55})$$

Under open circuit condition, $J_3=0$; thus from Eq. 25,

$$\eta_3^{(\text{Pt})} = -(\bar{S}_3^{(\text{Pt})} + \frac{Q_3^{\ddagger}(\text{Pt})}{T}) \quad (\text{Eq. 56})$$

Also applying Eq. 27 within the Pt phases,

$$\phi^{(a)} = \frac{1}{F} \eta_3^{(Pt)} = -\frac{1}{F} (\bar{S}_3^{(Pt)} + \frac{Q_3^*}{T}^{(Pt)}) \quad (\text{Eq. 57})$$

Under steady state conditions, since each volume element must remain electrically neutral, the fluxes J_2 and J_3 must be equivalent according to Eq. 29, $2J_2 = -J_3$.

Rewriting Eq. 30 gives:

$$\frac{\sigma_2}{2F^2} \left[\frac{d\eta_2}{dx} + (\bar{S}_2 + \frac{Q_2^*}{T}) \frac{dT}{dx} \right] = -\frac{\sigma_3}{F^2} \left[\frac{d\eta_3}{dx} + (\bar{S}_3 + \frac{Q_3^*}{T}) \frac{dT}{dx} \right] \quad (\text{Eq. 58})$$

Eq. 33, $\eta_2 = \frac{1}{2} \mu_{O_2} + 2\eta_3$, may be differentiated to give:

$$\frac{d\eta_2}{dx} = \frac{1}{2} \frac{d\mu_{O_2}}{dx} + 2 \frac{d\eta_3}{dx} \quad (\text{Eq. 59})$$

Substituting Eq. 59 into Eq. 58 and cancelling the common factor F ,

$$\frac{\sigma_2}{2} \left[\frac{1}{2} \frac{d\mu_{O_2}}{dx} + 2 \frac{d\eta_3}{dx} + (\bar{S}_2 + \frac{Q_2^*}{T}) \frac{dT}{dx} \right] = -\sigma_3 \left[\frac{d\eta_3}{dx} + (\bar{S}_3 + \frac{Q_3^*}{T}) \frac{dT}{dx} \right] \quad (\text{Eq. 60})$$

Regrouping Eq. 60 and solving for $\frac{d\eta_3}{dx}$,

$$\frac{d\eta_3}{dx} = -\frac{1}{4} \frac{\sigma_2}{\sigma_2 + \sigma_3} \frac{d\mu_{O_2}}{dx} - \frac{1}{2} \frac{\sigma_3}{\sigma_2 + \sigma_3} (\bar{S}_2 + \frac{Q_2^*}{T}) \frac{dT}{dx} - \frac{\sigma_2}{\sigma_2 + \sigma_3} (\bar{S}_3 + \frac{Q_3^*}{T}) \frac{dT}{dx} \quad (\text{Eq. 61})$$

Substituting $t_{ion} = \frac{\sigma_2}{\sigma_2 + \sigma_3}$ and $t_e = \frac{\sigma_3}{\sigma_2 + \sigma_3}$ into Eq. 61 and

removing the common factor dX , gives:

$$d\eta_3 = -\frac{t_{ion}}{4}d\mu_{O_2} - \frac{t_{ion}}{2}\left(\bar{S}_2 + \frac{Q_2^*}{T}\right)dT - t_e\left(\bar{S}_3 + \frac{Q_3^*}{T}\right)dT \quad (\text{Eq. 62})$$

Integrating Eq. 62 over the boundary conditions in Cell 5, gives:

$$\eta_3^{(ZrO_2)} = -\int_{\mu_{O_2}^1}^{\mu_{O_2}^2} \frac{t_{ion}}{4}d\mu_{O_2} - \int_{T_1}^{T_2} \frac{t_{ion}}{2}\left(\bar{S}_2 + \frac{Q_2^*}{T}\right)dT - \int_{T_1}^{T_2} t_e\left(\bar{S}_3 + \frac{Q_3^*}{T}\right)dT \quad (\text{Eq. 63})$$

where $\mu_{O_2}^1$ and $\mu_{O_2}^2$ are the chemical potentials of oxygen at the two electrodes; and T_2 and T_1 are the respective temperatures. The t_{ion} in Eq. 63 is a function of μ_{O_2} and T . The analytical solution of Eq. 63 is very complicated and is impossible to obtain. Substituting Eq. 63 into

$$\phi^{(\beta)} \equiv \frac{1}{F}\eta_3^{(ZrO_2)}$$

gives:

$$\phi^{(\beta)} = \frac{\bar{t}_{ion}}{4F}(\mu_{O_2}^1 - \mu_{O_2}^2) - \frac{\bar{t}_{ion}}{2F}\left(\bar{S}_2 + \frac{Q_2^*}{T}\right)(T_2 - T_1) - \frac{\bar{t}_e}{F}\left(\bar{S}_3 + \frac{Q_3^*}{T}\right)(T_2 - T_1) \quad (\text{Eq. 64})$$

where \bar{t}_{ion} is the effective ionic transport number of the

ZrO₂(+CaO) solid electrolyte in Cell 5, and $\bar{E}_0 = 1 - \bar{E}_{ion}$. The effective ionic transport number, \bar{E}_{ion} , is defined as:

$$\bar{E}_{ion} = \eta_3^{(ZrO_2)} / \left[-\frac{1}{4}(\mu_{O_2}'' - \mu_{O_2}') - \frac{1}{2} \left(\bar{S}_2 + \frac{Q_2^*}{T} \right) (T_2 - T_1) \right] \quad (\text{Eq. 65})$$

By definition,

$$\mu_{O_2}'' = \mu_{O_2}'' + RT_2 \ln Po_2'' \quad (\text{Eq. 66})$$

$$\mu_{O_2}' = \mu_{O_2}' + RT_1 \ln Po_2' \quad (\text{Eq. 67})$$

Subtracting Eq. 67 from Eq. 66 gives:

$$\begin{aligned} \mu_{O_2}'' - \mu_{O_2}' &= \mu_{O_2}'' - \mu_{O_2}' + RT_2 \ln Po_2'' - RT_1 \ln Po_2' \\ &= (S_{O_2}'' - S_{O_2}') \Delta T + RT_1 \ln (Po_2'' / Po_2') + R(T_2 - T_1) \ln Po_2'' \end{aligned} \quad (\text{Eq. 68})$$

where $\Delta T = T_2 - T_1$. Substituting Eq. 68 into Eq. 64 and collecting common terms:

$$\begin{aligned} \phi^{(\beta)} &= \frac{\bar{E}_{ion}}{4F} \left[-(S_{O_2}'' - S_{O_2}') \Delta T + RT_1 \ln (Po_2'' / Po_2') + R(T_2 - T_1) \ln Po_2'' \right. \\ &\quad \left. + 2 \left(\bar{S}_2 + \frac{Q_2^*}{T} \right) (T_2 - T_1) \right] - \frac{\bar{E}_e}{F} \left(\bar{S}_3 + \frac{Q_3^*}{T} \right) (T_2 - T_1) \end{aligned} \quad (\text{Eq. 69})$$

Regrouping Eq. 69:

$$\begin{aligned} \phi^{(\beta)} &= \frac{\bar{E}_{ion}}{4F} RT_1 \ln (Po_2'' / Po_2') + \frac{\bar{E}_{ion}}{2F} \left[-\frac{1}{2} (S_{O_2}'' - S_{O_2}') \Delta T + \frac{1}{2} R \Delta T \ln Po_2'' \right. \\ &\quad \left. + \left(\bar{S}_2 + \frac{Q_2^*}{T} \right) \Delta T \right] - \frac{\bar{E}_e}{F} \left(\bar{S}_3 + \frac{Q_3^*}{T} \right) \Delta T \end{aligned} \quad (\text{Eq. 70})$$

Substituting Eq. 70 and Eq. 57 into Eq. 52 ($E = \phi^{(a)} - \phi^{(b)}$) gives,

$$E = \frac{\bar{E}_{ion}}{4F} RT_1 \ln(P_{O_2}''/P_{O_2}') + \frac{\bar{E}_{ion}}{2F} \left[-\frac{1}{2} (S_{O_2}'' - S_{O_2}') \Delta T + \frac{R}{2} \Delta T \ln P_{O_2}'' \right. \\ \left. + (S_2 + \frac{Q_2}{T}) \Delta T \right] + \frac{\bar{E}_e}{F} (S_3 + \frac{Q_3}{T}) \Delta T - \frac{1}{F} (S_3^{(Pt)} + \frac{Q_3^{(Pt)}}{T}) \Delta T \quad (\text{Eq. 71})$$

This is the general EMF expression for a nonisothermal oxygen concentration cell with a $ZrO_2(+CaO)$ solid electrolyte. The expression derived this way is the same as results obtained by viewing the cell as an isothermal nonisobaric cell in series with an nonisothermal isobaric cell.

Considerations of electronic conduction in a nonisothermal cell with a $ZrO_2(+CaO)$ solid electrolyte

As we have considered before, the $ZrO_2(+CaO)$ solid electrolyte is an ionic conductor over a certain range of oxygen pressure at a given temperature. Outside the range, electronic conduction occurs.

The partial conductivity for each of the ionic and electronic defect species, i , is given by

$$\sigma_i = C_i q_i \mu_i \quad (\text{Eq. 72})$$

Therefore, the transport number of each species in the

electrolyte is defined by

$$t_i = \frac{\sigma_i}{\Sigma \sigma_i} \quad (\text{Eq. 73})$$

As discussed earlier, for the case of $\text{ZrO}_2(+\text{CaO})$,

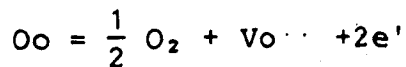
$$t_{\text{ion}} = \left[1 + \left(\frac{P_{\text{O}_2}}{P_h} \right)^{1/4} + \left(\frac{P_{\text{O}_2}}{P_e} \right)^{-1/4} \right]^{-1} \quad (\text{Eq. 74})$$

where P_e and P_h are constants previously defined for Eq. 15.

In this investigation, only electronic conduction at low oxygen pressures will be of concern. Therefore, the expression can be simplified into:

$$t_{\text{ion}} = \left[1 + \left(\frac{P_{\text{O}_2}}{P_e} \right)^{-1/4} \right]^{-1} \quad (\text{Eq. 75})$$

When the ambient oxygen pressure over $\text{ZrO}_2(+\text{CaO})$ is too low, the following reaction will occur:



Oxygen ions on normal sites will decompose into oxygen molecules, leaving oxygen vacancies and free electrons in the crystal. From the above reaction we can write:

$$C_e = K C_{\text{V}_o} \dots^{-1/2} P_{\text{O}_2}^{-1/4} \quad (\text{Eq. 76})$$

where C_e is the concentration of free electrons, K is the

reaction equilibrium constant, and C_{v_o} is the concentration of oxygen vacancies. As K is a constant at a given temperature and C_{v_o} is controlled by the aliovalent doping concentration, the two constants can be incorporated into K' , then:

$$C_e = K' P_{O_2}^{1/4} \quad (\text{Eq. 77})$$

From an earlier discussion in Section A of this chapter,

$$\omega_e = \nu_o \exp(-\Delta G_e^m/kT) \quad (\text{Eq. 78})$$

where ω_e is the jump frequency of electrons and ΔG_e^m is the free energy of migration of electrons. All other terms have the same meaning as defined for Eq. 3. Consequently, from Eq. 6 and 7,

$$\sigma_e = \frac{C_e a^2 q^2 \omega_e}{kT} \quad (\text{Eq. 79})$$

Substituting Eq. 74 and 75 into 76, and grouping all the constants into K_1 ,

$$\sigma_e = K_1 P_{O_2}^{-1/4} \frac{\exp(-\Delta G_e^m/kT)}{T} \quad (\text{Eq. 80})$$

Theoretically, it is not yet possible to calculate K_1 in Eq. 80. Nevertheless, this does not prevent us from

making comments on σ_e . From Eq. 80 it can be seen that σ_e increases as P_{O_2} decreases. Secondly, σ_e increases as temperature increases. To make more quantitative judgments on σ_e , an empirical parameter (P_e) may be introduced. P_e is defined as the oxygen partial pressure at which $t_e = t_{ion} = 0.5$. P_e has been measured experimentally and found to be temperature dependent in the form of⁽⁴³⁾

$$\ln P_e = -\frac{A}{T} + B \quad (\text{Eq. 81})$$

Substituting the above equation into Eq. 75 gives:

$$t_{ion} = \left[1 + \left(\frac{P_{O_2}}{\exp(B-A/T)} \right)^{-1/4} \right]^{-1} \quad (\text{Eq. 82})$$

This equation describes the temperature and oxygen pressure dependence of the ionic transference number.

It is well known that electronic conduction presents a major problem in isothermal oxygen probes, especially when the $ZrO_2(+CaO)$ solid electrolyte is applied under conditions of high temperature and low oxygen pressure. For a given temperature and oxygen pressure gradient, the EMF of an isothermal probe is (from Eq. 16)

$$E = \frac{RT}{F} \ln \frac{P_{O_2}^{7/4} + P_e^{1/4}}{P_{O_2}^{1/4} + P_e^{7/4}} \quad (\text{Eq. 83})$$

if the oxygen pressures at the electrodes of the cell are in such a range that the electronic hole conduction is

negligible. Here the electronic conductivity is represented through P_e . For a nonisothermal cell under the same oxygen pressure gradient but with a temperature gradient whose maximum temperature is T_2 , the EMF of the cell is obtained by substituting Eq. 63 into $\phi^{(Pt)} = \frac{1}{F} \eta_2^{(zrO_2)}$, and Eq. 57 into Eq. 52:

$$E = \frac{1}{4F} \int_{T_1}^{T_2} t_{ion} \frac{d\mu_{O_2}}{dT} dT + \frac{1}{2F} \int_{T_1}^{T_2} t_{ion} \left(\bar{S}_2 + \frac{Q_2^\circ}{T} \right) dT + \frac{1}{F} \int_{T_1}^{T_2} t_e \left(\bar{S}_2 + \frac{Q_2^\circ}{T} \right) dT - \int_{T_1}^{T_2} \alpha^{(Pt)} dT \quad (\text{Eq. 84})$$

where t_{ion} is given by Eq. 75. In the above equation, terms such as \bar{S}_2 and Q_2° are not measurable for mobile species. It was found that it was impossible to get an analytical expression for the integration in the above equation. However, the nonisothermal cell may be considered as an isothermal cell at T_1 in series with a nonisothermal cell at an oxygen pressure of $P_{O_2}^\circ$. This gives:

$$E = \frac{RT_1}{F} \ln \frac{P_{O_2}^\circ{}^{1/4} + P_e^{1/4}}{P_{O_2}^{1/4} + P_e^{1/4}} + \int_{T_1}^{T_2} \alpha dT \quad (\text{Eq. 85})$$

Earlier discussion in this chapter (Section E) demonstrated that the oxygen partial pressure in the expression for the Seebeck coefficient, α , should be $P_{O_2}^\circ$. The first term of the above equation is the same as the EMF expression for an isothermal cell under an identical oxygen gradient. In the second term of Eq. 85, α at $P_{O_2}^\circ$ is given by Eq. 49:

$$\alpha = \frac{t_{ion}}{2F} \left(-\frac{1}{2} S \dot{O}_2 + \frac{1}{2} R \ln P_{O_2} + \bar{S}_2 + \frac{Q_2}{T} \right) - \frac{t_e}{F} \left(\bar{S}_2 + \frac{Q_2}{T} \right) - \alpha^{(Pt)}$$

The t_{ion} in the above expression is very close to unity at the usual high reference oxygen partial pressure, P_{O_2} . Therefore, the above equation can be simplified into

$$\alpha = \frac{1}{2F} \left(-\frac{1}{2} S \dot{O}_2 + \frac{1}{2} R \ln P_{O_2} + \bar{S}_2 + \frac{Q_2}{T} \right) - \alpha^{(Pt)} \quad (\text{Eq. 86})$$

This indicates that the second term of Eq. 85 is not affected by electronic conduction. As the first term in Eq. 85 is the same as Eq. 83, it is evident that errors caused by lowering of the theoretical emf due to electronic conduction in oxygen cells will be the same whether it is isothermal or not.

The above analysis points out that the accuracy of a nonisothermal cell is not any better than that of an isothermal one. That is to say, changing conditions at the reference electrode, be it temperature or oxygen partial pressure, will not improve the overall accuracy of the cell.

Even so the probe employed here still presents the advantage of being more stable due to the low oxygen flux through the $ZrO_2(+CaO)$ solid electrolyte. Generally, the oxygen flux through a solid electrolyte of a galvanic oxygen cell with oxygen pressures P_{O_2} and P_{O_2}' at the anode and cathode can be expressed as⁽²⁰⁾:

$$J_{O_2} = \frac{RT\sigma_1}{2F^2L} \frac{P_e^{1/4}}{P_{O_2}^{1/4}} \frac{P_{O_2}'^{1/4} - P_{O_2}^{1/4}}{P_{O_2}^{1/4}}$$

where L is the length that oxygen ions must travel, that is, the length or thickness of the solid electrolyte. All other terms have the same definition as in the previous discussion.

This oxygen flux problem is especially significant if one of the electrodes has a low concentration of an electroactive species. Etsell and Flengas⁽⁴⁸⁾ made electrochemical measurements of oxygen partial pressures in CO-CO₂ and Ar-O₂ gas mixtures using a pure oxygen reference electrode. It was found for mixture dilute in CO, CO₂, or O₂ that the cell voltage is strongly dependent on the flow rate of the gas mixture passing over the working electrode.

A very likely explanation given for this flow rate dependence was concentration polarization arising from electronic oxygen transference, that is, the transfer of oxygen from the electrode with the higher oxygen partial pressure to the one with the lower oxygen pressure. A high flow rate is, therefore, necessary to remove the oxygen at the low oxygen electrode, whose oxygen activity is changed by the oxygen transferred from the other electrode. The sensitivity of an oxygen cell $\frac{dE}{dP_{O_2}}$ is highest when the concentration of an electroactive species is low.

Experimentally it was found⁽⁴³⁾

$$\sigma_1 = 837 e^{-25300/RT} \quad (\text{Eq. 88})$$

and

$$\log P_e = -54500/T + 14.0 \quad (\text{Eq. } 89)$$

for $ZrO_2(+CaO)$ solid electrolyte (10 mol % CaO).

As can be seen from the above equations, both σ_i and P_e decrease exponentially with decreasing temperature. Thus a nonisothermal cell with a lower temperature at its reference electrode will help in reducing oxygen transfer through the electrolyte. Perhaps more importantly, for the nonisothermal cell used in the present study, the electrolyte length is about 100 times the length of a disc electrolyte, usually 1 to 5 mm, used in the isothermal cell. This alone can correspondingly reduce the oxygen flux through the electrolyte according to Eq. 87. Use of a lower reference oxygen pressure, P_{O_2} , can also help in reducing oxygen transfer. Consequently, the solid reference oxygen probe, which has a lower reference electrode oxygen pressure, was adopted in this study. As a whole, nonisothermal cells present significant advantages over isothermal cells in minimizing the polarization problem.

Further considerations of effective ionic transport number

As was pointed out in the last section, an analytical expression of \bar{t}_{ion} for a nonisothermal oxygen probe is impossible to obtain. However, approximations of \bar{t}_{ion} can be obtained by first considering the effective ionic transport number for an isothermal oxygen probe.

The effective ionic transport number, t_{ion}' , for an isothermal oxygen probe is defined as

$$t_{ion}' = \frac{E}{E^0} = [1/(\mu_{O_2}'' - \mu_{O_2}')] \int_{\mu_{O_2}'}^{\mu_{O_2}''} t_i d\mu_{O_2} \quad (\text{Eq. 90})$$

Substituting Eq. 75 into the above equation and integrating, give:

$$t_{ion}' = 4 \frac{\log(P_{O_2}''^{1/4} + P_e^{1/4}) - \log(P_{O_2}'^{1/4} + P_e^{1/4})}{\log P_{O_2}'' - \log P_{O_2}'} \quad (\text{Eq. 91})$$

For nonisothermal conditions P_e is dependent on temperature. Therefore \bar{t}_{ion} is dependent on temperature. Substituting Eq. 81 into the above equation, gives the t_{ion}' for nonisothermal conditions:

$$\bar{t}_{ion} =$$

$$4 \frac{\log(P_{O_2}''^{1/4} + [\exp(B-A/T)]^{1/4}) - \log(P_{O_2}'^{1/4} + [\exp(B-A/T)]^{1/4})}{\log P_{O_2}'' - \log P_{O_2}'} \quad (\text{Eq. 92})$$

Integrating the above equation over T_1 and T_2 , gives

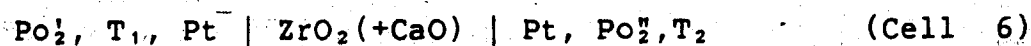
$$\bar{t}_{ion} = \frac{4}{T_2 - T_1}$$

$$\int_{T_1}^{T_2} \frac{\log(P_{O_2}''^{1/4} + [\exp(B-A/T)]^{1/4}) - \log(P_{O_2}'^{1/4} + [\exp(B-A/T)]^{1/4})}{\log P_{O_2}'' - \log P_{O_2}'} dT \quad (\text{Eq. 93})$$

The above equation is solved by the numerical integration for some typical values of $P_{O_2}^r$, $P_{O_2}^s$, T_1 , and T_2 . The obtained \bar{t}_{ion} values are listed in Table 3 and the Fortran program used is included as Appendix I. The effective ionic transport number for the isothermal conditions (at 1600°C and the same oxygen gradient), t_{ion} is also listed in Table 3 for comparison.

F. Calculation of dissolved oxygen in molten steel from the EMF measured by nonisothermal oxygen probes

As mentioned earlier, the probe used for continuous oxygen determination in molten steel is actually a nonisothermal galvanic cell with a $ZrO_2(+CaO)$ solid electrolyte. The cell can be represented as



where $P_{O_2}^r$ is the reference electrode oxygen pressure, T_2 is the reference electrode temperature, $P_{O_2}^s$ is the unknown oxygen pressure in equilibrium with dissolved oxygen in molten steel, and T_1 is the steel temperature.

The cell can be represented as in Fig. 6. The EMF of this cell is given by

$$E = \frac{RT_1}{F} \ln \frac{P_{O_2}^r^{1/4} + P_e^{1/4}}{P_{O_2}^s^{1/4} + P_e^{1/4}} + \alpha \Delta T + E_{lead} \quad (\text{Eq. 94})$$

In the above expression all terms have been explained

Table 3 \bar{E}_{ion} values for typical nonisothermal conditions

Po_2^I	Po_2^I	TC	\bar{E}_{ion}	t_{ion}
0.21	1.487×10^{-9}	1273	0.9986	0.9951
0.21	1.487×10^{-11}	1273	0.9972	0.9878
0.21	1.487×10^{-13}	1273	0.9936	0.9698
0.21	1.487×10^{-15}	1273	0.9850	0.9317
0.21	1.487×10^{-9}	1473	0.9981	0.9951
0.21	1.487×10^{-11}	1473	0.9960	0.9878
0.21	1.487×10^{-13}	1473	0.9905	0.9698
0.21	1.487×10^{-15}	1473	0.9778	0.9317
4.934×10^{-11}	1.487×10^{-9}	1273	0.9927	0.9552
4.934×10^{-11}	1.487×10^{-11}	1273	0.9877	0.9654
4.934×10^{-11}	1.487×10^{-13}	1273	0.9777	0.8967
4.934×10^{-11}	1.487×10^{-15}	1273	0.9579	0.8099
1.981×10^{-9}	1.487×10^{-9}	1473	0.9946	0.9858
1.981×10^{-9}	1.487×10^{-11}	1473	0.9899	0.9679
1.981×10^{-9}	1.487×10^{-13}	1473	0.9794	0.9331
1.981×10^{-9}	1.487×10^{-15}	1473	0.9572	0.8678
1.556×10^{-15}	1.487×10^{-9}	1273	0.9667	0.8288
1.556×10^{-15}	1.487×10^{-11}	1273	0.9543	0.7640
1.556×10^{-15}	1.487×10^{-13}	1273	0.9333	0.6480
1.556×10^{-15}	1.487×10^{-15}	1273	0.8988	0.5968
2.504×10^{-12}	1.487×10^{-9}	1473	0.9836	0.9361
2.504×10^{-12}	1.487×10^{-11}	1473	0.9742	0.8799
2.504×10^{-12}	1.487×10^{-13}	1473	0.9559	0.8781
2.504×10^{-12}	1.487×10^{-15}	1473	0.9215	0.7679

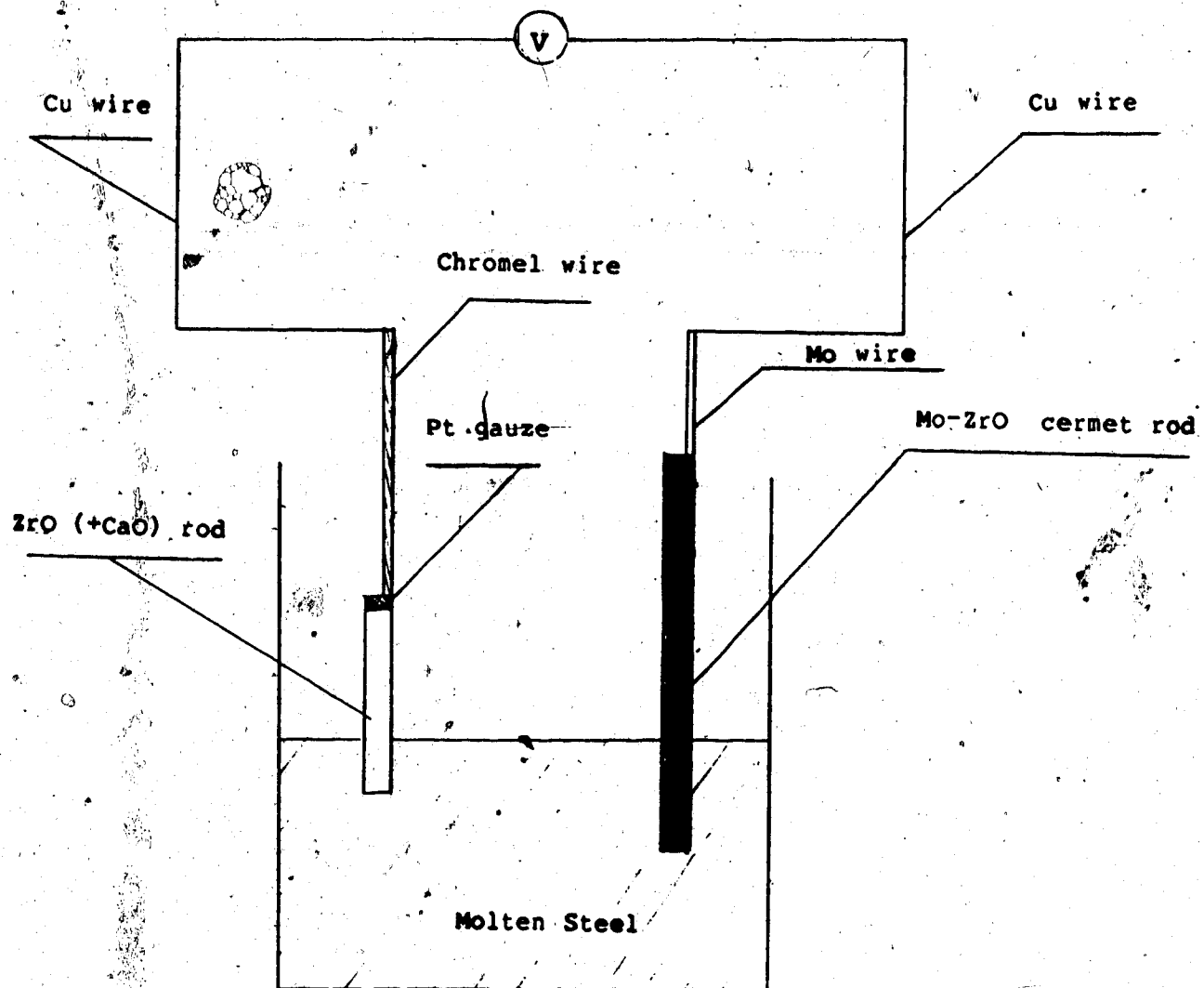


Fig. 6 Figurative representation of the laboratory-made cell

previously except for E_{lead} .

Thermoelectric EMF caused by different leads to an oxygen concentration cell

E_{lead} is an electromotive force caused by the thermocouple effect of different leads for the probe. Thermoelectric EMF arises in all electrochemical cells where the lead wires are not identical, even if the temperatures at each lead is the same.

Given an isothermal cell as in Fig. 7, if the Pt-Rh13% wire is replaced by a Pt wire then:

$$E = \frac{RT_1}{F} \ln \frac{P_{O_2}^{n/4} + P_e^{1/4}}{P_{O_2}'^{1/4} + P_e^{1/4}} - E' \quad (\text{Eq. 95})$$

where E' is the thermoelectric EMF of the thermocouple Pt vs. Pt-Rh13%, Furthermore, if the cell is nonisothermal as it is represented in Fig. 8, then the EMF of the cell should be

$$E = \frac{RT_1}{F} \ln \frac{P_{O_2}^{n/4} + P_e^{1/4}}{P_{O_2}'^{1/4} + P_e^{1/4}} + \alpha \Delta T - E'' \quad (\text{Eq. 96})$$

where α is the Seebeck coefficient of $ZrO_2(+CaO)$ at the oxygen pressure, P_{O_2}' , and E'' is the thermoelectric EMF of the thermocouple Pt vs. Pt+Rh13% at temperature T_2 .

The thermoelectric corrections, such as E' and E'' can be readily found in handbooks for thermocouples.

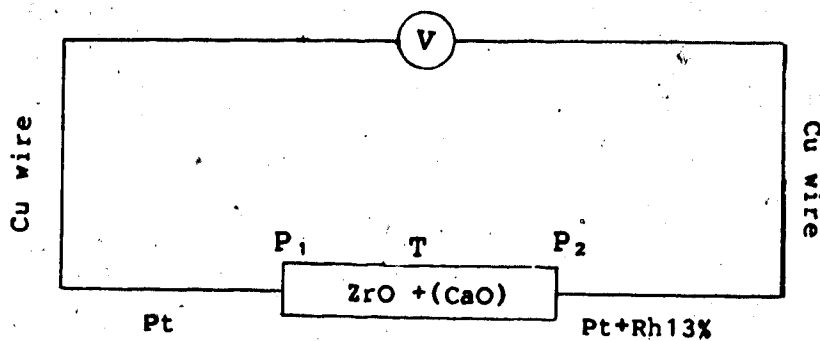


Fig. 7 Isothermal cell with different leads

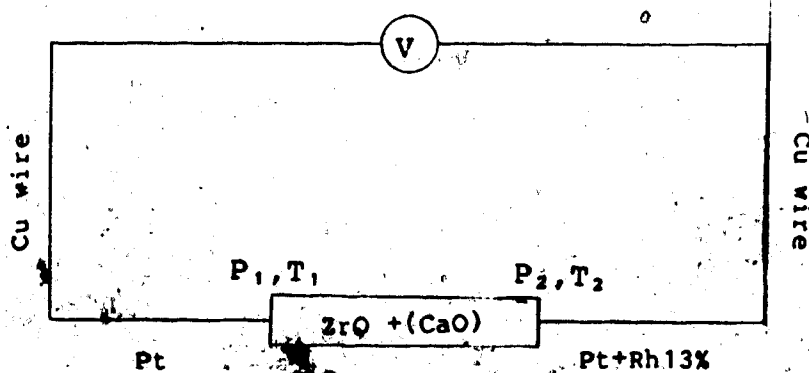


Fig. 8 Nonisothermal cell with different leads

The above two equations are corrected to platinum because in the Seebeck coefficient expression

$$\alpha = \alpha^{(\text{ZrO}_2)} - \alpha^{\text{metal}}$$

the α^{metal} term is $\alpha^{(\text{Pt})}$ for the available Seebeck coefficient data on $\text{ZrO}_2(+\text{CaO})$ solid electrolytes. If any nonisothermal cell does not use a Pt lead, a thermoelectric correction has to be made.

The cell as represented in Fig. 6 will now be considered. In order to be consistent with Seebeck coefficient measurements, the thermoelectric EMF correction is described by the last two terms in the following equation:

$$E = \frac{RT_1}{F} \ln \frac{P_{\text{O}_2}^{7/4} + P_e^{1/4}}{P_{\text{O}_2}^{1/4} + P_e^{1/4}} + \alpha_{(\text{at } p_2)} \Delta T + E_{(\text{cpt}2)} - E_{(\text{mpt}1)} \quad (\text{Eq. 97})$$

where $E_{(\text{cpt}2)}$ is the thermoelectric EMF of a chromel wire vs. Pt at T_2 , and $E_{(\text{mpt}1)}$ is the thermoelectric EMF of a Mo-ZrO₂ rod vs. Pt at T_1 . From Etsell's⁽⁵⁰⁾ measurement:

$$E_{(\text{cpt}2)} - E_{(\text{mpt}1)} = 3.76 + 0.0177T_2 - (-8.92 + 0.0261T_1) \quad (\text{Eq. 98})$$

Notice the nomenclature in the above equation is different with T_2 standing for the reference electrode temperature and T_1 for the steel temperature.

Oxygen partial pressure and temperature dependence of the Seebeck coefficient

Under a given oxygen pressure the Seebeck coefficient of $ZrO_2(+CaO)$ was given by Eq. 22,

$$\alpha = \frac{1}{2F} \left(-\frac{1}{2} S_{O_2} + \frac{1}{2} R \ln P_{O_2} + \bar{S}_2 + \frac{Q_2^\circ}{T} \right) - \alpha^{(Pt)}$$

assuming the $ZrO_2(+CaO)$ is predominantly an ionic conductor, where \bar{S}_2 and Q_2° indicate the partial molar entropy and heat of transport for oxygen ions.

As can be seen from Eq. 22, α is oxygen pressure dependent. When the oxygen pressure is 0.21 atm, α is found to be -0.505 mV/°C over a wide range of temperature for the $ZrO_2(+CaO)$ solid electrolyte.⁽⁵⁰⁾ It would be natural to expect α to be temperature dependent since S_{O_2} , \bar{S}_2 and $\frac{Q_2^\circ}{T}$ are all temperature dependent. However, α is experimentally found virtually temperature independent, fortuitously due to the cancellation of the temperature effect when the three terms are summed.

Whether α is temperature dependent or not, it appears safe to assume:

$$\alpha = K + \frac{R}{4F} \ln P_{O_2} \quad (\text{Eq. 99})$$

under given temperature conditions.

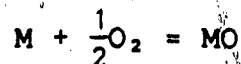
If $P_{O_2} = 0.21$ atm, and $\alpha = K + \frac{1.987}{4F} \ln 0.21 = -0.505$ mV/°C, then

$$\alpha(\text{Po}_2=1\text{atm}) = K = -0.471 \text{ mV}/^\circ\text{C}$$

Thus the oxygen pressure dependence of α is:

$$\alpha = -0.471 + \frac{R}{4F} \ln \text{Po}_2 \quad (\text{Eq. 100})$$

Sometimes the oxygen pressure in the expression for α is controlled by a metal-metal oxide mixture, for example:



with $\Delta G^\circ_{\text{MO}} = A + BT$

Then the oxygen pressure over the mixture at equilibrium is

$$\text{Po}_2 = \left[\exp\left(\frac{\Delta G^\circ_{\text{MO}}}{RT}\right) \right]^2 \quad (\text{Eq. 101})$$

Substituting the above equation into Eq. 100 gives:

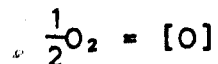
$$\alpha = -0.471 + \frac{B + A/T}{2F} \quad (\text{Eq. 102})$$

Calculation of the oxygen activity in steel from the measured EMF

Given all the considerations above, for a measured oxygen probe voltage, T_1 , T_2 , Po_2^1 , and P_e , the unknown oxygen pressure Po_2^2 can be calculated from Eq. 93. This Po_2^2 is the oxygen partial pressure in equilibrium with dissolved

oxygen in molten steel.

Furthermore, according to the reaction



$a_{[O]}$, the activity of the dissolved oxygen in steel, can be determined from the calculated oxygen pressure. For the above reaction⁽⁵¹⁾,

$$\Delta G^*_{[O]} = -28000 - 0.67T_1 \quad (\text{Eq. 103})$$

where $\Delta G^*_{[O]}$ is the free energy of dissolution of oxygen and T_1 is the steel temperature. At equilibrium

$$\Delta G_{[O]} = \Delta G^*_{[O]} + RT_1 \ln \frac{a_{[O]}}{P_{O_2}^{1/2}} = 0 \quad (\text{Eq. 104})$$

From Eq. 99 and 100 it follows that,

$$a_{[O]} = \exp\left(\frac{-\Delta G^*_{[O]}}{RT_1}\right) P_{O_2}^{1/2} \quad (\text{Eq. 105})$$

Sometimes it is desirable to know the weight percentage of oxygen in steel from the oxygen activity obtained. However, molten steel usually contains several alloying elements in dilute solution. Typical alloying elements are Si, C, Al, Mn. They affect the oxygen activity coefficient to different extents because of their interactions with dissolved oxygen in steel.

By definition

$$[\%O] = \frac{a_{[O]}}{f_o} \quad (\text{Eq. 106})$$

where the oxygen activity coefficient, f_o , in molten steel with alloying elements added is defined as

$$f_o = f_o^0 \times f_o^m \times f_o^n \times \dots \quad (\text{Eq. 107})$$

where f_o^i is the activity interaction coefficient of the i^{th} component in a multicomponent molten steel system containing O, M, N etc.. A more convenient way of looking at this problem is

$$\log f_o = [\%O]e_o^0 + [\%M]e_o^m + [\%N]e_o^n + \dots \quad (\text{Eq. 108})$$

where $[\%O]$ is weight percentage of dissolved oxygen, $[\%i]$ is weight percentage of the i^{th} solute and the term e_o^i is defined by

$$e_o^i = \frac{\partial \log f_o}{\partial [\%i]} \quad (\text{Eq. 109})$$

Values of e_o^i can be readily found in thermodynamic data tables⁽⁵¹⁾.

In the present study, samples of molten steel were taken periodically for chemical analysis of alloying elements. Oxygen content was analyzed by the inert gas fusion method. After those analyses were done, f_o was

calculated according to the following formula

$$\log f_0 = [\%O]e_0^O + [\%C]e_0^C + [\%Al]e_0^{Al} + [\%Si]e_0^{Si} + \dots$$

Substituting values⁽⁵¹⁾ for e_0^i

$$\log f_0 = -0.2[\%O] - 0.13[\%C] - 0.94[\%Al] - 0.14[\%Si] + \dots$$

(Eq. 110)

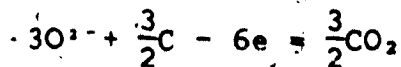
Once f_0 was determined and $a_{(O)}$ measured electrochemically, $[\%O]$ was obtained from Eq. 102.

G. Fundamentals of the $\text{Na}_3\text{AlF}_6\text{-Al}_2\text{O}_3$ system

Today, one hundred years after its invention, the Hall-Heroult method remains the predominant process of commercial aluminum production. Though many technological improvements have been made, principles of the process remain the same. It probably will continue to be the dominant method for the foreseeable future.

In the Hall-Heroult process, aluminum is electrochemically reduced from Al_2O_3 , dissolved in molten Na_3AlF_6 , at a temperature around 960°C . Usually about 3 to 8 weight percent Al_2O_3 is added to the molten cryolite which acts as the electrolyte in an aluminum electrolysis cell. A voltage of around 4.5 volts is impressed onto the cell through which a direct current passes. This results in oxidation of oxygen ions at the carbon anode and reduction

of aluminum ions at the cathode. After the oxygen ion is oxidized it will react with the carbon anode to form CO_2 . The electrode reaction can be written as

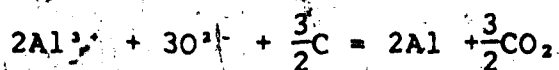


at the carbon anode; and



at the cathode, which is a layer of liquid Al at the bottom of the cell.

The overall cell reaction is the sum of two electrode reactions:



During normal electrolysis, the anode reaction, in principle, involves the discharge of oxygen ions from complex oxygen-carrying ions at the anode. However, the actual mechanism is much more complicated.

Properties of the $\text{Na}_3\text{AlF}_6\text{-Al}_2\text{O}_3$ electrolyte

Pure cryolite (Na_3AlF_6) melts at $1011 \pm 2^\circ\text{C}$ with a slight dissociation of the complex anion AlF_6^{3-} . The most probable scheme of the dissociation was found by Grjotheim⁽⁵²⁾ to be:



This scheme is supported by many studies, in particular, Raman spectroscopy⁽⁵³⁾ which indicated about 25 % AlF_6^- dissociated into AlF_4^- in the molten cryolite.

When alumina is added into molten cryolite, it will dissolve and introduce O^{2-} ions and additional Al^{3+} into the system. Aluminum ions are already present in the system in the complex ions AlF_6^- and AlF_4^- . The added O^{2-} ions are quite similar in size to the F^- ions; therefore O^{2-} ions can replace F^- ions structurally. It is now commonly assumed that the O^{2-} ions introduced into the system will occupy essentially the same type of sites as F^- ions, and that they will be statistically distributed around Al^{3+} ions in the melt as AlOF_x^{3-x} complex ions. Holm⁽⁵⁴⁾ has measured the freezing-point depression in molten cryolite by the addition of alumina. For additions of less than 2 mol % alumina, one unit of Al_2O_3 creates three units of "foreign" species. This strongly suggested that species with a single oxygen ion caused the observed freezing-point depression in the dilute solution region, where ideal behaviour may be expected.

Phase diagram studies of the quasi-binary system, $\text{Na}_3\text{AlF}_6-\text{Al}_2\text{O}_3$, show that the system has a single eutectic point at 960-963°C and 10.0-11.5 wt% Al_2O_3 . The earlier belief in the existence of a solid solution in $\text{Na}_3\text{AlF}_6-\text{Al}_2\text{O}_3$ has now been disproved by more recent investigations.

Anode Effect

In industrial aluminum cells a kind of abnormal behaviour, known as the "anode effect", can occur during electrolysis. Under galvanostatic conditions, an anode effect manifests itself by a sudden increase in cell voltage. In industrial cells the voltage can rise abruptly to 30-50 V while the current remains approximately constant or decreases slightly. Simultaneously, the normal gas discharge at the anode almost ceases, and the current passes from the melt to the anode by way of a series of small arcs. A rise in the temperature of the anode and its vicinity also takes place.

The anode effect occurs when the Al_2O_3 content of the cell becomes too low (usually below 1-2 wt %) to maintain normal electrolysis. A parameter, known as the critical current density, is introduced to help characterize the anode effect. It is defined as the maximum current density at a given Al_2O_3 content, which is attained before the normal anode reaction is superceded by the anode effect. Hence, this current density can be considered as a limiting current density for oxidation of the oxygen-containing ions.

Relationships between the critical current density and concentration of Al_2O_3 has been investigated extensively.⁽⁵³⁾ Experimental values of critical current density at a given Al_2O_3 content do not always agree with one another due to many different factors, such as geometric shape of the anode, anode material, and external pressure. Nevertheless,

most investigations seem to point out that critical current density increases as the Al_2O_3 concentration in the melt increases. This can be expressed by Sand's equation

$$\frac{i\tau^{1/2}}{C} = \frac{1}{2} \pi^{1/2} n F D^{1/2} \quad (\text{Eq. 111})$$

where i is the current density, τ is the transition time, C is the concentration, n is the number of electrons involved in the reaction, F is the Faraday constant, and D is the diffusion coefficient of the oxygen-containing ions.

The term $\frac{i\tau^{1/2}}{C}$ attains a constant value in very short transition times. Ideally, by measuring $\tau^{1/2}$, corresponding concentrations of oxygen-containing species can be determined. However, further studies found deviations from Sand's equation occurred if the melt contained more than 2 wt % Al_2O_3 . Therefore, Grjotheim⁽⁵³⁾ proposed an empirical equation

$$i\tau^{1/2} = K C^n \quad (\text{Eq. 112})$$

where K is an experimental constant, i is the current density, C is the alumina concentration in the melt, and n has empirical values between 0.5 and 0.6. Accordingly, there still is not a mature technique for determining $[\text{Al}_2\text{O}_3]$ in industrial cells.

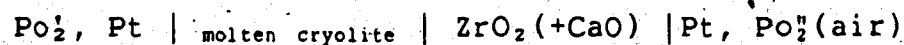
Though many different explanations have been given for the anode effect, it is now generally agreed that before or during the anode effect, fluoride ions are oxidized and

react with the carbon anode surface to form gaseous CF_4 , which blocks the carbon anode surface. The fluoride ions will only be oxidized when the content of Al_2O_3 in the $Na_3AlF_6-Al_2O_3$ melt has dropped too low.

Frequent anode effects are unwanted because of the extra energy consumption and possible overheating of the cells. In addition, anode effects disrupt normal cell operation. On the other hand, anode effects serve the purpose of keeping a check on the alumina concentration in the electrolyte so that overfeeding can be avoided. If another means of alumina monitoring is found, the effect may be abolished completely.

H. Oxygen pressure determination in a molten $Na_3AlF_6-Al_2O_3$ system

A nonisothermal oxygen probe, basically the same as the one used in molten steel, is used here for oxygen measurements in molten $Na_3AlF_6-Al_2O_3$ solutions. The probe, with an air reference electrode, can be represented as

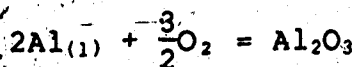


(Cell 7)

Similar to Eq. 94, the cell voltage is given by:

$$E = \frac{RT_1}{F} \ln \frac{Po_2^{1/4} + P_e^{1/4}}{Po_2^{1/4} + P_e^{1/4}} + \alpha \Delta T + E_{lead}$$

Here α and E_{load} can be treated in exactly the same way as was discussed for measuring oxygen in molten steel. Therefore, for a given T_1 , T_2 , and P_o , dependence on temperature, the P_{O_2} in equilibrium with a molten $Na_3AlF_6-Al_2O_3$ mixture can be calculated from the measured cell voltage. As in industrial cells, aluminum is added into the molten $Na_3AlF_6-Al_2O_3$ system. After the addition of aluminum and if the equilibrium is reached within the melt, the P_{O_2} in the melt is controlled by the following reaction



The free energy change for the reaction is

$$\Delta G = \Delta G^\circ + RT \ln \frac{a(Al_2O_3)}{P_{O_2}^{3/2}} \quad (\text{Eq. 113})$$

where $a(Al_2O_3)$ is the activity of Al_2O_3 in the melt, and P_{O_2} is the oxygen partial pressure in equilibrium with the Al_2O_3 in the melt. If the amount of Al_2O_3 added to the system exceeds the solubility limit of Al_2O_3 in cryolite, one will have $a(Al_2O_3) = 1$. In addition, $a_{Al} = 1$ holds for pure Al added into the cell. Then at equilibrium where $\Delta G = 0$,

$$\Delta G^\circ = \frac{3}{2} RT \ln P_{O_2} \quad (\text{Eq. 114})$$

By measuring the oxygen partial pressure at this equilibrium condition ΔG° for the reaction of Al and O_2 in the

$\text{Na}_3\text{AlF}_6\text{-Al}_2\text{O}_3\text{-Al}$ system can be obtained from Eq. 114.

After ΔG° is obtained, the activity of Al_2O_3 can then be determined by measuring the oxygen partial pressure in equilibrium with melts of different Al_2O_3 contents according to a rearrangement of Eq. 113:

$$\ln a(\text{Al}_2\text{O}_3) = -\frac{\Delta G^\circ}{RT} + \frac{3}{2} \ln P_{\text{O}_2} \quad (\text{Eq. 115})$$

The activity of Al_2O_3 in a Na_3AlF_6 melt can provide us with the information about the thermodynamics of the melt. This is very important to the understanding of the aluminum electrolysis process. In addition, the activity of Al_2O_3 in a $\text{Na}_3\text{AlF}_6\text{-Al}_2\text{O}_3$ melt can be correlated to the anode effect, hence providing a tool for in situ monitoring of the Al_2O_3 concentration in the cell. This would have immense value for operational control in the aluminum electrolysis process.

III. Experimental

A. Experimental set-up

The basic experimental set-up used in the current study can be represented by Fig. 9.

An Inductotherm 30 KW induction furnace was used to melt the steel, which was supplied by Stelco. The oxygen partial pressure in equilibrium with the dissolved oxygen in molten steel was determined by measuring the voltage of a laboratory-made nonisothermal oxygen probe. The probe voltage was measured by a Keithley 616 Digital Electrometer, then recorded with an Keithley 6162 Isolated Input/Control connected to a 750 Printer. At the same time, the probe voltage was followed by a chart recorder. The temperature at the reference electrode of the oxygen probe was measured with a Chromel vs. Alumel thermocouple connected to a Fluke 2165A Digital Thermometer. Steel temperature was measured with a quartz tube-sheathed Pt vs. Pt+Rh13% thermocouple connected to a Fluke 2168A Digital Thermometer. During the run, argon was continuously flushed over the surface of the molten steel.

About $1\frac{1}{2}$ hr was required to melt down a full charge of steel using the induction furnace. The original composition of the steel stock, supplied by Stelco, is listed as the following: 0.56-0.61% C, 0.65-0.85% Mn, 0.28% Si, 0.65% Cr,

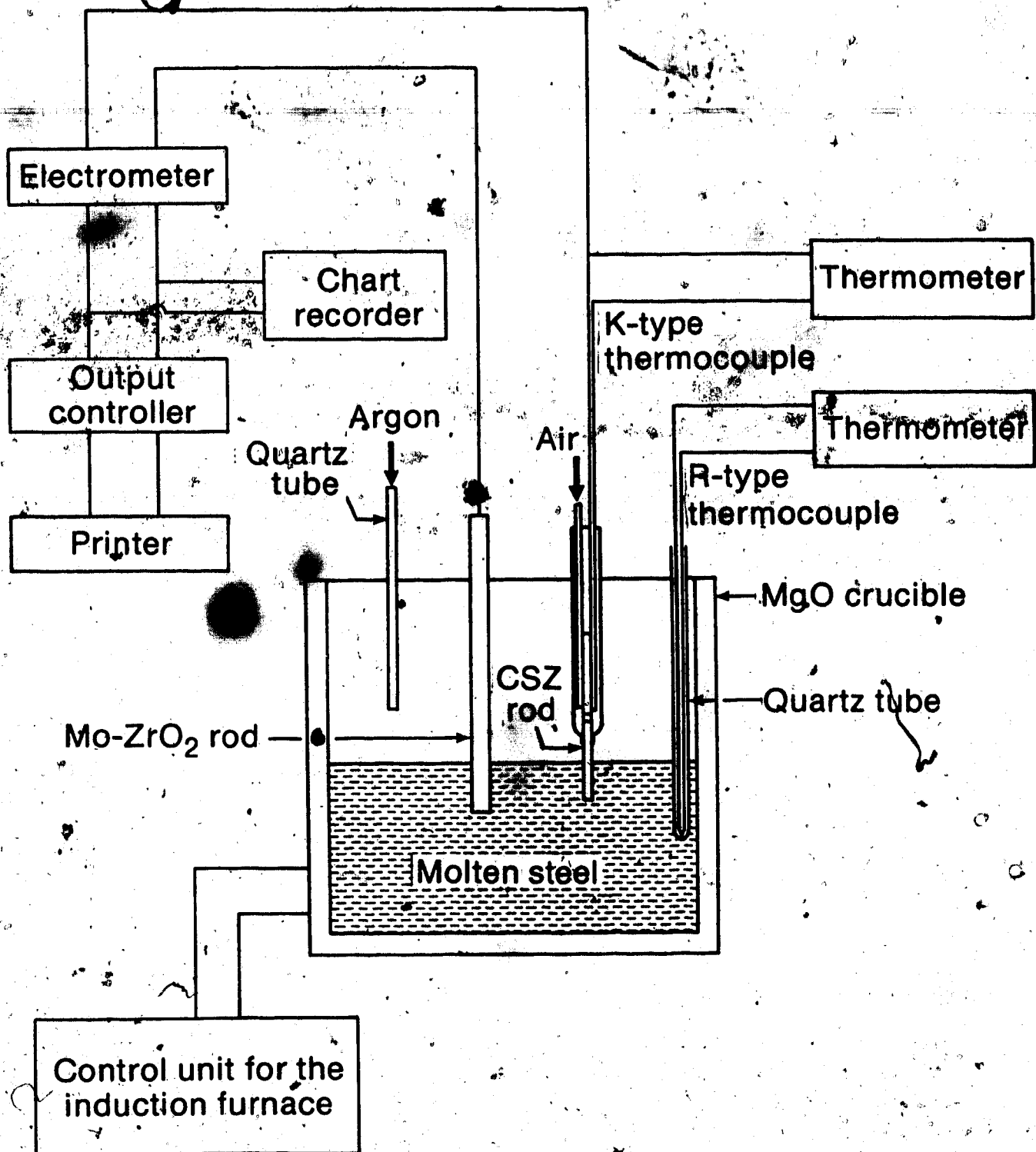


Fig. 9 Experimental set-up for tests on molten steel

and 0.035% Nb. Power input to the furnace was maintained at 20 KW throughout the melting process and was reduced to about 14 KW to keep the steel temperature constant once the steel had melted. The steel temperature was easily maintained within 5°C of the usual operating temperature, which was between 1500-1530°C depending on individual heats.

Initially, great difficulty was encountered in attempting to measure the temperature of the molten steel. High temperature mullite and alumina protection sheaths for the thermocouple all cracked upon being immersed into steel. A pyrometer was tried but its readings were too unreliable to be valuable for the present study. Finally the solution was found to be a Pt vs. Pt-Rh13% thermocouple placed in a closed end quartz tube. The quartz tube usually lasted for a single run which could take from 30 to 90 minutes.

As the steel was melted in the induction furnace, argon gas was flushed over the melt to help prevent possible oxidation of molten steel by oxygen in the air. To make the argon protection more effective, a laboratory-made cover was put on top of the induction furnace. It was found that the cover helped reduce the oxidation to a certain extent; therefore, it helped to maintain a more stable experimental environment. Even though every effort was made to maximize the effectiveness of the argon protection, oxidation of steel still occurred due to limitations of the experimental conditions.

First, even with the cover on, oxygen in air could still get into contact with the molten steel. When this happened, oxidation of steel was inevitable. Secondly, there may be refractory lining decomposition which can introduce additional oxides into the steel melt. Every time the MgO crucible was replaced, it could be seen that the crucible was penetrated by the steel and may be attacked by the steel.

The oxygen probe was immersed into molten steel to measure the oxygen activity in steel. Usually the Mo-ZrO₂ cermet rod was immersed to about 2 cm whereas the ZrO₂(+CaO) electrolyte rod was dipped into steel to a depth of 1 cm. The probe voltage was measured between a Mo wire connected to the cermet rod and one of the thermocouple wires which was in electrical contact with the Pt, air reference electrode. The quartz tube with a Pt-Pt+Rh13% thermocouple inside was fully immersed to record the steel temperature.

B. Construction of the nonisothermal oxygen probe

Oxygen probe with an air reference electrode

A detailed drawing of the probe design is shown in Fig. 10. Also a photograph of the the probe is presented (Plate 1). The rod on the right side of the photograph is a Mo-ZrO₂ cermet rod.

The major component of the probe was the electrolyte rod which was a CaO partially stabilized ZrO₂ rod with a

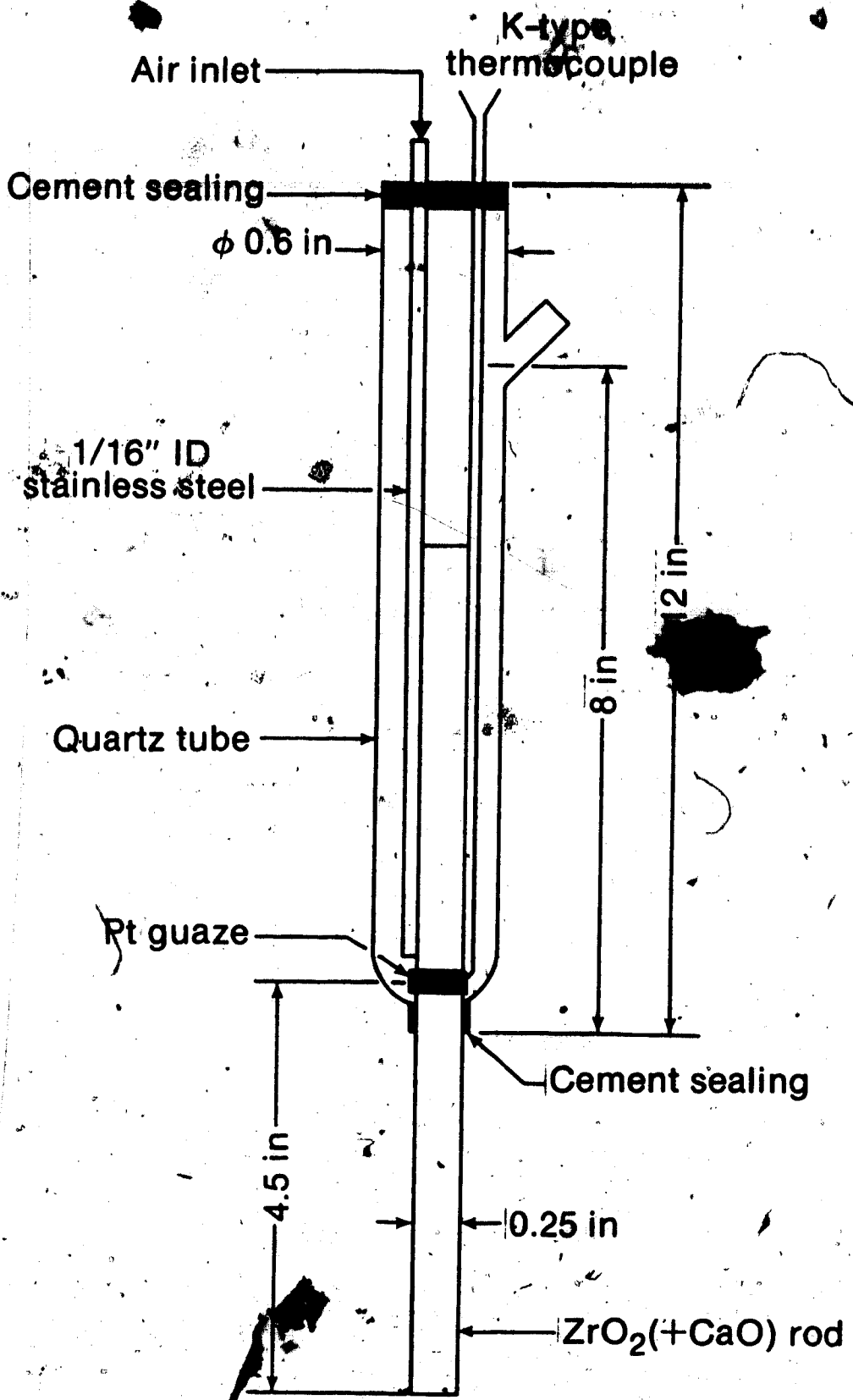


Fig. 10 Design of the air reference electrode probe.

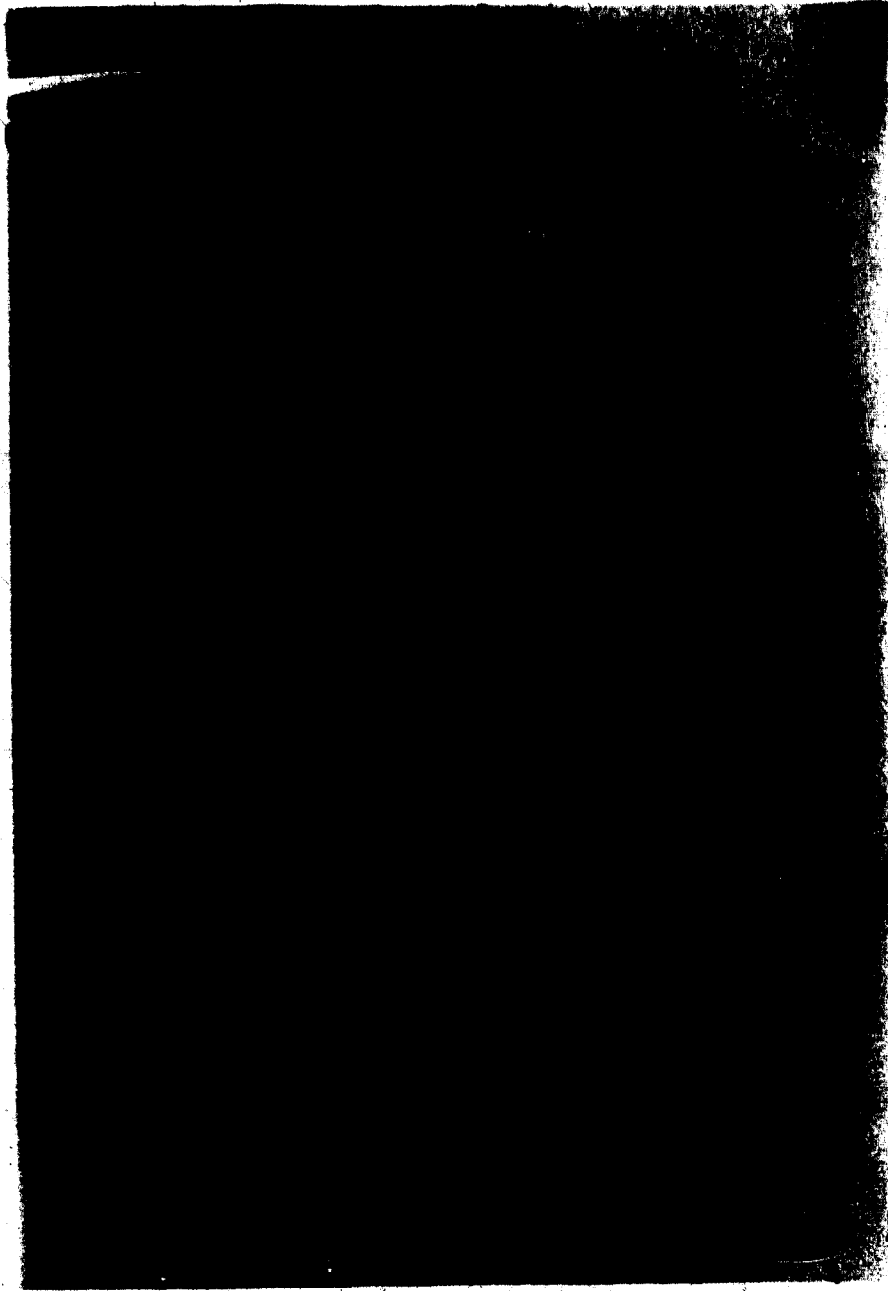


Plate 1 Photograph of a typical air reference probe

diameter of 6.4 mm. A typical chemical analysis of the electrolyte was the following: ZrO_2+HfO_2 94.69%, SiO_2 0.60%, CaO 3.5%, MgO 0.79%, Fe_2O_3 0.11%, Al_2O_3 0.20%, and TiO_2 0.11%. A piece of platinum gauze was attached onto the electrolyte rod at a distance of 8-12 cm away from the tip to constitute the reference electrode. This distance could not be too far from the tip because the reference electrode could not be at a temperature out of the range required for suitably low impedance. Air was led into the probe by a 3 mm OD-1.5 mm ID stainless steel tube and impinged upon the Pt gauze to maintain a constant oxygen partial pressure over the reference electrode.

Normally the air flow rate was set at 85 ml/min, which was relatively slow. Air flow was used simply to keep the atmosphere at the reference electrode from being stagnant. Therefore a low flow rate was sufficient, especially since a high air flow rate would have cooled the reference electrode too much.

A Chromel-Alumel (K-type) thermocouple was positioned in contact with the Pt gauze to measure the reference electrode temperature. One leg of this thermocouple also served as the electric lead for the reference electrode. The whole reference electrode was contained in a specially shaped quartz tube.

Sealing is required at the joint of the quartz tube and electrolyte rod. The sealing material used was either Ceramacoat 512 or Sauereisen, both of which performed

reasonably well.

To make the measurements the tip of the electrolyte rod was dipped into the molten steel which is the working electrode of the probe. The tip of the Mo-ZrO₂ rod was dipped into the steel and served as the electric lead for the working electrode. The Mo-ZrO₂ had a composition of 40 volume percent ZrO₂, that is, 26.4 wt % ZrO₂ and 73.6 wt % Mo metal.

Since the reference electrode was several centimeters above the molten steel, the reference electrode temperature is naturally lower than the working electrode temperature, that is, the steel temperature. Therefore, the voltage measured between the working electrode and the reference electrode will include a thermoelectric contribution due to the temperature gradient and the different leads used for the two electrodes.

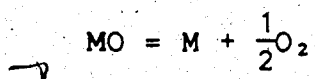
Oxygen probe with solid metal-metal oxide reference electrodes

The choice of the metal-metal oxide mixture to be used as the reference electrode was limited since it had to fulfill certain basic requirements: (1) it could not melt at the temperature of interest, (2) it could not react with the probe components, (3) the oxygen dissociation pressure of the oxide had to be in the range where there was no significant electronic conductivity in the electrolyte.

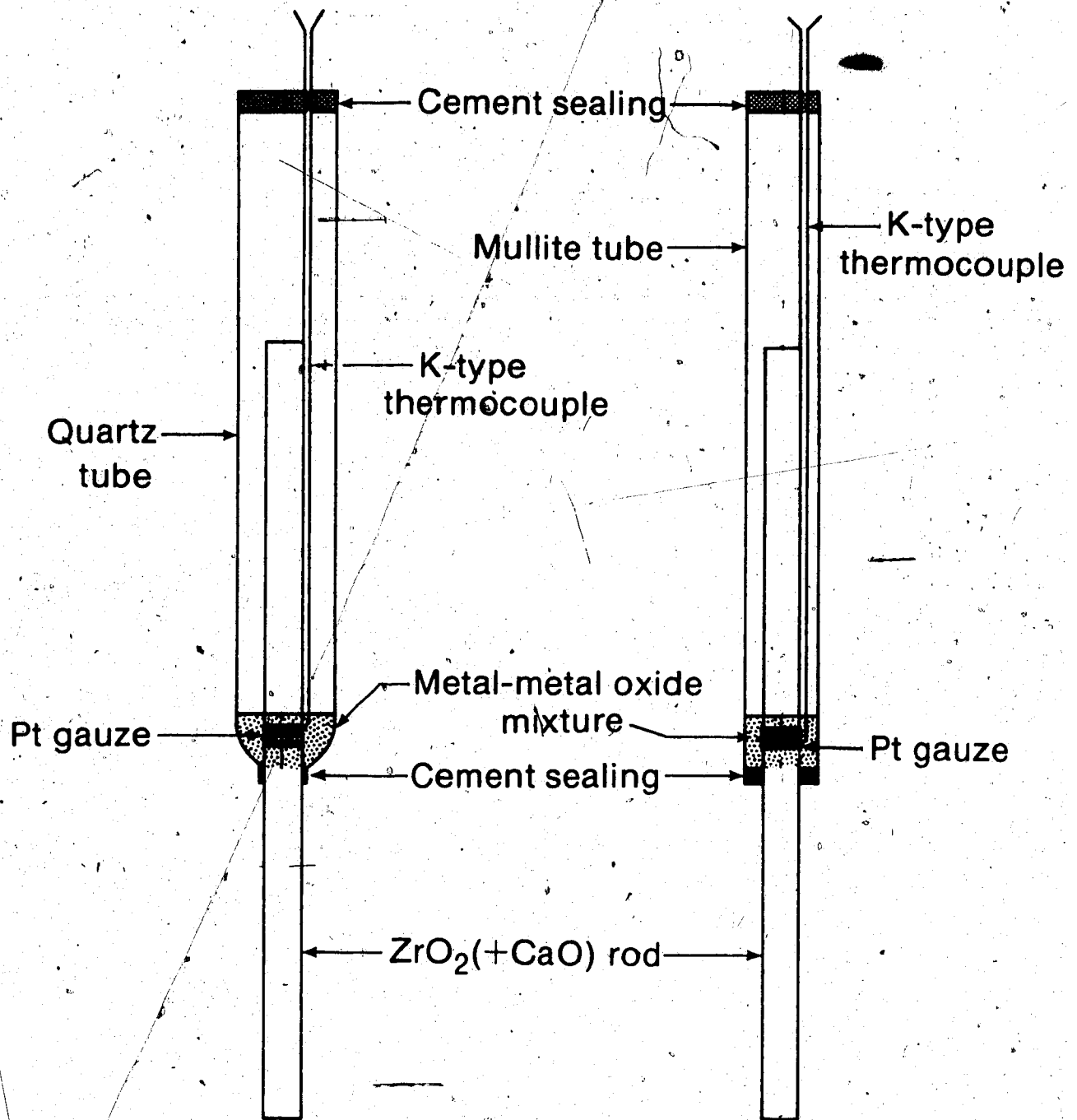
Two kinds of metal-metal oxide mixtures, Ni-NiO and Mo-MoO₂, were used because they fulfilled these requirements. The nickel oxide used was Fisher certified and the nickel powder was grade NFTM from Sherritt Gordon. The MoO₂ is 99.9% pure powder from Research Org/Inorg. Chem. Corp. and the molybdenum was 99.98% pure 100 mesh powder from Apache Chemicals.

The probe design for the solid metal-metal oxide reference electrode was a little different from that of the air reference electrode probes. A detailed illustration of probe design is shown in Fig. 11 and a photograph of the probe is also included in Plate 2.

Under equilibrium conditions the oxygen pressure over the reference electrode was controlled by the reaction



In order to keep the oxygen partial pressure at the reference electrode unaffected by the surrounding atmosphere, the reference electrode was sealed. A good seal here was more important than the one used in the air reference electrode. Zirconia cement was used first and was found to crack under working conditions. Ceramacoat 512, a high temperature ceramic adhesive was tried later and behaved reasonably. The best choice, however, was found to be Sauereisen from the Sauereisen Cement Company.



(a) Probe with quartz tube

(b) Probe with mullite tube

Fig. 11 Design of solid metal-metal oxide reference probes.



Plate 2 Photograph of a typical solid reference probe

In all cases, wet plaster-like cement was applied onto the area to be sealed and left alone to dry in air for at least 24 hr.. Subsequently the sealed probe was put into a drying-oven to further drive off moisture from the cement. Finally, a smooth, dry and apparently crack-free seal was obtained. The maximum continuous operating temperature for Ceramacoat 512 was specified to be 2500°F. Both cements were mainly composed of SiO_2 and binders.

The metal-metal oxide mixture was always made rich in metal powder, usually a ratio of 3 to 1 for the metal to its oxide. Therefore, even if the cement sealing was not perfect and some air leaked into the reference electrode compartment, the extra oxygen introduced by the air would be buffered by the excess metal present in the mixture. In this way slight leaks, if any ever occurred, would not disturb the equilibrium oxygen pressure in the reference electrode compartment. Metal-metal oxide mixtures were analyzed after use to see if metal was consumed by oxygen which had leaked into the reference electrode compartment. The analysis indicated that metal powder was still present in all mixtures after they were used.

The solid reference electrode probe worked basically on the same principles as the air reference electrode probe. However, there are differences. First, solid reference electrode probes did not need the gas outlet and inlet. This would make the probe simpler, hence easier to handle and implement in plant applications. Secondly, the oxygen

partial pressure at the reference electrode was much lower than the oxygen partial pressure in air. In the case of the Ni-NiO mixture, the oxygen pressure over the reference electrode was very close to the oxygen pressure in equilibrium with dissolved oxygen in steel. Therefore the oxygen concentration gradient across the electrolyte rod was much smaller for the solid reference probe than for the air reference probe. This helped reduce possible electrode polarization problems due to electronic conduction in the $ZrO_2(+CaO)$ electrolyte. As was discussed in Section E of the theoretical part, this presents a significant advantage under very low oxygen pressure conditions. However, care had to be taken to ensure the solid reference electrode probe was sealed well. This ensured stable and enduring performance.

C. Measuring equipment

The probe voltage was measured by a Keithley high input impedance electrometer with an accuracy of ± 1 mV. The probe voltage could be printed out at an interval from every two seconds to every hour. Sometimes a chart recorder was also used to follow cell voltage. The input for the chart recorder came from the output of an operational amplifier inside the electrometer. In this way the chart recorder, which had a smaller input impedance, could follow the probe voltage without drawing any current from the cell. Hence this prevented cell equilibrium from being disturbed.

The reference electrode and working electrode temperatures were measured by a Fluke digital thermometer with an accuracy of $\pm 1^\circ\text{C}$. The temperature readings were taken manually once every minute.

D. Steel deoxidation and reoxidation

After the original steel charge was melted down the oxygen level in steel was often too high. In order to measure lower oxygen levels, deoxidation had to be carried out. The usual deoxidants were ferro-manganese, ferro-silicon, and calcium-silicon, which were all supplied by Stelco. In some cases, pure aluminum was added to help lower oxygen levels even further.

Deoxidation was also necessary because every time the charge in the furnace was melted some reoxidation of steel occurred. After it was melted, the steel needed to be deoxidized to bring the oxygen level down to acceptable values. Otherwise the oxygen level in the steel would increase cumulatively since the steel in the furnace would be used up to 5 times before it was replaced by a new charge.

It was observed that a combination of the above mentioned deoxidants gave better results in terms of deoxidation than the addition of a single one. Rare earth, titanium and boron deoxidants were also experimented with but were found not to be overly effective, so they were not used regularly in the present study.

To achieve very low oxygen levels in steel, down to a few ppm, it was found that a considerable amount of aluminum had to be added. Sometimes the amount was several times what should have been necessary according to values calculated from thermodynamic equilibrium data.

Increasing the oxygen level in steel was usually much easier. Pieces of 99.9% pure Fe_2O_3 from Cerac Incorporated were added into the molten steel. The Fe_2O_3 pieces were 13 to 3 mm chunks. A typical chemical analysis was the following: Al 0.007%, Ca 0.001%, Cu < 0.001%, Mg 0.001%, Mn 0.08%, Si 0.005%. It usually took a few minutes for the oxygen level in the steel to increase after lumps of Fe_2O_3 were added.

E. Oxygen measurement in cryolite

For oxygen measurements in a cryolite-alumina melt, the entire experimental set-up was basically the same as that used for molten steel with one notable exception, i.e., the induction furnace was replaced by a Lindberg Hevi-Duty pot furnace. The pot furnace had a power of 20 kw and its temperature could be controlled within $\pm 5^\circ\text{C}$.

The probe used for oxygen measurements in $\text{Na}_3\text{AlF}_6\text{-Al}_2\text{O}_3$ melts was the same as the air reference electrode oxygen probe used for molten steel. Metal-metal oxide reference electrode probes were used as well. They were Ni-NiO and Cr-Cr₂O₃ reference probes.

Cryolite melts with Al_2O_3 , added were contained in a graphite crucible. Graphite crucibles had to be used here because molten cryolite is so corrosive that any ordinary refractory oxide crucible is unsatisfactory. However, graphite crucibles had their own disadvantages. At the operating temperature (1030°C), graphite was gradually oxidized by oxygen in the air. After a few runs, the graphite crucible slowly burned away. Nevertheless, graphite was the only material found suitable.

The Na_3AlF_6 - Al_2O_3 melt composition varied from 0 to 20% Al_2O_3 . The pure cryolite and alumina (anhydrous) were from Fisher. Typical impurity analysis of cryolite was: chloride 0.001%, iron 0.001%, loss on ignition, heavy metals 0.0004%, sulfate 0.014%, silicate 0.01%, alkalies and alkaline earths 0.28%, water soluble substances 0.06%.

To compensate the loss of aluminum fluoride due to the evaporation, pure aluminum fluoride was added to make the mole ratio in cryolite for AlF_3 : NaF from 1:3 to 1:2.6. The concentration of alumina was varied in the run by adding aluminum oxide powder into the cryolite melt.

It took an hour and a half to heat up the Lindberg pot furnace. After it reached the preset operating temperature, the graphite crucible with a weighed mixture of Na_3AlF_6 - Al_2O_3 was put into the furnace. It took another 20 to 30 minutes to melt the mixture. During the test, the furnace temperature was automatically maintained by the temperature controller inside the furnace. Argon gas was

flushed over the melt and crucible to extend the life of the graphite crucible and to help maintain an inert atmosphere over the melt.

The oxygen probe and a piece of Pt wire attached on to the other end of the electrolyte rod were immersed into the $\text{Na}_3\text{AlF}_6\text{-Al}_2\text{O}_3$ melt to complete the circuit for cell voltage measurements. This is illustrated by Fig. 12. The platinum wire serves as the working electrode. One of the thermocouple wires served as the lead for the air reference electrode. The probe voltage is measured between those two leads by an electrometer and followed by a chart recorder similar to oxygen measurements in molten steel. The temperatures at the probe electrodes were measured by thermometers and recorded manually.

F. Sampling and sample analysis

Steel samples

When oxygen in molten steel was being measured by an oxygen probe, pin samples of steel were regularly taken for analyses of alloying elements and oxygen content. Steel samples were taken with a sampling gun which is shown in Plate 3. An ordinary Pyrex tube with an 8 mm OD and 3 mm ID was inserted into the barrel of the sampling gun. When the trigger was pulled molten steel was drawn up into the glass tube. After the sample cooled down, the Pyrex tube was broken and a piece of the pin steel sample was ready for

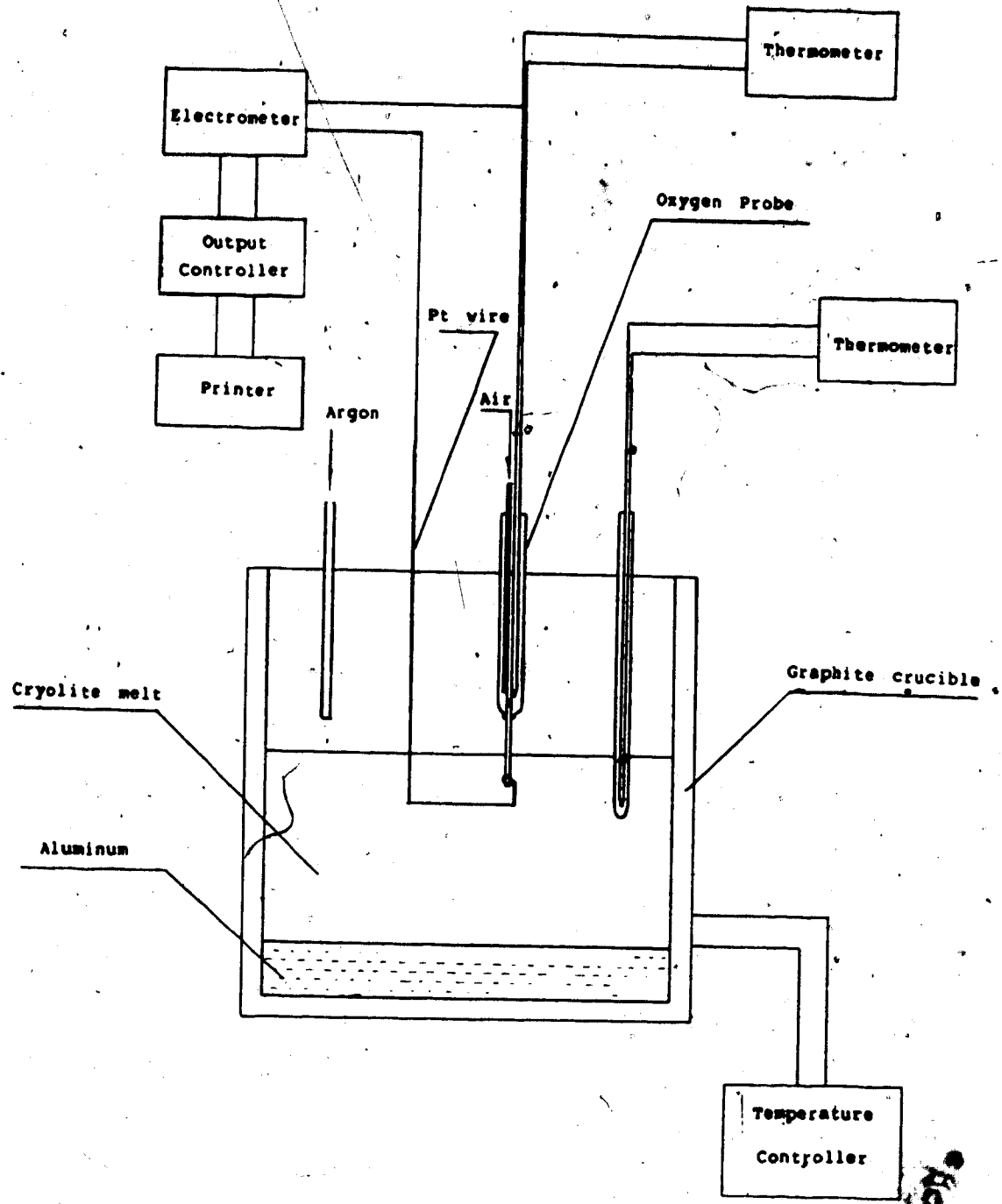


Fig. 12 Experimental set-up for tests on the $\text{Na}_3\text{AlF}_6\text{-Al}_2\text{O}_3$ system

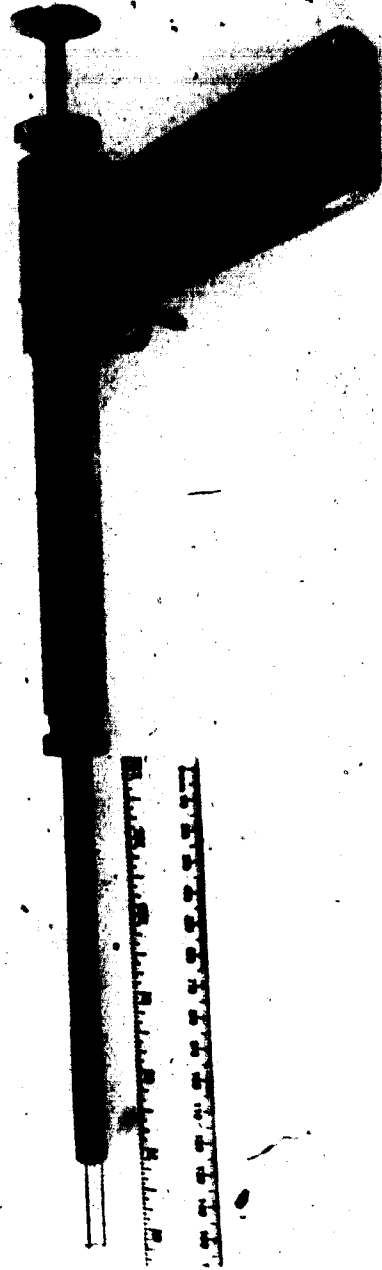


Plate 3 Sampling gun used for taking steel samples

analysis.

Later in this study another sampling technique was tried. Plate 4 shows the simple device used. An evacuated glass tube with a thin-walled tip was put into a hole at the end of a stick. The glass tube was held in position by a small screw. With the sampling glass tube in position, the tip of the tube was immersed into the molten steel. Upon immersion, the thin walled tip of the vacuum tube melted immediately. Steel then was drawn into the tube which had to be pulled out of the steel bath quickly before it completely melted. Finally the glass tube was broken to obtain a steel sample the same size as with the sampling gun.

Sampling was done regularly when the oxygen probe was immersed in a steel melt. It was also done before and after any deoxidants were added. Probe voltages corresponding to each sample were recorded. Later these samples were sent to Stelco's research lab in Hamilton for oxygen content analysis by the inert gas fusion technique. Alloying element analysis was done in our lab by atomic absorption.

From the probe voltage the oxygen content in steel was calculated according to the formulae derived in the theoretical part of this thesis. Some studies have claimed that if the oxygen content was not too high or too low the probe measurement should agree with the inert gas fusion analysis. Other researchers have stated that the inert gas fusion method should always give a higher oxygen content

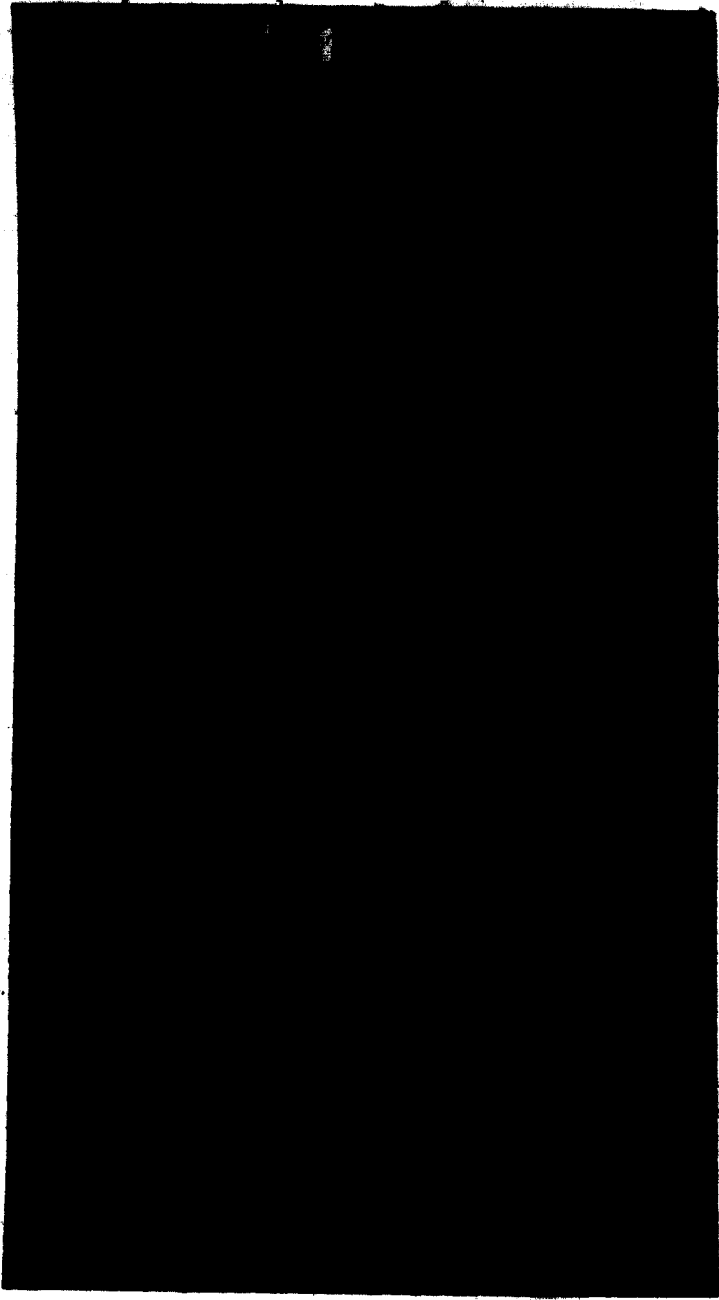


Plate 4 Devices used for taking steel samples

than the electrochemical measurement.

In the inert gas fusion method, steel samples first were pickled by dilute acid. Only the middle section of a pin sample was used. After these preliminary treatments, the samples were heated to a very high temperature so that oxides or dissolved elemental oxygen in the sample were reduced by carbon. From the amount of carbon dioxide evolved total oxygen content in the steel can be determined.

Samples for alloying element analysis were first dissolved in aqua regia. This solution was diluted to a suitable concentration for atomic absorption analysis. Typical elements analyzed were Al, Si, Cr, Mn, Mo and Ti.

Accuracy of the method was 2-3%.

It is particularly important to mention that only acid soluble aluminum is determined by this method. Since Al_2O_3 does not dissolve in aqua regia. From thermodynamic data we know aluminum is probably the strongest deoxidant used in the steel industry. It is the amount of elemental aluminum rather than the total aluminum that is controlling the oxygen levels in steel. Aluminum already tied up as Al_2O_3 will certainly not help in reducing oxygen levels in steel.

It was also desirable to analyze other alloying elements in steel because all of them influence the oxygen activity coefficient.

$\text{Na}_3\text{AlF}_6\text{-Al}_2\text{O}_3$ samples

There are a number of methods, such as conventional wet chemical analysis,⁽⁵⁵⁾ high temperature vacuum evaporation or reduction, microscopy, X-ray diffraction⁽⁵⁶⁾ and chronopotentiometry^(35,36) for determining alumina concentrations in $\text{Na}_3\text{AlF}_6\text{-Al}_2\text{O}_3$ mixtures. Among these the conventional wet chemistry method is probably the most straightforward and therefore the most widely used. The fluoride phase in $\text{Na}_3\text{AlF}_6\text{-Al}_2\text{O}_3$ mixtures is extracted by a suitable solvent and the alumina residue is determined gravimetrically.

The procedure for the analysis of Al_2O_3 in $\text{Na}_3\text{AlF}_6\text{-Al}_2\text{O}_3$ was given in the paper by Thonstad⁽⁵⁴⁾. According to his results, the accuracy of the method was very good ($\pm 3\%$) for low Al_2O_3 concentrations (1-3%) and for high Al_2O_3 concentrations (7-12%). The accuracy for intermediate concentrations was about $\pm 10\%$. Because the $\text{Na}_3\text{AlF}_6\text{-Al}_2\text{O}_3$ mixture used in the present study was pre-weighed, analysis of the Al_2O_3 concentration was unnecessary.

IV. Results and Discussion

A. Experimental data processing with a computer program

Computer programs were designed to help with repetitive calculations involving experimental results and serve to improve the reliability of calculations.

The chemical analysis data of the alloying elements were first read into the computer to calculate the oxygen activity coefficient which was used throughout the whole set of experimental data.

The programs were designed so that for every measured cell voltage, E , reference electrode temperature, T_2 , working electrode temperature, T_1 , and a given reference electrode oxygen pressure, P_{O_2} , the oxygen pressure at the working electrode was calculated. After finishing with one group of E , T_1 , T_2 data the program went back for another loop to treat another group of data.

A typical input data file, output data file, and the program itself are listed in the Appendices.

This program has the following advantages. First of all, for each T_2 and T_1 recorded, the Seebeck contribution ($\alpha\Delta T$) is calculated for each measured cell voltage (E), which is recorded at the same time as T_2 and T_1 . Likewise, the thermoelectric contribution E_{lead} caused by using different leads for the electrodes of the oxygen probe is calculated for each different T_2 and T_1 by the program.

Secondly, as P_e is temperature dependent, it changes as the temperature at the working electrode (T_1) changes. Rather than using a fixed P_e , the program changes the P_e according to its temperature function.

Thirdly, the free energy change of dissolution of oxygen into molten steel also changes as the steel temperature changes. The program uses changing $\Delta G_{(o)}$ according to its temperature dependence and the steel temperature.

Finally, in the case of the solid metal-metal oxide reference electrodes, the oxygen pressure inside the reference electrode compartment changes as the temperature at the reference electrode changes. This is because the oxygen pressure at the reference electrode is controlled by the equilibrium of the metal-metal oxide, which is temperature dependent. The program can change the P_{O_2} , the reference electrode oxygen pressure, according to the reference electrode temperature and the given thermodynamic equilibrium between the metal and metal oxide.

Instead of trying to keep T_1 , T_2 constant, hence keeping $\alpha\Delta T$, P_e , $\Delta G_{(o)}$ and P_{O_2} constant, this program can follow the changes and make consequent adjustments. As a result, large amounts of experimental data can be processed more accurately and conveniently.

The analog electrical signals of the oxygen probe and thermocouples can be converted into digital information. Then the information can be processed by a dynamic program

as described above. Therefore, such a program would be able to provide instantaneous information about the oxygen level in steel for different steelmaking processes.

B. Performance of the air reference oxygen probe

Resistance against chemical attack

During oxygen measurements in steel the tip of the electrolyte rod was immersed in molten steel continuously. Usually a test was run for about an hour or a little longer. At the end of every run, the probe and Mo-ZrO₂ rod were pulled out of the steel. From visual observation afterwards, the ZrO₂(+CaO) rod was not corroded.

This was expected because ZrO₂ is reasonably inert and in its highest oxidation state. The fact the rod is sintered at a very high temperature and has a melting point of about 2680°C also helps explain the good resistance to chemical attack.

Qualitative analysis of a ZrO₂(+CaO) rod after use by X-ray diffraction only showed the presence of monoclinic and tetragonal zirconia.

Energy dispersive X-ray analysis indicated there were other elements present in the electrolyte. They were Si, Al, Ca, Ti, Ni, Fe. The presence of Ca was expected while the other elements found were not surprising since they were listed as impurities.

Quantitative energy dispersive X-ray analysis was also attempted. However, these results did not reflect the absolute amount of each element in the electrolyte. Relatively speaking, quantitative analysis on used rods did not show any increase in impurities compared with quantitative analysis on an unused rod. The results of three analyses are shown in Table 4. where Sample 1 represents the unused electrolyte, Sample 2 is the electrolyte used in steel, and Sample 3 is the electrolyte used in cryolite. The $ZrO_2(+CaO)$ rod appears sufficiently stable in molten steel to withstand possible chemical attack.

A micrograph of a used $ZrO_2(+CaO)$ rod was taken to compare with that of a unused rod (Plate 5 and 6). As can be seen from the photographs some microscopic changes were found.

A Mo- ZrO_2 rod was used as the electrical contact between steel and the probe. It was definitely an electronic conductor as simple test showed the rod had very low resistance at room temperature.

Any other metallic rod would probably dissolve into molten steel and form its own ferro-alloy. But Mo- ZrO_2 was only slightly attacked after being used in steel for extended periods of time. The rod was, to some extent, weakened by molten steel where it was in contact with slag on the surface. Slag forming at the surface of steel was usually more corrosive than the steel itself. From a

Table 4 Quantitative analysis of the rods by EDXA

	Element	Relative K	WT %	Oxide %
Sample 1	Al	0.0330	6.02	11.37
	Si	0.0139	2.11	4.51
	Ca	0.0098	1.36	1.90
	Zr	0.5440	60.86	82.22
Sample 2	Al	0.0345	6.26	11.82
	Si	0.0205	3.13	6.69
	Ca	0.0196	2.69	3.76
	Zr	0.5054	57.47	77.64
Sample 3	Al	0.0363	6.60	12.48
	Si	0.0136	2.10	4.48
	Ca	0.0096	1.32	1.85
	Zr	0.5343	60.10	81.19



Plate 5 Micrograph of an unused $ZrO_2(+CaO)$ rod

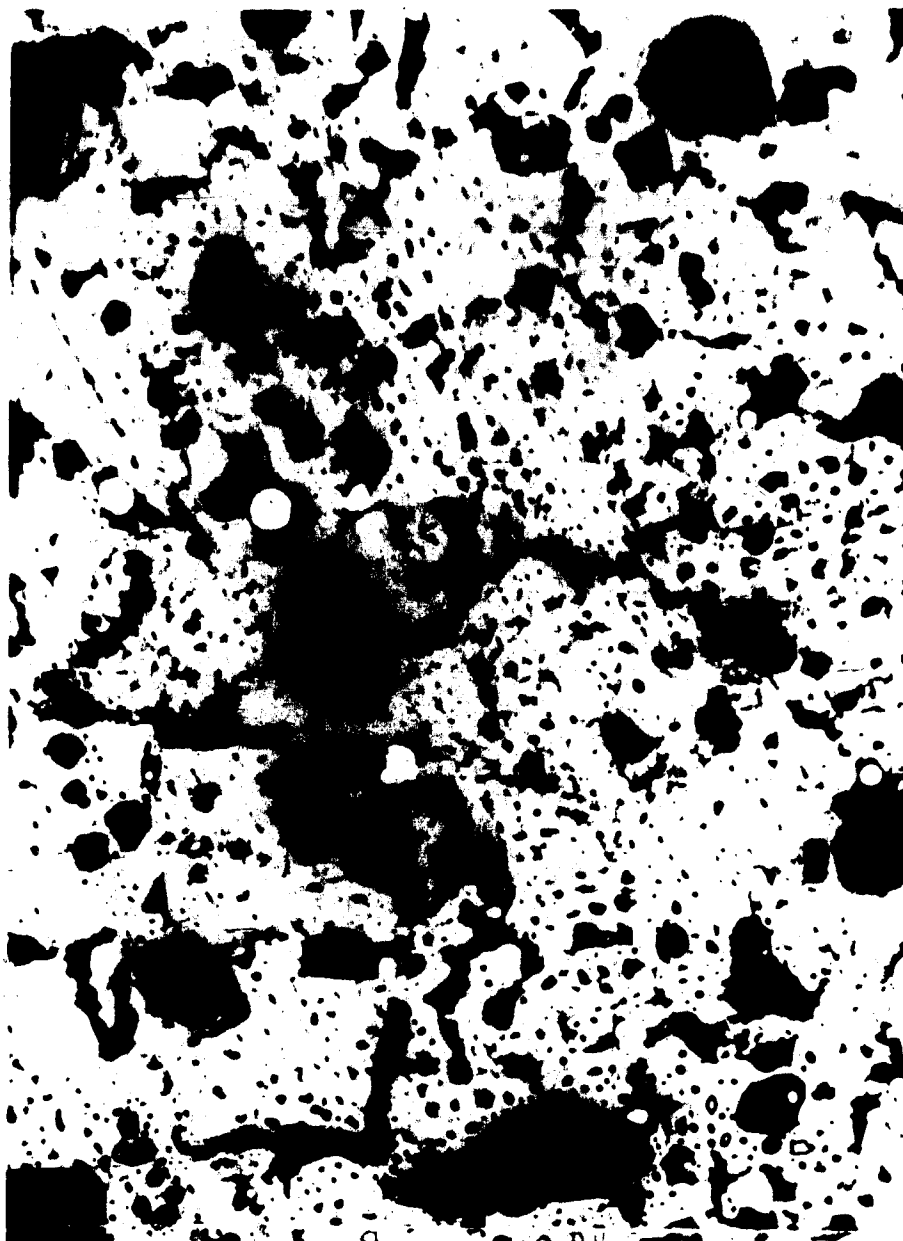


Plate 6 Micrograph of a used $ZrO_2(+CaO)$ rod

comparison between photographs of the used (Plate 1) and unused probe (Plate 2) it can be seen how well it withstood attack.

Overall, the nonisothermal oxygen probe would usually last two or three runs, each of which was about an hour long. The probe then had to be reconstructed because the quartz tube gradually devitrifies after being used at temperatures of 1000°C or above for an extended period of time. The quartz tube accordingly became very brittle and cracked upon any slight mechanical stress. However, the major components of the probe, the $ZrO_2(+CaO)$ and the Mo- ZrO_2 rods, could still be used after the quartz tube was replaced.

Measurement of dissolved oxygen in molten steel

When it was immersed in steel the probe could give a steady EMF output when the oxygen level in steel was relatively stable. Results of several tests at different oxygen levels were plotted as cell voltage vs. time in Fig. 13-19 for 5, to 155 ppm oxygen levels in steel.

The figures provide a clear indication of the stability of the oxygen probe. However, due to the limits of the experimental conditions, longer times meant the steel could be gradually reoxidized by the oxygen in the air. As a result, the oxygen level in the steel went up and the probe voltage drifted down correspondingly. In those cases, a drifting probe voltage did not necessarily indicate that the

Fig. 13 Cell voltage vs. time at 5 ppm [O]

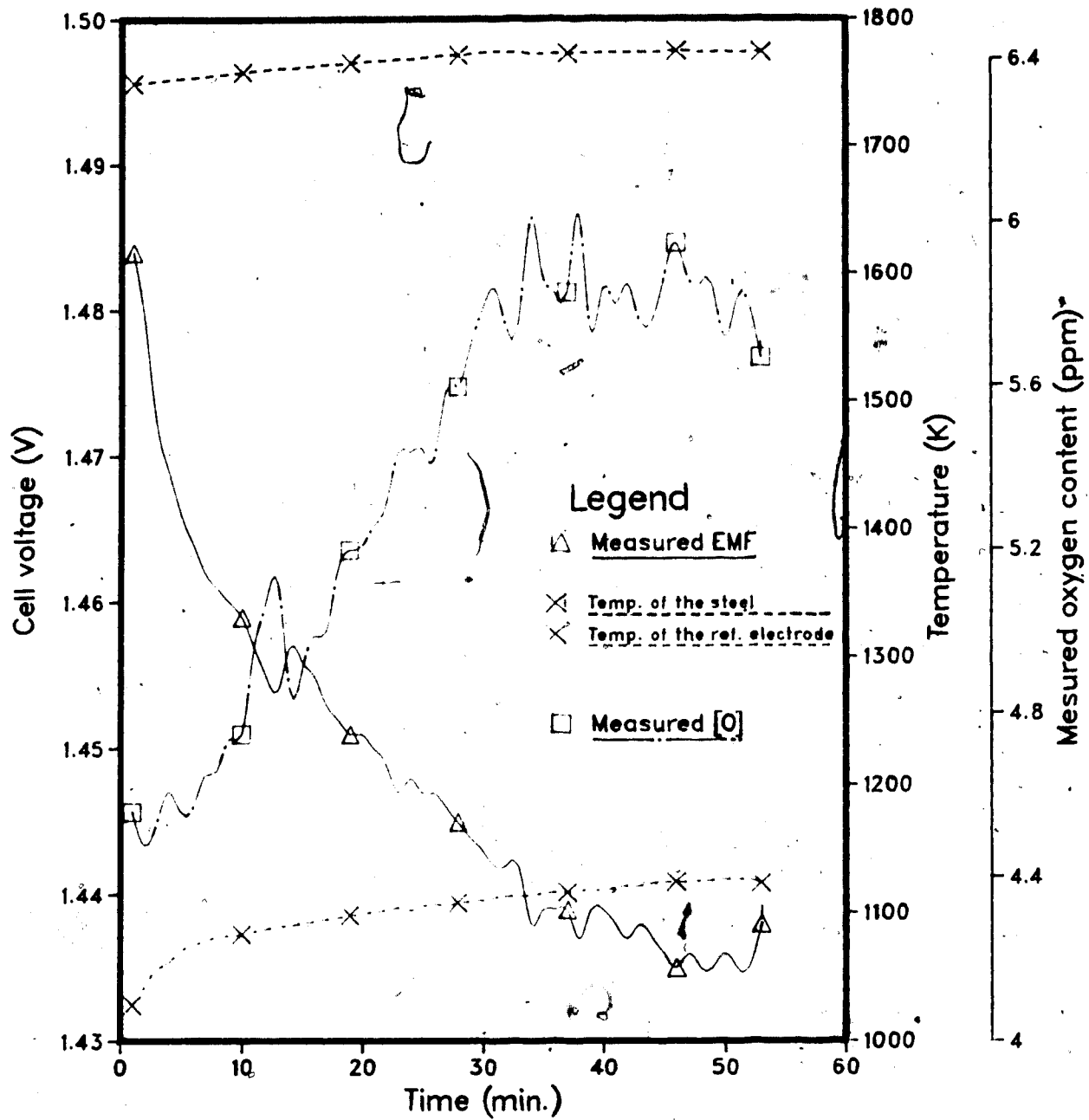


Fig. 14 Cell voltage vs. time at 7 ppm [O]

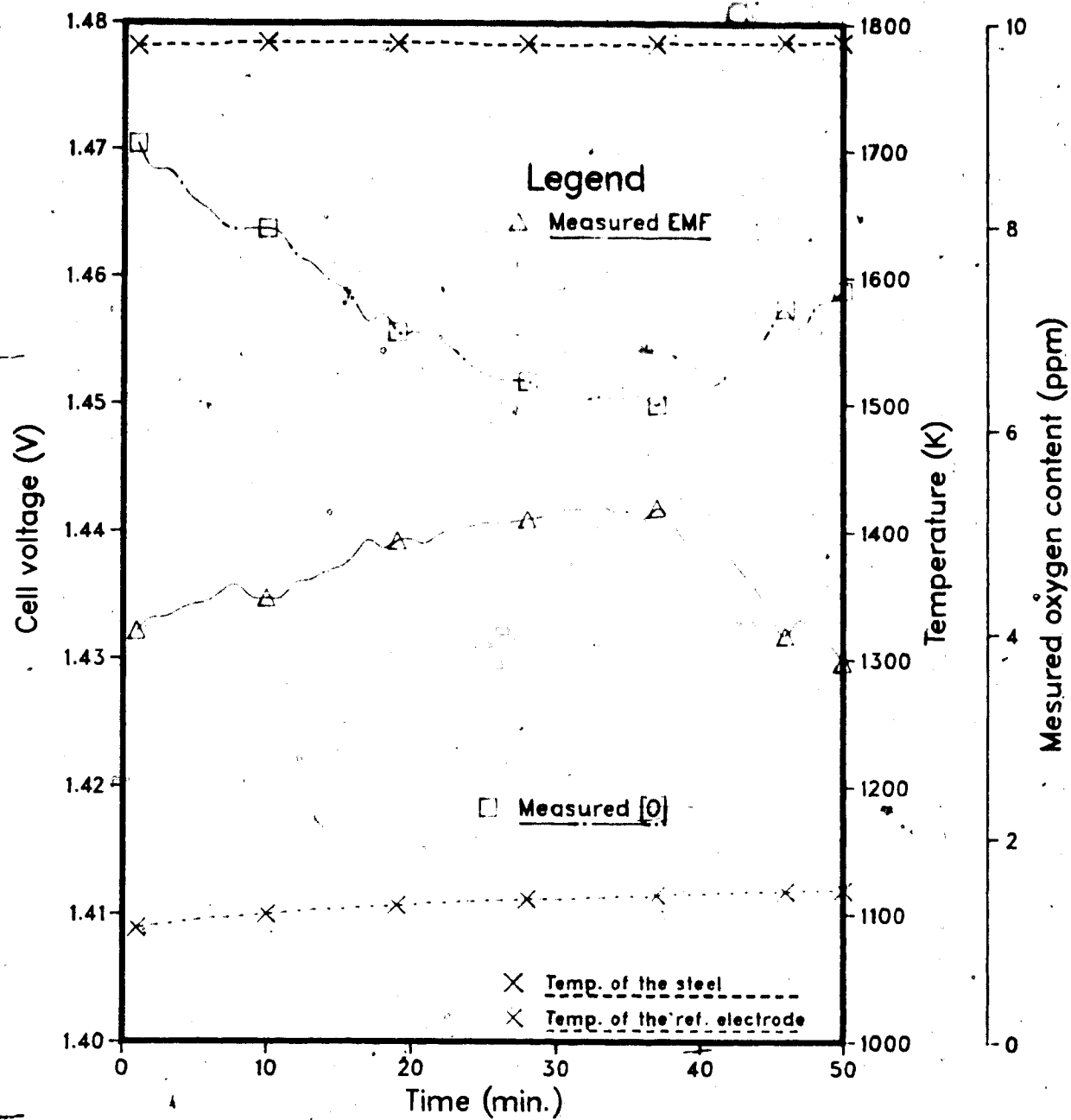


Fig. 15 Cell voltage vs. time at 15 ppm [O]

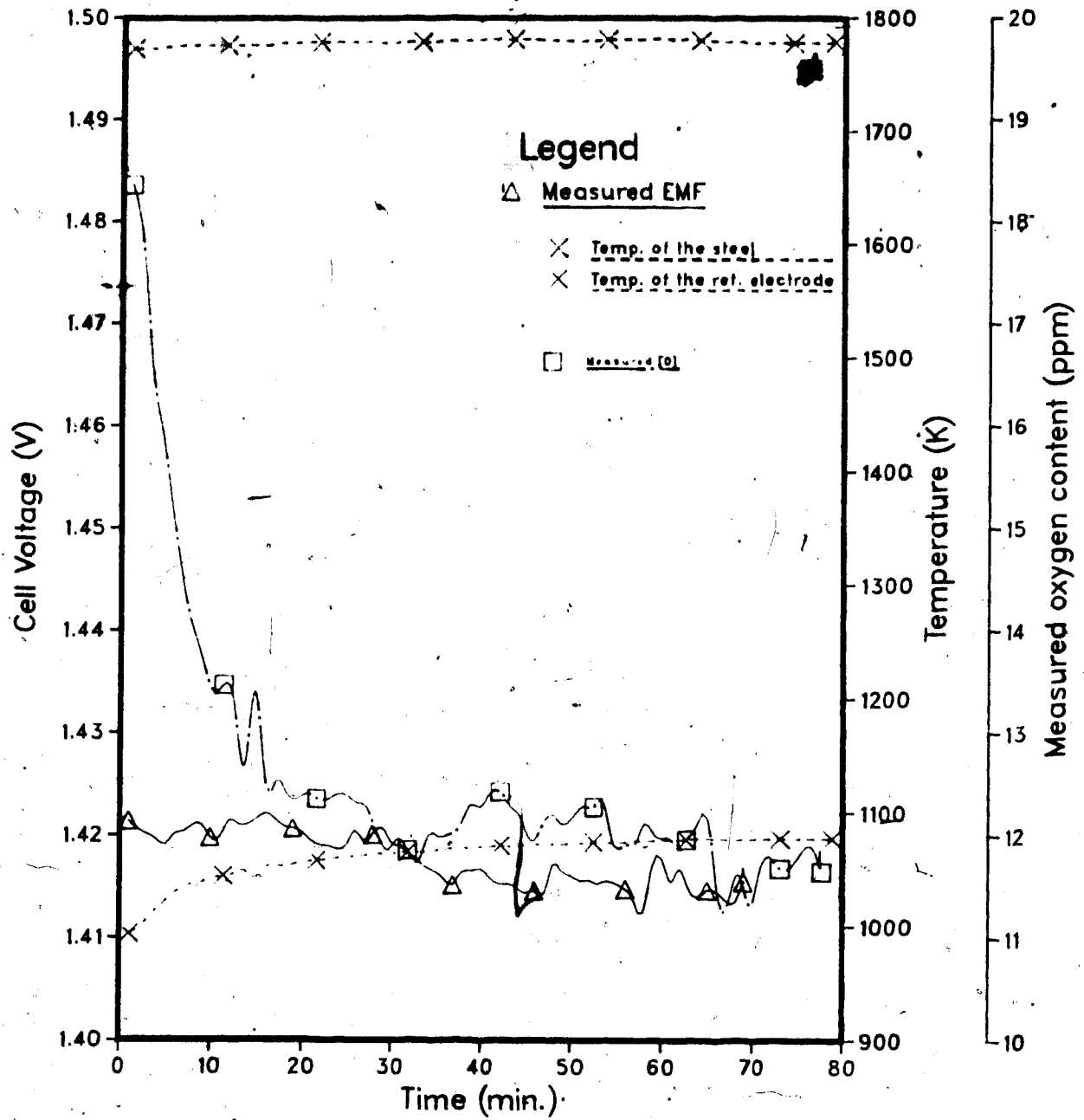


Fig. 16 Cell voltage vs. time at 30 ppm [O]

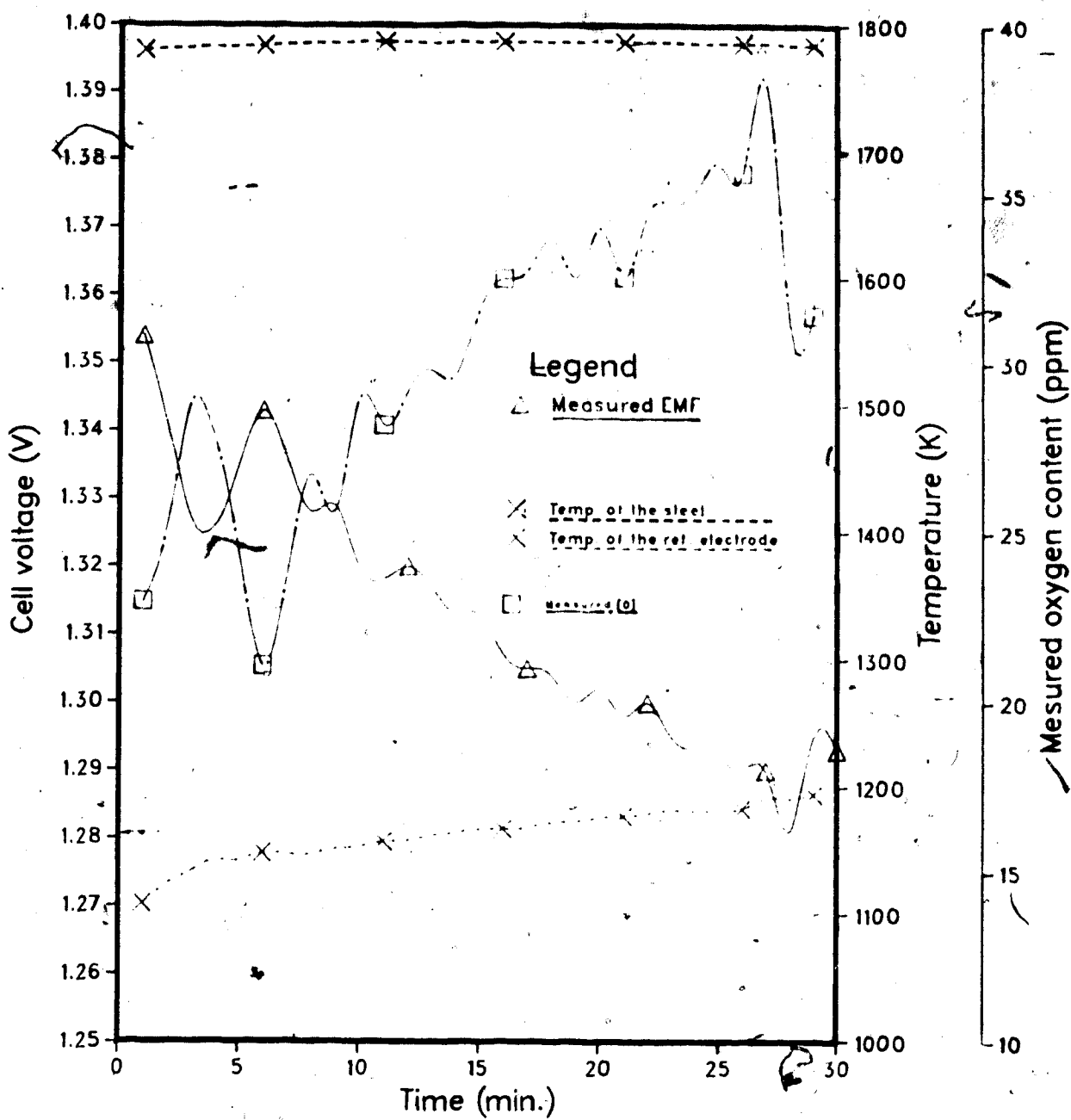


Fig. 17 Cell voltage vs. time at 55 ppm [O]

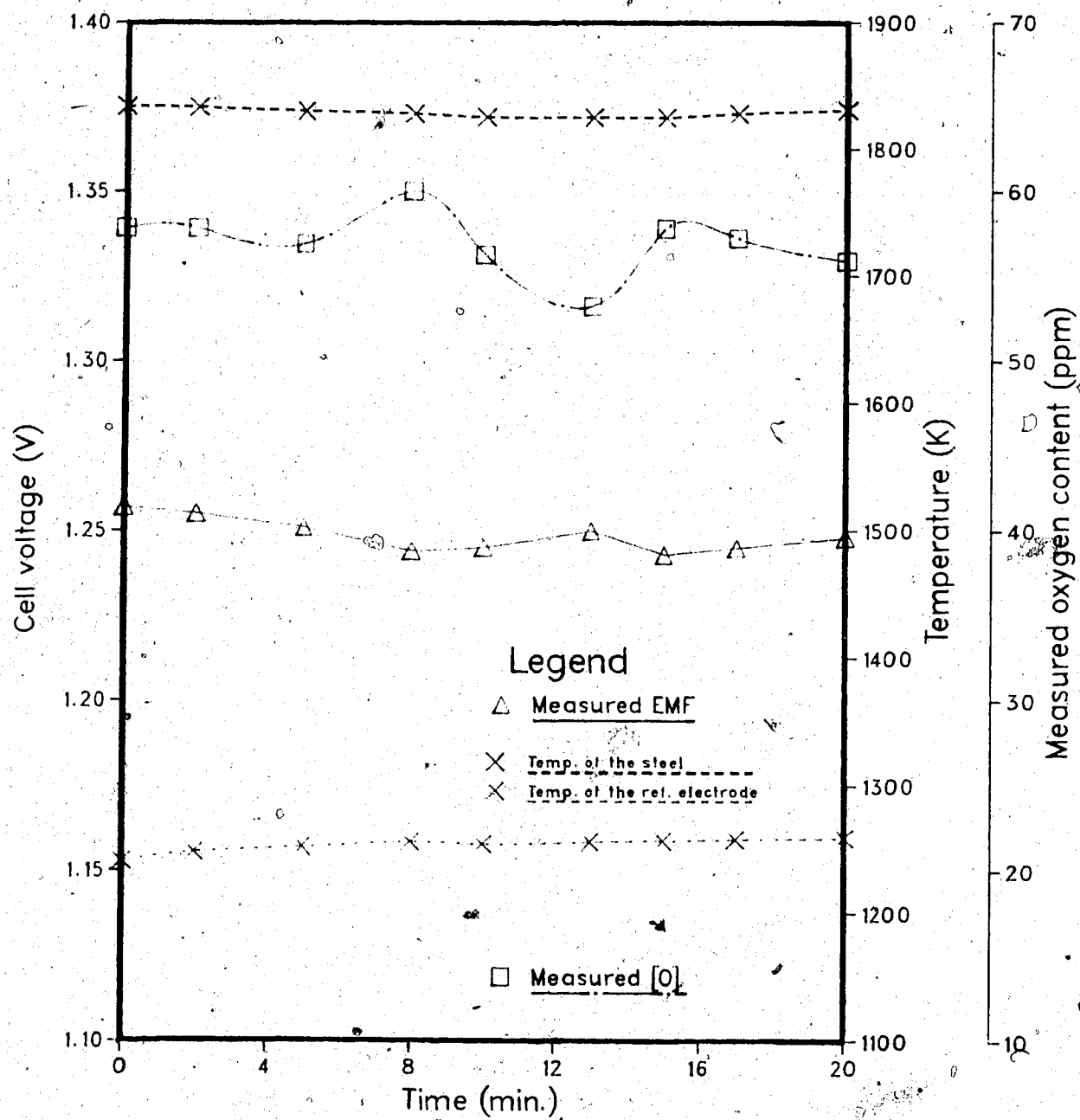


Fig. 18 Cell voltage vs. time at 100 ppm [O]

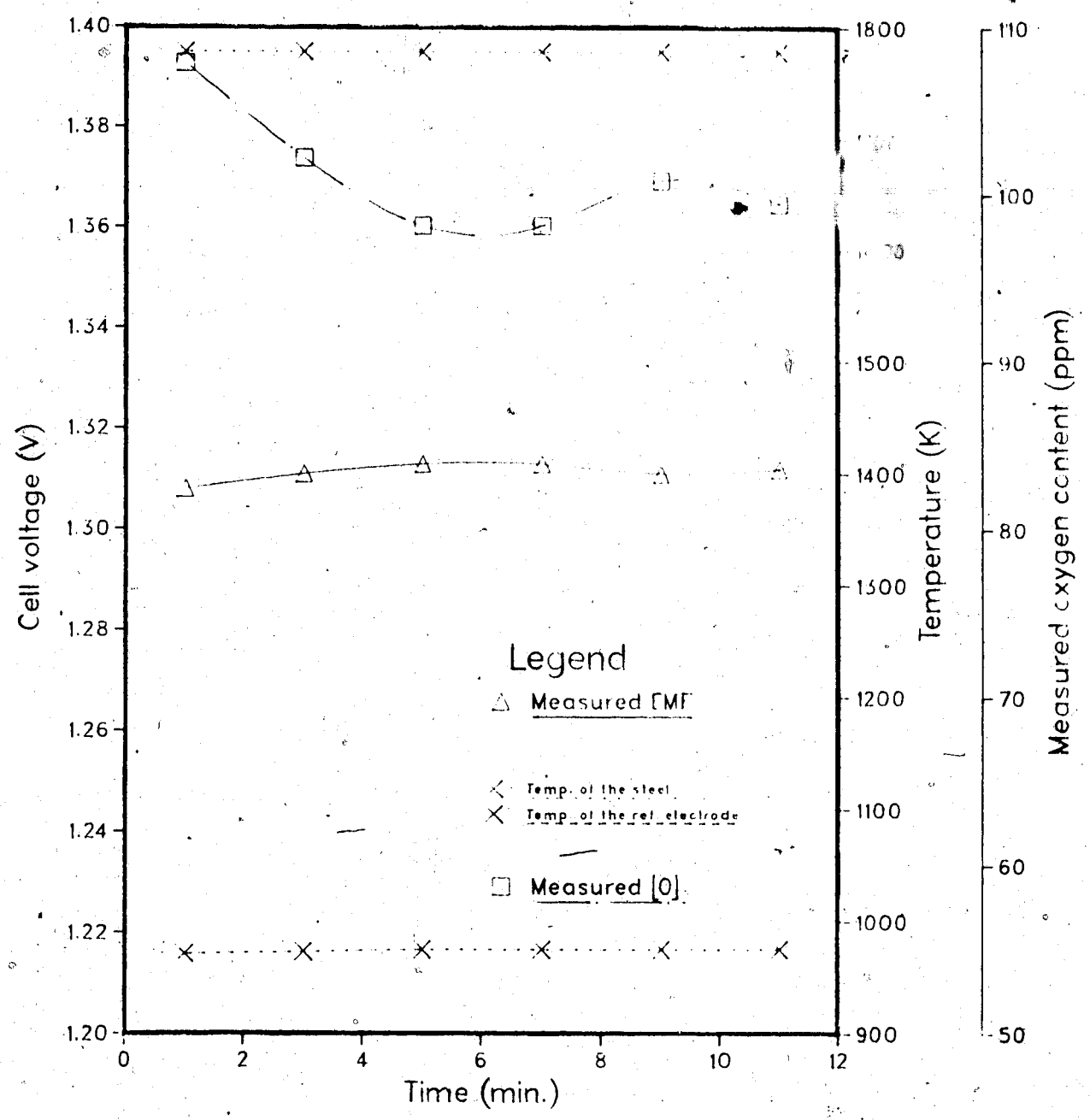
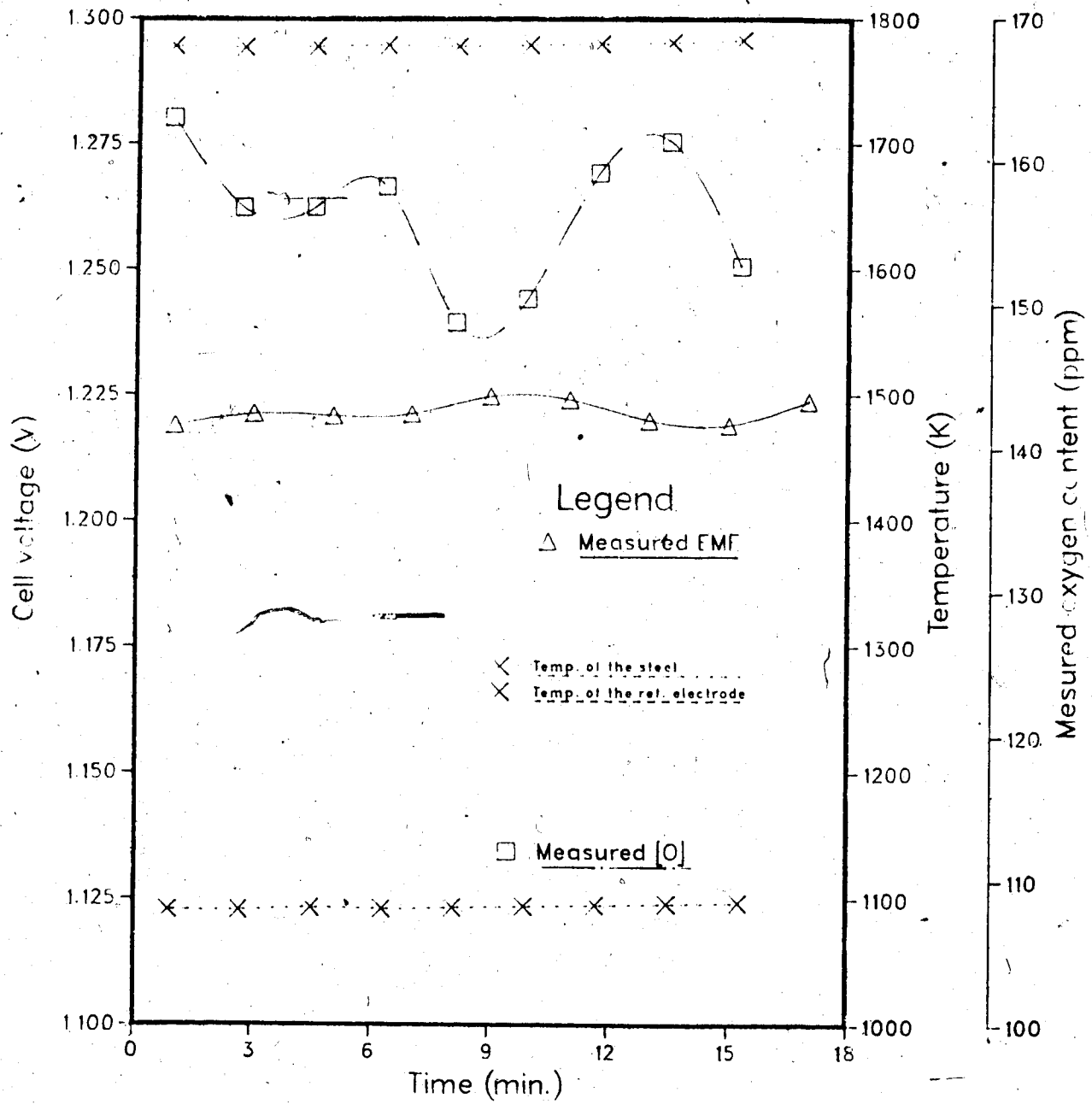


Fig. 19 Cell voltage vs. time at 155 ppm [O]



probe was deteriorating.

Aluminum-killed steel has been found to contain total oxygen contents of 0.003-0.0120%.⁽⁵⁷⁾ The activity values of dissolved oxygen in such steel can, however, be estimated at below 0.001%. This is because, after deoxidation treatment, an appreciable amount of oxides are left suspended in the steel. Oxygen in those suspended oxides will be included in the total oxygen content by conventional inert gas fusion analysis, whereas oxygen activity measured by electrochemical methods does not include the content of chemically combined oxygen.

Our experimental results confirmed the above discussion: oxygen contents in steel determined by inert gas fusion analyses showed consistently higher oxygen values than those determined by the oxygen probe. This can be seen from Fig. 20.

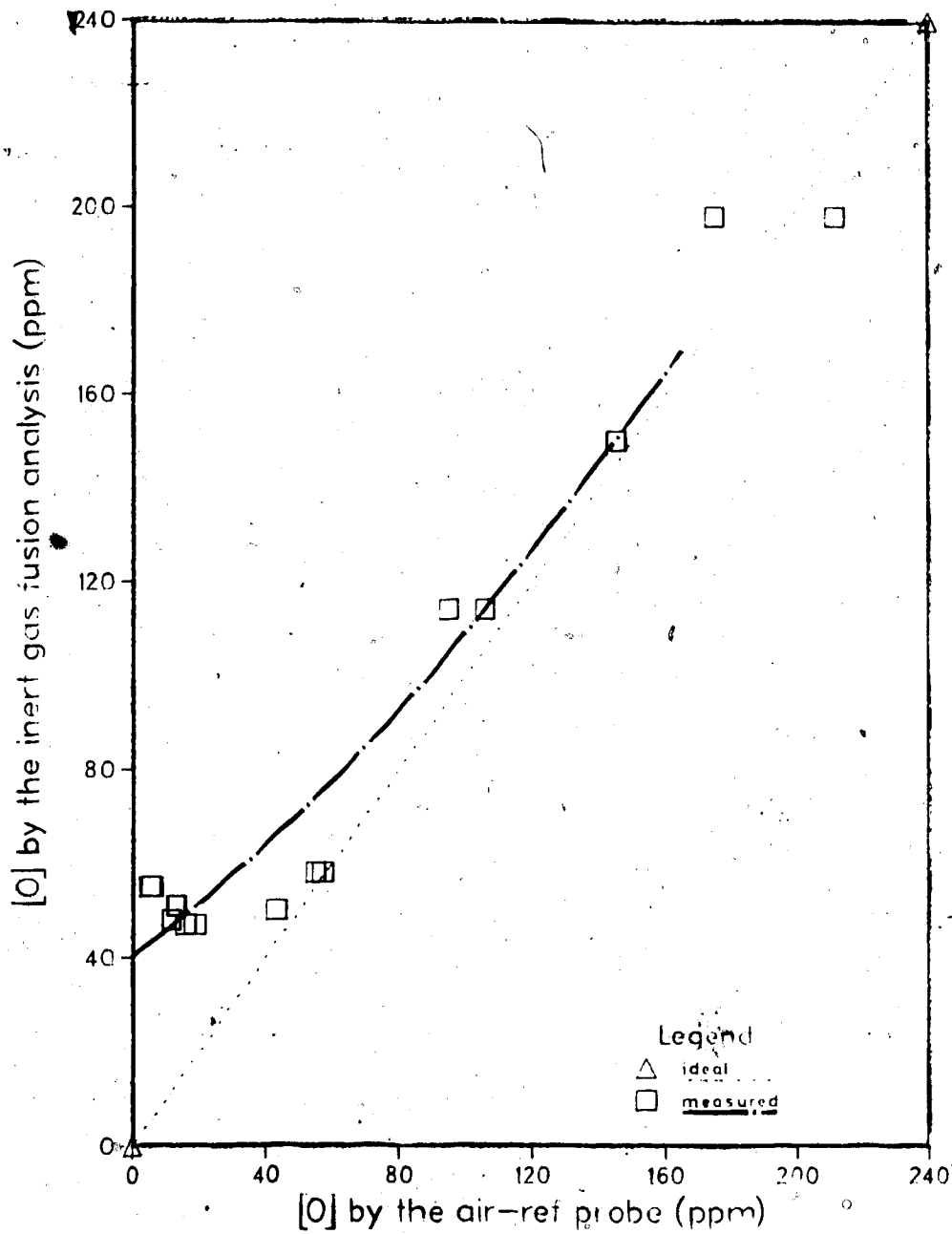
In the present study strongly deoxidized steel was studied. Oxygen levels of 1-5 ppm in molten steel were measured with the air reference electrode oxygen probe. Results of a run on a very low oxygen level are listed in Table 5, where E is EMF measured by the probe, TH, TC are temperatures of molten steel and the reference electrode, respectively, and O is the oxygen content calculated from the EMF measured.

The steel used in the present study was reused for up to 5 heats before new steel replaced the old charge. Each time the steel was melted down, it was reoxidized to some

Table 5 Results of a run on very low oxygen level

E (V)	TH (K)	TC (K)	O (ppm)
1.4510	1784	1276	1.47
1.4450	1783	1282	1.54
1.4240	1782	1284	2.16
1.4250	1784	1283	2.18
1.4350	1784	1287	1.78
1.4280	1784	1292	1.92
1.4210	1785	1293	2.17
1.4200	1785	1294	2.19

Fig. 20 [O] determined by the air-ref. probe vs. that by the inert gas fusion analysis.



extent. Later, during the run, the steel was usually deoxidized with Al or other deoxidants. Not all of the products of deoxidation, i.e., the various oxides formed, go into the slag. Some of those oxides remained suspended in the molten steel, especially the finer oxide particles such as Al_2O_3 which have a high melting point. These oxide inclusions accumulated in the steel before re-charging. Therefore, inert gas fusion analysis would inevitably give higher oxygen contents than those by electrochemical measurement.

In conclusion, care should be taken in interpreting oxygen analysis results from inert gas fusion analyses, especially where the amount of various oxides that could be present in the steel samples is unknown. While special techniques may have to be developed to separate oxides from steel to make inert gas fusion analysis more meaningful, dissolved oxygen activity is determined by electrochemical oxygen probes.

If near-equilibrium conditions can be established in liquid Al-killed steel, the dissolved oxygen content can be determined from the amount of the dissolved aluminum through established thermodynamics of the reaction:



Plant practice has indicated that this state of equilibrium can be approached by gas purging of liquid steel in the

casting ladle. This equilibrium was investigated by Janke⁽⁵⁸⁾ using a $ZrO_2(+CaO)$ tubular oxygen sensor. The temperature function of the reaction constant $K(Al_2O_3)$ was obtained as:

$$\log K(Al_2O_3) = \frac{62680}{T} - 20.54 \quad (\text{Eq. 116})$$

in the temperature range 1550°C to 1650°C. If the interaction coefficient e_{Al}^{Al} is neglected, the following relationship is expected:

$$\log a_{[O]} = -\frac{2}{3} \log [\%Al] - \frac{1}{3} \log K(Al_2O_3) \quad (\text{Eq. 117})$$

Janke's results confirmed data determined earlier for the Al-O reaction equilibrium in pure iron melts. Results of $K(Al_2O_3)$ in steel are listed in Table 6 for comparison⁽⁵⁸⁾.

To check the oxygen content determined by the oxygen probe used in the present study, steel samples were subjected to acid-soluble aluminum analysis. Corresponding oxygen contents were calculated by assuming the relationship in Eq. 117. Oxygen content determined by the oxygen probe is plotted versus the oxygen level predicted from Eq. 117 in Fig. 21.

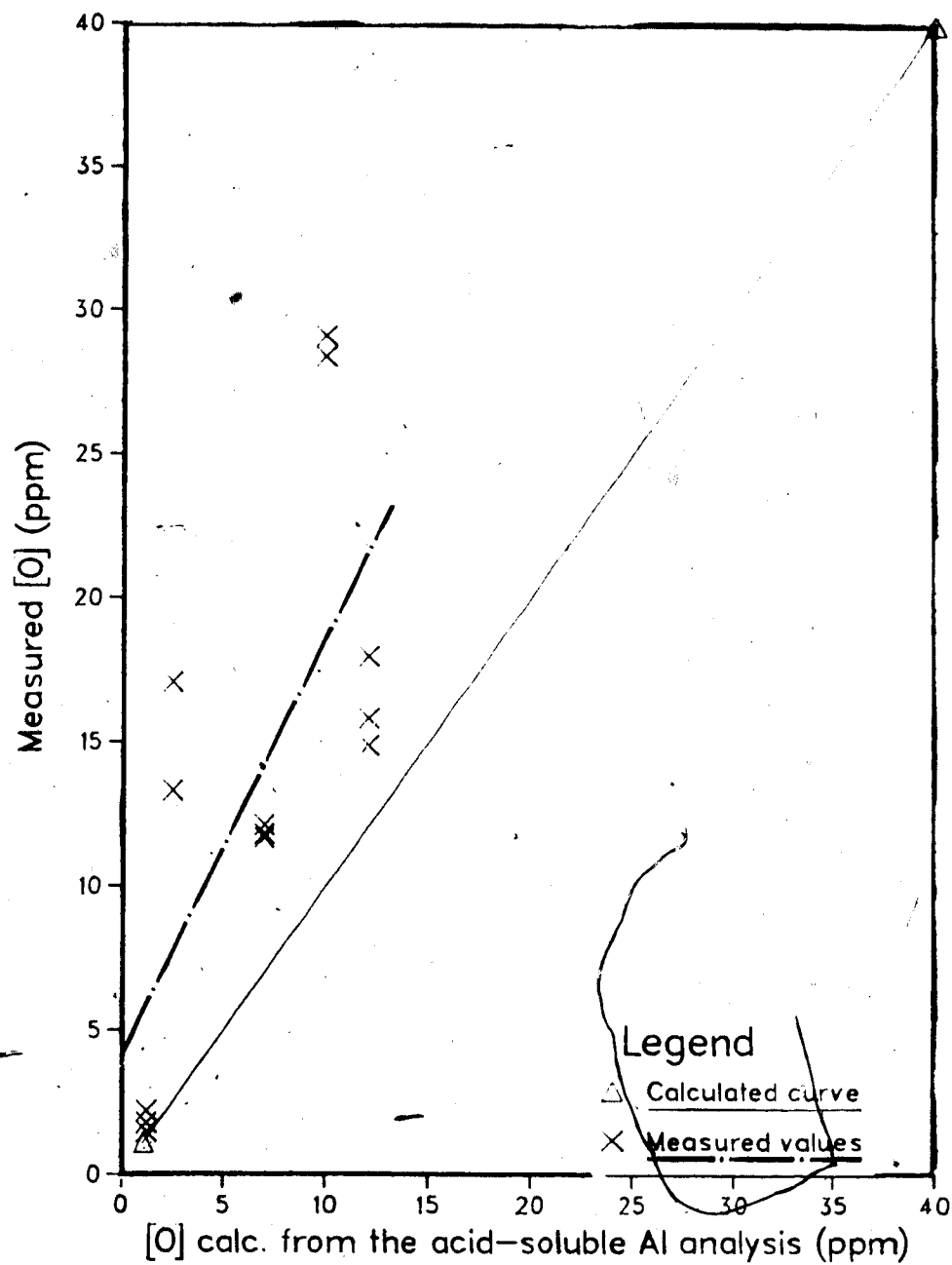
Probe response to varying oxygen content

The oxygen content in steel was increased by adding pieces of Fe_2O_3 . The oxygen probe responded to the increase

Table 6 $K(\text{Al}_2\text{O}_3)$ by various researchers

$\log K(\text{Al}_2\text{O}_3)$	% Al	Method	Author(s)
64000/T-20.48	<0.1	H ₂ O-H ₂ Equilibrium	Gokoen, Chipman 1953
60300/T-18.6	<1	H ₂ O-H ₂ Equilibrium	McClean, Bell 1956
64290/T-20.56	-	Calculated	Buzek, Hutla 1969
62780/T-20.17	-	Calculated	Fruehan 1970
64000/T-20.57	<3	Metal-slag Equilibrium	Rohde et al. 1971
62680/T-20.54	<2	EMF/ThO ₂ (Y ₂ O ₃) Electrolyte	Jacquemot et al. 1973
	<1.3	EMF/ThO ₂ (Y ₂ O ₃) Electrolyte	Janke, Fischer 1976

Fig. 21 [O] level determined by the oxygen probe vs. that calculated from the acid-soluble Al analysis



rapidly. This response was recorded clearly on the chart recorder. As can be seen from Fig. 22 which is a photocopy of the chart paper, the probe voltage dropped after a couple of minutes as oxygen level in steel was increased by the addition of the pieces of Fe_2O_3 . Alternatively, the oxygen level was lowered by adding deoxidants and this change was not recorded.

When Fe_2O_3 was added into molten steel, the oxygen probe was left in the steel melt. From the chart recorder output we can see the transition period between low and raised oxygen levels. In contrast, the oxygen probe was pulled out of the steel to make deoxidation additions since deoxidation was usually vigorous, and since the products of deoxidation, i.e., slags, had to be removed before the probe was again immersed.

In actual plant applications, the probe could be positioned at some slag-free area, such as at the wall of a tundish, where it would not have to be pulled out to make deoxidation additions.

C. Performance of solid metal-metal oxide reference oxygen probes

A quartz tube was first tried for constructing the metal-metal oxide reference electrode oxygen probe. The reference electrode compartment was sealed with Ceramacoat 512 or Sauereisen cement. When this probe was used for

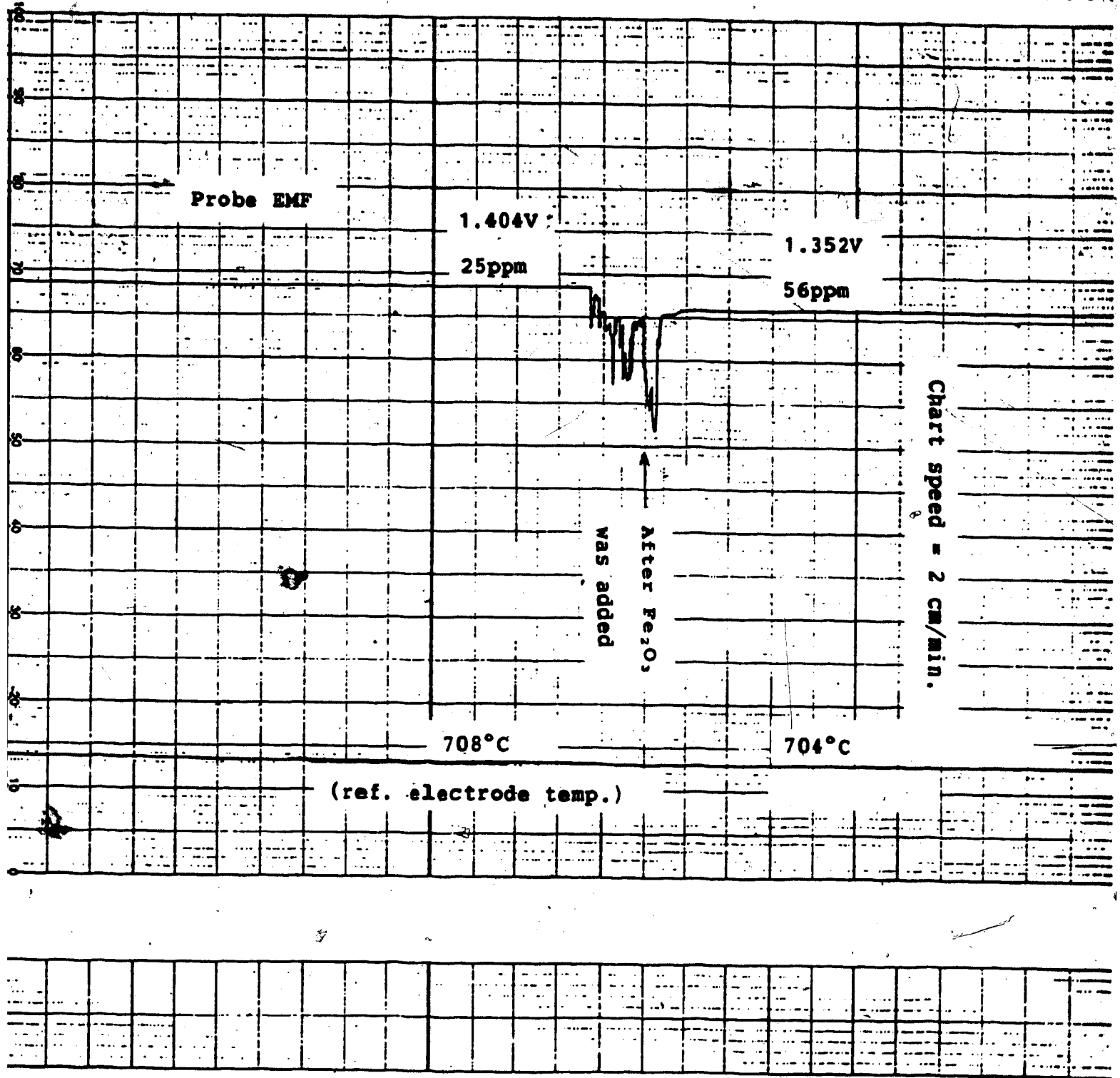


Fig. 22 The probe response to varying oxygen content

oxygen measurement in the induction furnace, it was found that the cement sealing or quartz tube cracked because the thermal expansion coefficient for $ZrO_2(+CaO)$ did not match that of the quartz tube. Therefore a mullite tube was used instead to construct the probe. The cracking problem did not occur anymore because the thermal expansion coefficient of mullite is reasonably close to that of the electrolyte.

Discovering the proper materials for constructing the probe represented a major breakthrough in this study. The tests using a metal-metal oxide reference electrode oxygen probe were basically the same as with the air reference probe.

The solid reference probe, as a whole, was simpler and easier to handle because it was not necessary to keep a gas flowing into and out of the probe. The lifetime of the solid reference probe was actually longer than the air reference probe because mullite had no devitrification problem.

Measurement of dissolved oxygen in steel

1. Ni-NiO reference oxygen probe

The oxygen results obtained by a Ni-NiO reference probe were compared with oxygen levels determined by acid-soluble aluminum analysis. Oxygen content values by the solid reference probe agreed reasonably well with values from acid-soluble aluminum analysis. This is shown in Fig. 23.

Fig. 23 [O] level determined by the Ni-NiO ref. probe vs. that calculated from the acid-soluble Al analysis

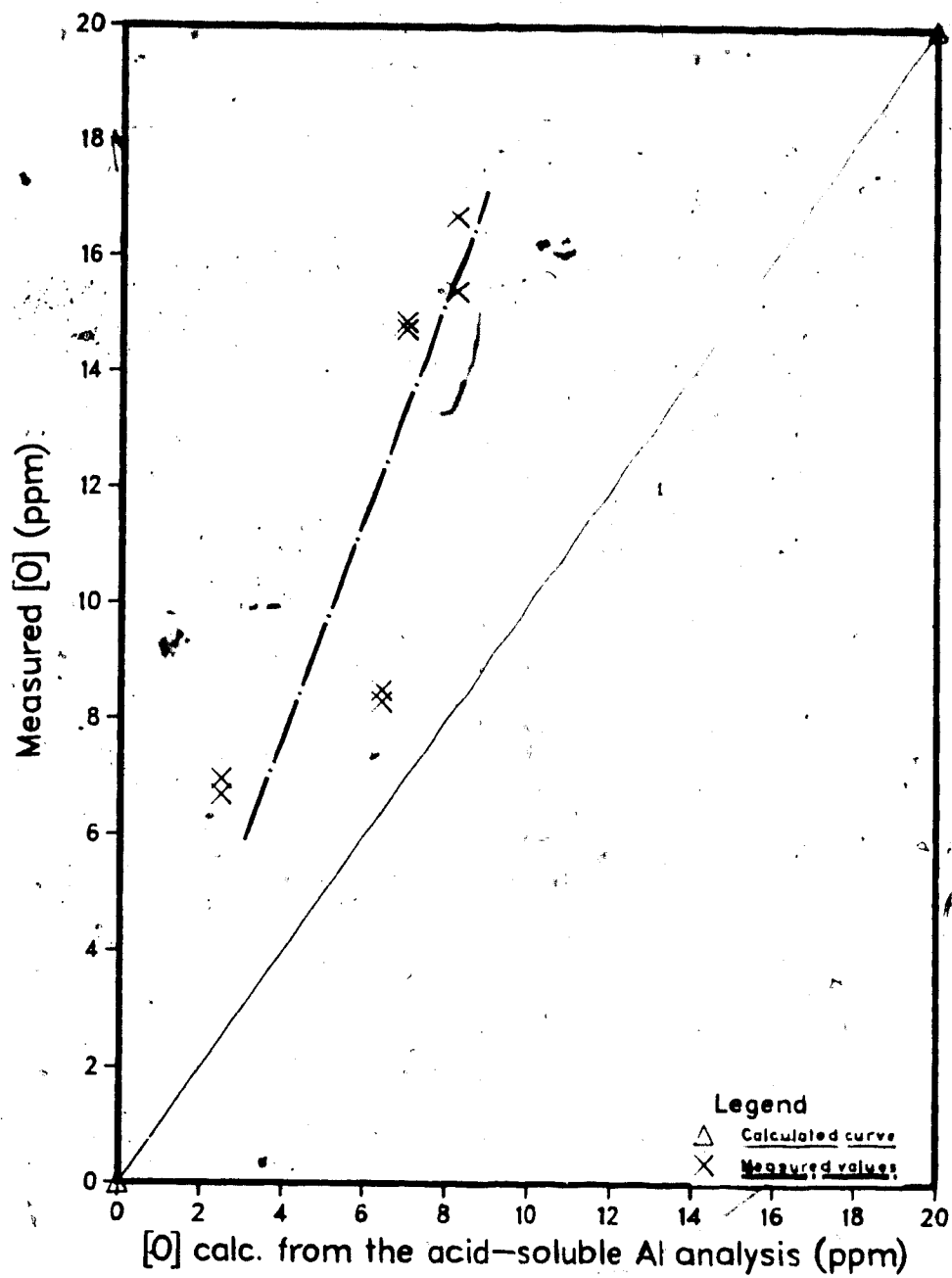
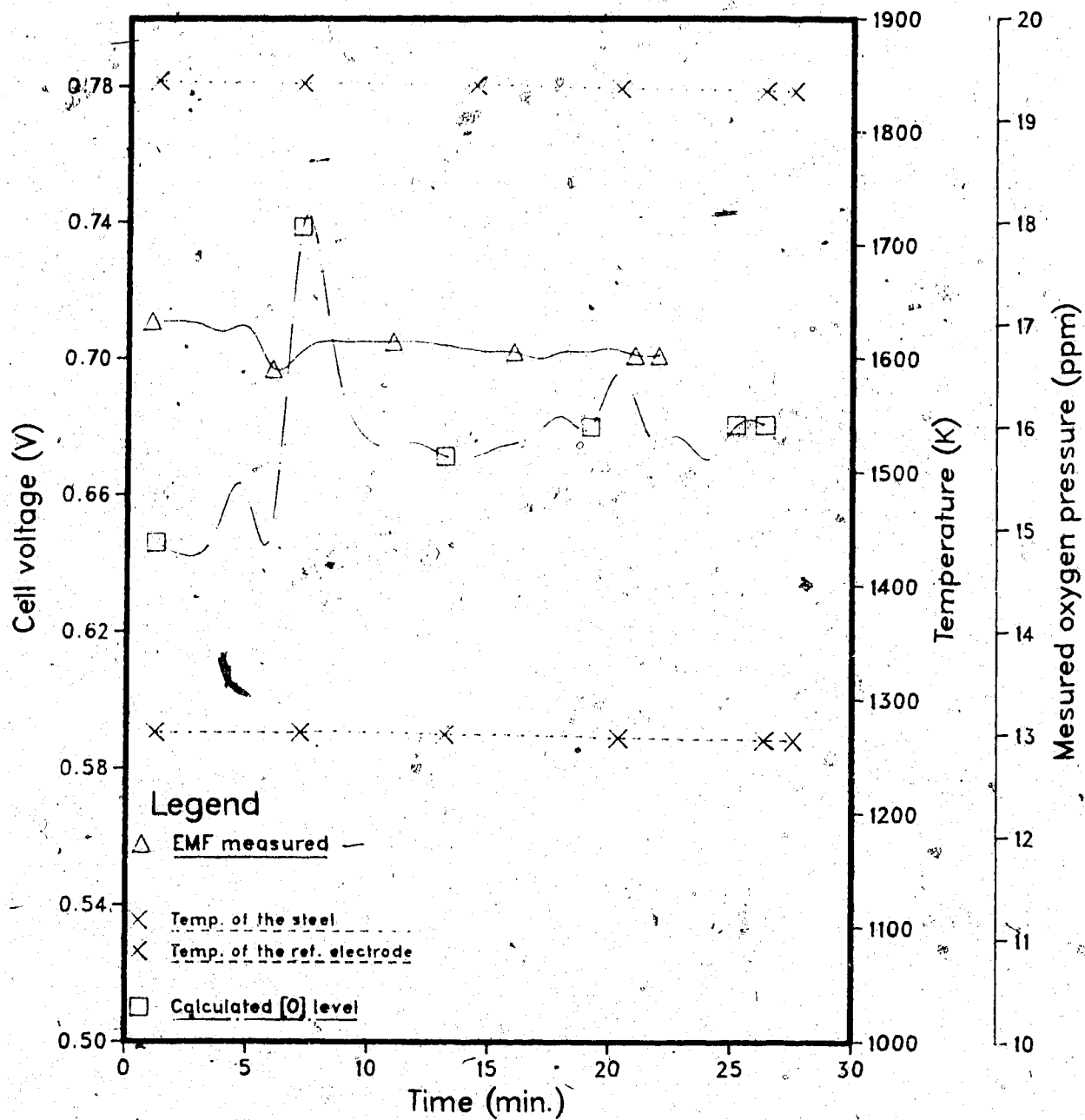


Fig. 24 [O] in steel determined by the Ni-NiO ref. probe



The probe can also give stable EMF output for a period of at least half an hour as shown in Fig. 24.

Comparison between [O] results obtained by the Ni-NiO reference probe is compared with that by the air reference probe in Fig. 25. The results obtained by the Ni-NiO probe were lower compared with that by the air reference probe. It may be possible that air reference probe tends to give higher values due its greater oxygen gradient across the electrolyte, inducing higher oxygen flux through the electrolyte.

2. Mo-MoO₂ reference oxygen probe

The oxygen probe with a Mo-MoO₂ reference electrode generally behaved poorly in comparison with the Ni-NiO reference probes. Though a Mo-MoO₂ reference probe could sometimes give a stable EMF for half an hour, the [O] level calculated according to its EMF values disagreed markedly with the level determined by the air reference probe, which was used in the same run. Since previous⁽²⁰⁾ and present studies all confirmed the air reference probe works well, the Mo-MoO₂ reference probe appears unreliable.

Results of a typical run using air and Mo-MoO₂ reference probes are listed in Table 7 and 8, respectively. As can be seen from the table, [O] level according to the Mo-MoO₂ probe is much higher than that determined by the air reference electrode probe. In both tables, E, TH, TC, and O have the same meaning as they do in Table 5.

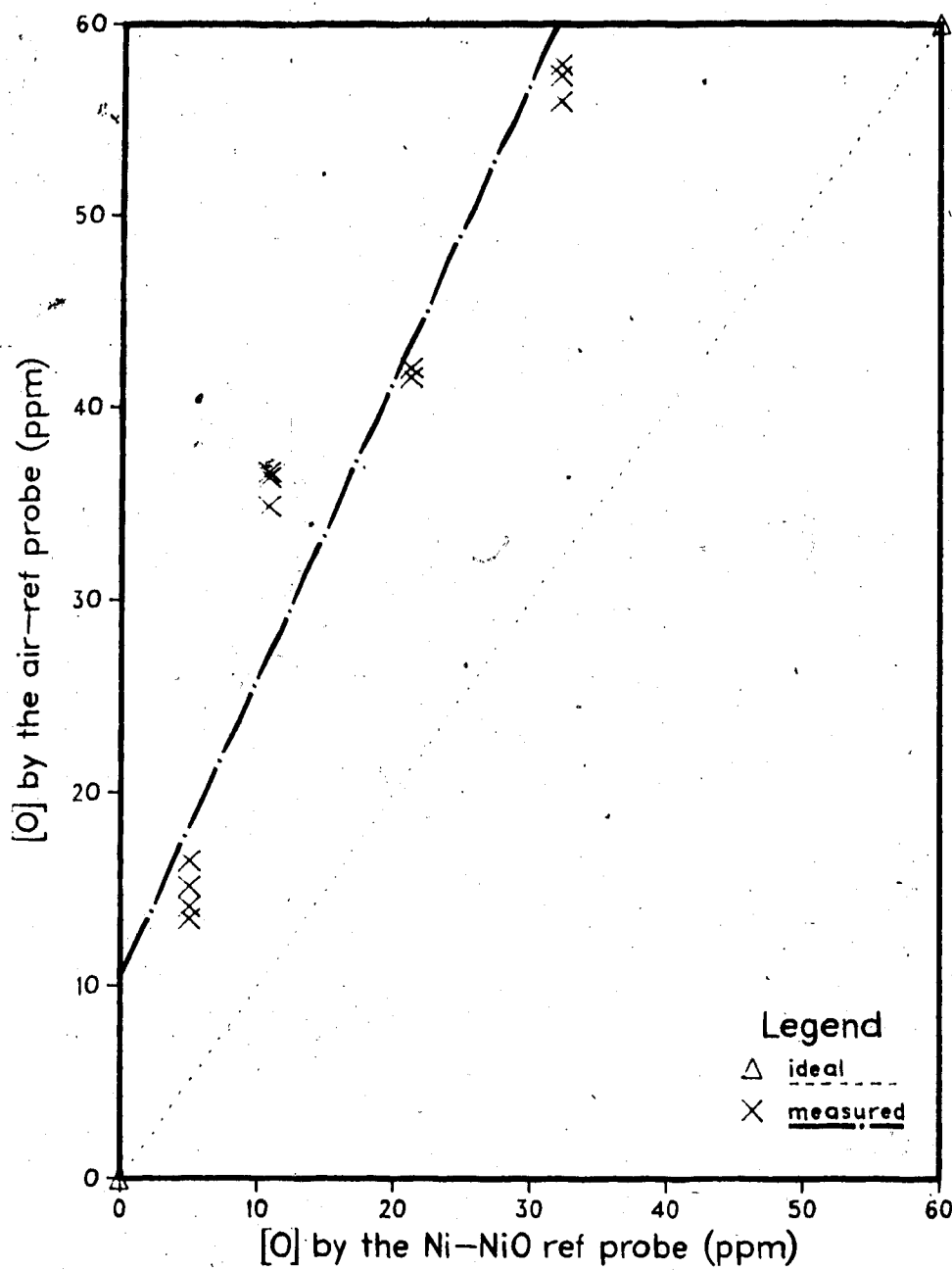
Table 7 [O] level determined by the air reference probe

E (V)	TH (K)	TC (K)	O (ppm)
1.3700	1779	1090	20.54
1.3670	1780	1104	19.62
1.3670	1781	1109	19.11
1.3670	1782	1111	19.02
1.3670	1782	1112	18.88
1.3690	1789	1118	18.71
1.3710	1789	1118	18.18
1.3680	1790	1119	19.01
1.3700	1787	1118	18.12
1.3730	1783	1116	16.99
1.3740	1779	1114	16.39

Table 8 [O] level determined by the Mo-MoO₂ probe

E (V)	Th (K)	TC (K)	O (ppm)
0.5880	1790	1053	234.89
0.5400	1784	1059	318.62
0.5270	1780	1066	281.15
0.5270	1778	1071	233.60
0.5280	1778	1073	218.94
0.5410	1777	1075	169.97
0.5390	1777	1078	161.88
0.5420	1777	1080	147.88

Fig. 25 [O] determined by the air-ref. probe vs. that by the Ni-NiO ref. probe



It was not clear why the Mo-MoO₂ reference probe behaved poorly. However, a possible explanation is that the oxygen partial pressure over Mo-MoO₂ is relatively low; hence, it was very sensitive to any environmental disturbance or impurities in the metal-metal oxide mixture. Problems have been reported with Cr-Cr₂O₃ as a reference electrode for oxygen probes because it has lower oxygen partial pressures at specific temperatures compared with other reference oxides.

In conclusion, Ni-NiO metal-metal oxide mixtures are recommended for solid reference electrode oxygen probes rather than Mo-MoO₂.

Advantages of the solid reference electrode oxygen probe over the air reference electrode probe when used under very low oxygen conditions

Oxygen flux through the ZrO₂(+CaO) solid electrolyte in oxygen probes depends on the difference of the oxygen partial pressures at the two electrodes.

$$J_{O_2} = \frac{RT\sigma_1}{2F^2L} \frac{P_e^{1/4}}{P_{O_2}^{1/4}} \frac{(P_{O_2}^n)^{1/4} - (P_{O_2}^r)^{1/4}}{P_{O_2}^{n/4}} \quad (\text{Eq. 118})$$

With a metal-metal oxide reference electrode, the oxygen pressure at the reference electrode is much lower than 0.21 atm, the oxygen pressure at an air reference electrode. Within the temperature range of 900-1500°C, the oxygen partial pressure over a Ni-NiO system is 1.144×10^{-12} to

1.262×10^{-9} atm. The thermodynamic data used here are from Charette and Flengas⁽⁵⁹⁾.

These oxygen partial pressure values match reasonably well with the oxygen partial pressures that were measured in steel. From the above equation, it can be seen that J_{O_2} decreases as P_{O_2} and $P_{O_2}^{\circ}$ approach each other. Theoretically, if P_{O_2} equals $P_{O_2}^{\circ}$, the oxygen flux through the electrolyte will be zero. With Ni-NiO metal-metal oxide mixtures as the reference electrode, that objective is nearly attained at certain combinations of electrode temperatures and oxygen activity in steel.

For the Mo-MoO₂ system in the same temperature range as for the Ni-NiO system, the oxygen pressure varies from 1.508×10^{-11} to 7.123×10^{-9} atm, calculated from Katayama and Kozuka's data.⁽⁶⁰⁾

Oxygen levels in steel were measured by air reference and Ni-NiO reference oxygen probes. It was found that the measurement for low oxygen levels by the Ni-NiO reference electrode probe was closer to what was determined by acid-soluble aluminum analysis than the measurement by the air reference electrode oxygen probe. This is shown in Fig. 25 which is a comparison for the same oxygen level in steel measured by the air reference and Ni-NiO reference probes.

D. Oxygen pressure measurement by the air reference oxygen probe in the $\text{Na}_3\text{AlF}_6\text{-Al}_2\text{O}_3$ system

Oxygen partial pressures, associated with $\text{Na}_3\text{AlF}_6\text{-Al}_2\text{O}_3$ melts were measured for different Al_2O_3 compositions by the oxygen probes with different reference electrodes. The results are listed in Table 9, 10, and 11 for air, Ni-NiO, and Cr-Cr₂O₃ reference probes respectively. The results agreed reasonably well. As before, a $\text{ZrO}_2(+\text{CaO})$ solid electrolyte rod was used in the oxygen probes.

Rolin and Bernhard⁽⁶¹⁾ reported their study on the phase diagram of the $\text{ZrO}_2\text{-Na}_3\text{AlF}_6$ system very briefly, in one sentence actually. They found that ZrO_2 was soluble in cryolite to some extent. No any other details were given.

Naturally, the corrosiveness of cryolite was of concern here. To test its resistance to chemical attack by cryolite, a rod was left in molten $\text{Na}_3\text{AlF}_6\text{-Al}_2\text{O}_3$ for over an hour, with no apparent chemical attack. Later in other regular runs, it was found that the $\text{ZrO}_2(+\text{CaO})$ rod did not show any substantial dissolution after being used in the system for around an hour.

X-ray diffraction analysis and energy dispersive X-ray analysis both did not detect any compounds that might result from the chemical attack of the rod by cryolite. Quantitative EDXA analysis of an electrolyte rod used in $\text{Na}_3\text{AlF}_6\text{-Al}_2\text{O}_3$ is listed in Table 4. A micrograph of a rod used in $\text{Na}_3\text{AlF}_6\text{-Al}_2\text{O}_3$ for one hour is shown in Plate 7. It can be compared with the photograph of an unused rod. The

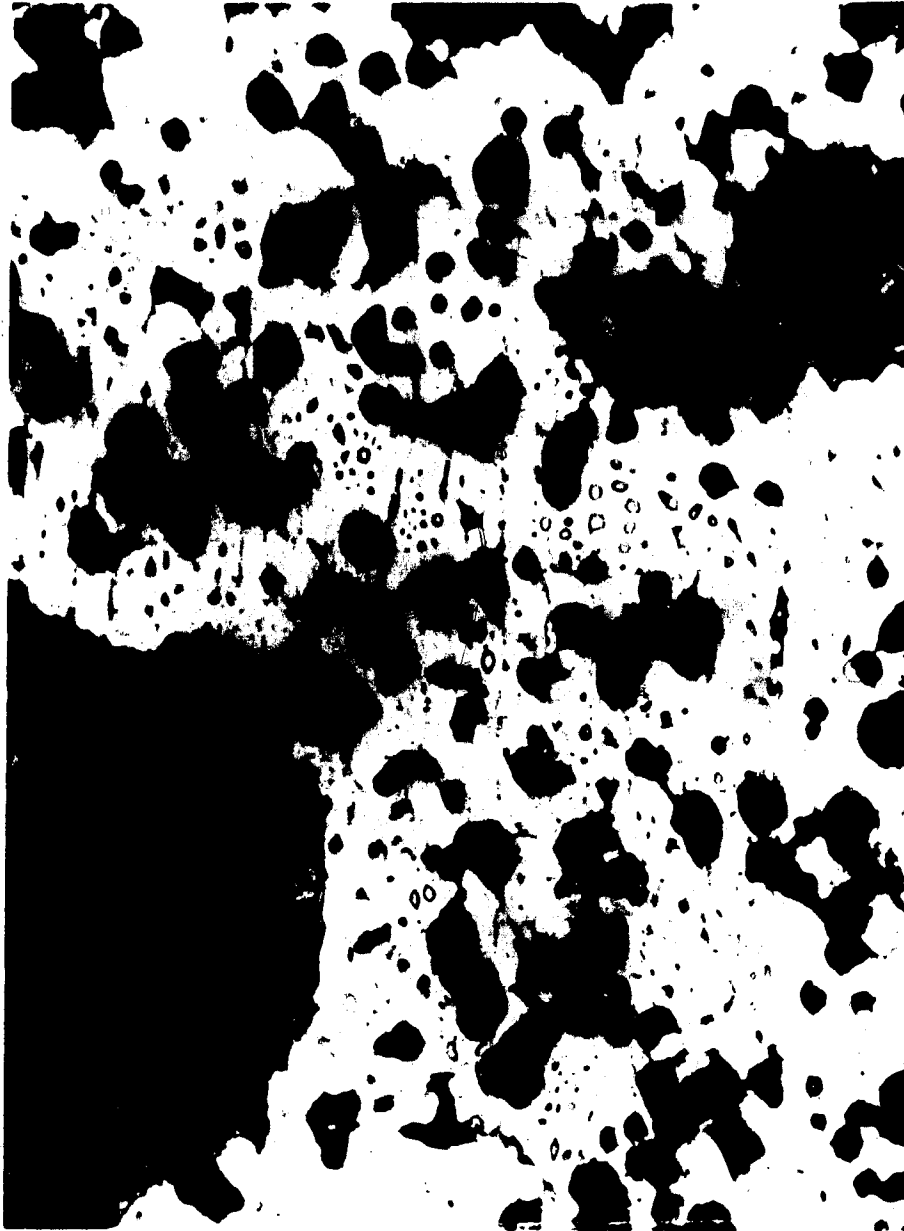


Plate 7 Micrograph of a $\text{ZrO}_2(+\text{CaO})$ rod after use in
 $\text{Na}_3\text{AlF}_6-\text{Al}_2\text{O}_3$

result indicated that the sintered $ZrO_2(+CaO)$ rod seemed to withstand chemical attack by molten $Na_3AlF_6-Al_2O_3$.

EMF responses of the probes for a run in the $Na_3AlF_6-Al_2O_3$ system with alumina concentrations from 1% to saturation appear in Table 9, 10, and 11. The corresponding oxygen pressures calculated from EMF values are also listed. For the calculations in the above three tables, thermodynamic data on NiO is from Charette⁽⁵⁹⁾ and data on Cr_2O_3 from H. A. Fine et al.⁽⁶²⁾

In general, EMF readings obtained by the probe in cryolite were less stable than those obtained with oxygen probes in steel. Sometimes EMF readings fluctuated by as much as 20 mV. Results of EMF recorded by a chart recorder of a typical run using air reference probe is shown in Fig. 26. In Fig. 27 similar response to the addition of the alumina into the melt is shown in Fig. 27. In both cases, chart paper speed is 2 cm/min. and the full scale voltage is 2 volts. Perhaps this is related to the nature of the $Na_3AlF_6-Al_2O_3$ melt itself. More work is needed to gain deeper insight into the thermodynamic and structural properties of the $Na_3AlF_6-Al_2O_3$ system. Furthermore, the relationship expected between the alumina concentration and oxygen partial pressure measured in the melt is yet to be established.

Table 9 Results of the emf obtained on the $\text{Na}_3\text{AlF}_6\text{-Al}_2\text{O}_3$ system by the air reference probe

Time (min.)	Alumina conc. (wt %)	EMF	TH	TC	Po_2 (atm)
0	1%	1.5710	1322	1179	0.176×10^{-23}
2		1.5700	1320	1180	0.161×10^{-23}
4		1.5700	1319	1179	0.155×10^{-23}
7		1.5800	1319	1179	0.104×10^{-23}
8		1.5140	1319	1179	0.136×10^{-22}
11	3%	1.6590	1317	1168	0.396×10^{-25}
13		1.6330	1316	1173	0.108×10^{-24}
16		1.6060	1316	1174	0.335×10^{-24}
20		1.6170	1317	1176	0.214×10^{-24}
26	5%	1.6580	1318	1170	0.419×10^{-25}
29		1.6310	1317	1176	0.117×10^{-24}
31		1.6230	1316	1177	0.153×10^{-24}
34		1.6110	1314	1177	0.228×10^{-24}
39	8%	1.7070	1316	1169	0.321×10^{-26}
41		1.7070	1318	1172	0.329×10^{-26}
44		1.6920	1318	1174	0.706×10^{-26}
46		1.6770	1318	1174	0.152×10^{-25}

47		1.6730	1318	1174.	0.186×10^{-25}
42	10%	1.5570	1315	1165	0.274×10^{-23}
45		1.5920	1319	1172	0.738×10^{-24}
47		1.5830	1319	1172	0.106×10^{-23}
50		1.5600	1318	1172	0.251×10^{-23}
56	satured	1.4940	1315	1167	0.292×10^{-22}
58		1.5210	1316	1170	0.105×10^{-22}
60		1.5840	1316	1171	0.880×10^{-24}
63		1.6390	1315	1172	0.800×10^{-25}

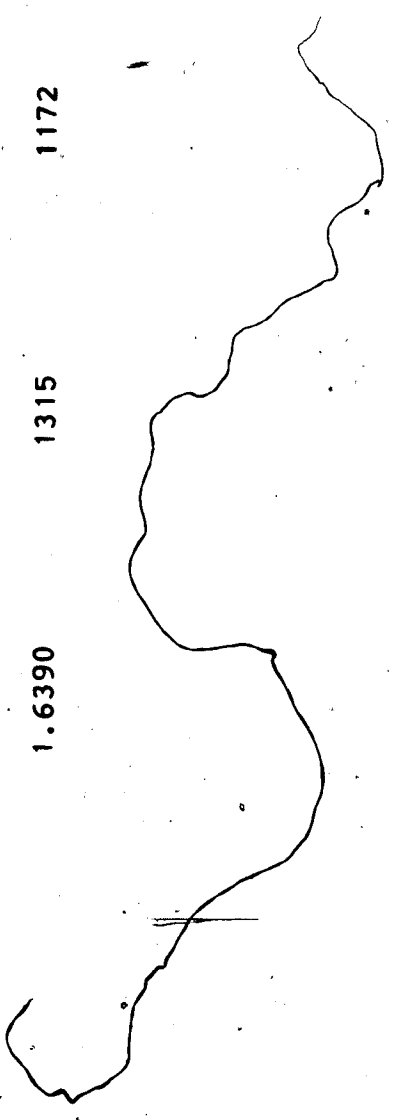


Table 10 Results of the emf obtained on the $\text{Na}_3\text{AlF}_6\text{-Al}_2\text{O}_3$ system by the Ni-NiO reference

Time (min.)	Alumina conc. (wt %)	EMF	TH	TC	Po_2 (atm)
0	1%	0.8800	1288	1091	0.129×10^{-23}
3		0.9920	1291	1128	0.144×10^{-25}
5		1.0060	1292	1134	0.794×10^{-26}
9		0.9920	1291	1140	0.141×10^{-25}
13	5%	1.2980	1290	1121	$0. > 124 \times 10^{-28}$
16		1.2530	1290	1130	0.441×10^{-29}
19		1.2790	1290	1131	0.873×10^{-29}
22		1.2870	1290	1131	0.103×10^{-28}
27	8%	1.2490	1289	1133	0.357×10^{-29}
30		1.2530	1290	1141	0.446×10^{-29}
33		1.2500	1290	1143	0.405×10^{-29}
35		1.2380	1291	1144	0.281×10^{-29}
39	10%	1.2460	1288	1134	0.296×10^{-29}
42		1.2340	1289	1142	0.200×10^{-29}
46		1.2270	1289	1144	0.142×10^{-29}
49		1.1890	1289	1144	0.374×10^{-31}

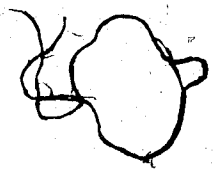
52		1.1160	1289	1145	0.742×10^{-29}
58	saturation	1.2400	1290	1111	0.269×10^{-29}
61		1.2720	1290	1111	0.735×10^{-29}
63		1.2900	1290	1114	0.108×10^{-28}
66		1.3020	1290	1116	0.132×10^{-28}
69		1.3180	1290	1118	0.166×10^{-28}

Table 11 Results of the emf. obtained on the $\text{Na}_3\text{AlF}_6\text{-Al}_2\text{O}_3$ system by the $\text{Cr-Cr}_2\text{O}_3$ reference

Time (min.)	probe		TH (K)	Po_2 (atm)
	alumina conc. (%wt)	EMF (V)		
0	1%	0.5370	1308	0.204×10^{-28}
2		0.6090	1309	0.262×10^{-30}
5		0.6960	1309	0.313×10^{-28}
8		0.6860	1309	0.244×10^{-28}
12		0.7390	1309	0.744×10^{-28}
15	3%	0.6690	1309	0.135×10^{-31}
18		0.4370	1306	0.118×10^{-25}
21		0.4070	1305	0.191×10^{-25}
24		0.3570	1304	0.111×10^{-24}
28	5%	0.4010	1304	0.159×10^{-24}
31		0.3410	1302	0.134×10^{-24}
34		0.4560	1302	0.351×10^{-27}
36		0.3540	1301	0.398×10^{-25}
41	8%	0.2250	1301	0.516×10^{-22}
44		0.2290	1300	0.597×10^{-23}
46		0.2870	1300	0.429×10^{-24}

49	0.2820	1299	1174	0.285×10^{-24}
52	0.2580	1301	1161	0.126×10^{-22}
55	0.3190	1300	1171	0.140×10^{-24}
58	0.3310	1299	1173	0.440×10^{-25}
61	0.3550	1299 ^a	1174	0.121×10^{-25}
64	0.4870	1300	1164	0.148×10^{-27}
68	0.4340	1299	1172	0.288×10^{-27}
70	0.4360	1300	1174	0.193×10^{-27}

10%



saturation

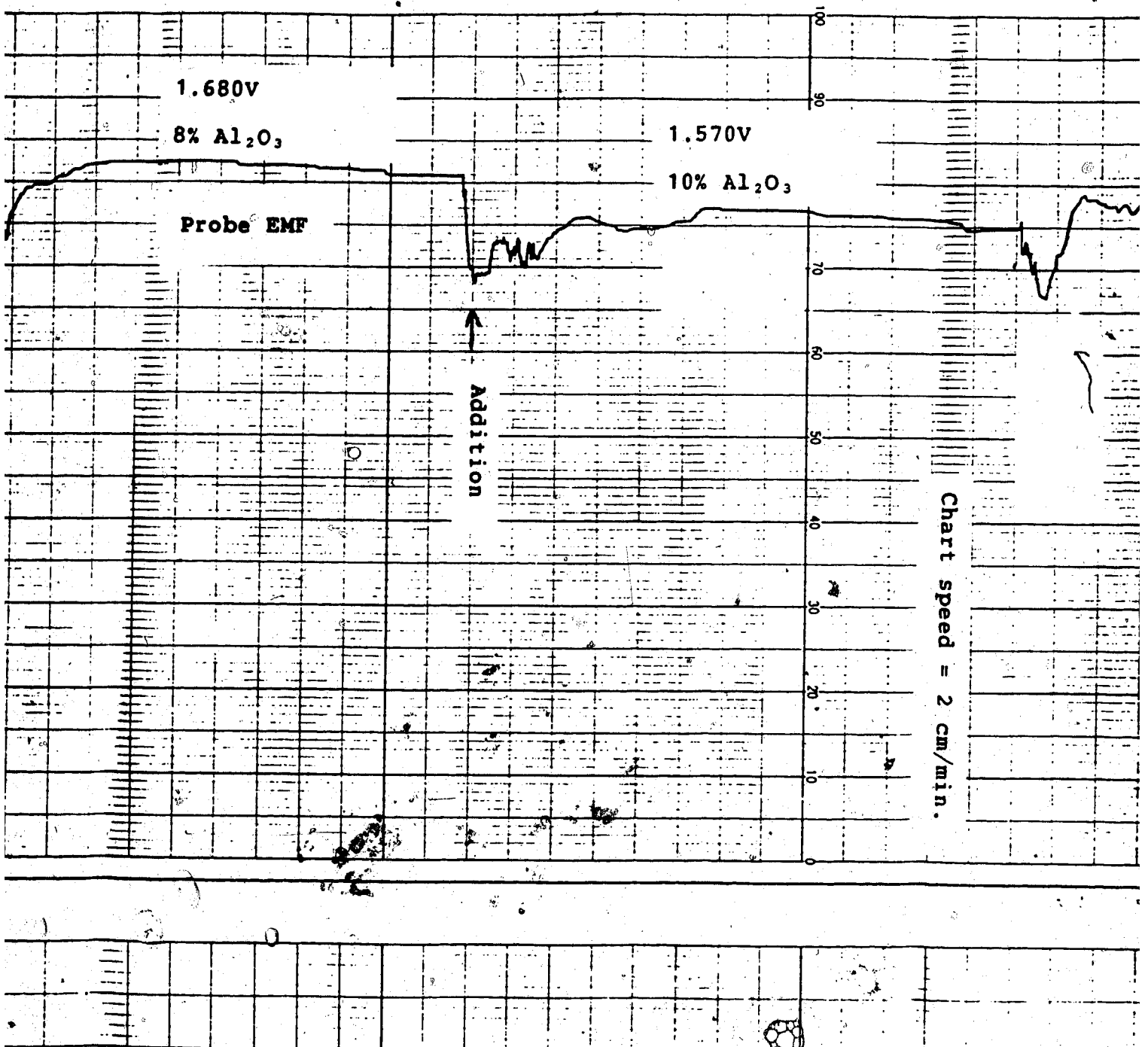
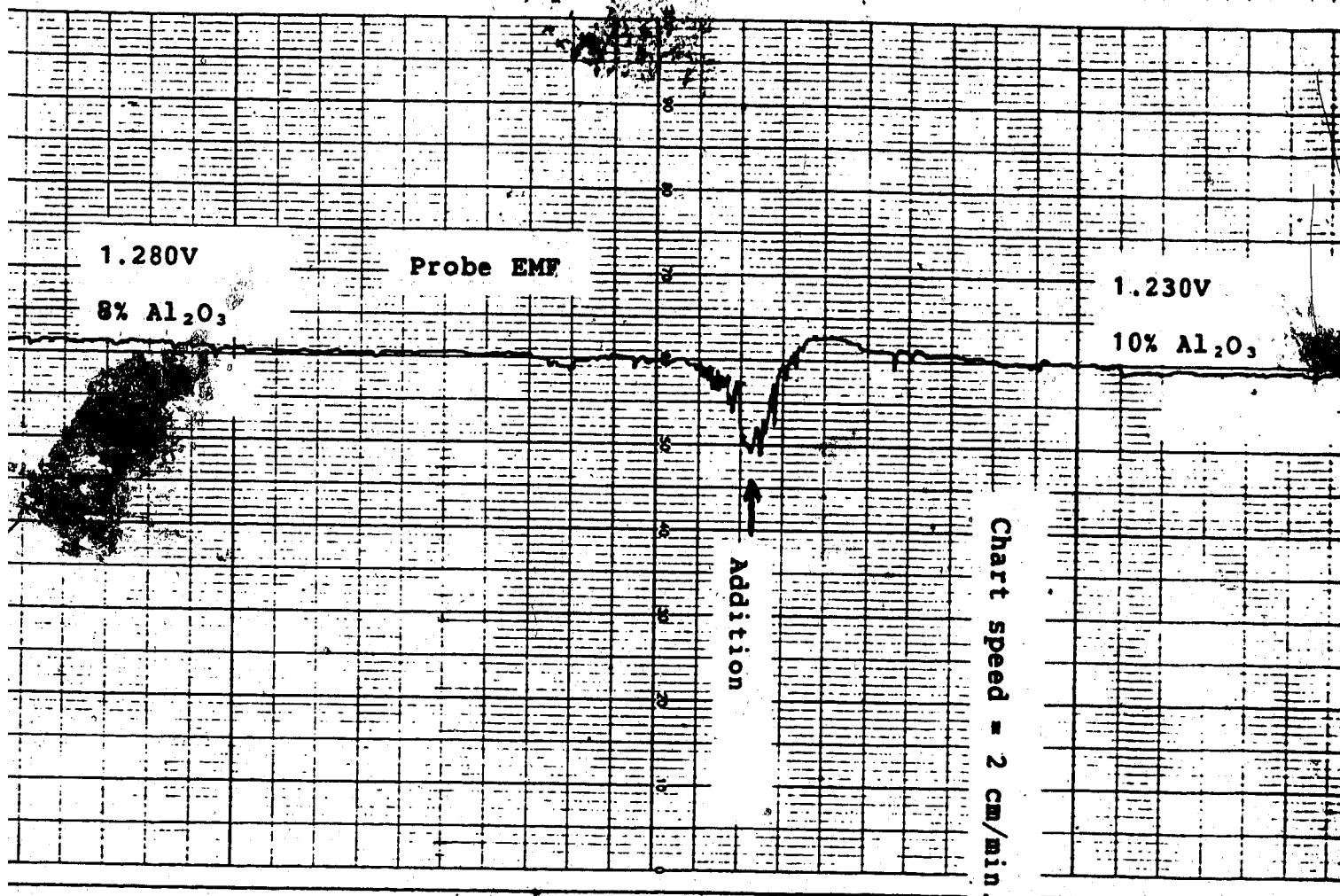


Fig. 26 EMF response of an air reference probe on the
Na₃AlF₆-Al₂O₃ system



RECORDS 5384-43

Fig. 27 EMF response of a Ni-NiO reference probe on the
 $\text{Na}_3\text{AlF}_6\text{-Al}_2\text{O}_3$ system

E. Possible industrial applications

Continuous oxygen measurement in steelmaking processes

It is only natural to think of continuous oxygen measurement in molten steel after intermittent measurement has proven to be so successful. Continuous oxygen measurements can give on-line information about steelmaking processes. This would be very helpful in providing valuable in-situ information for process control in general.

With minor adaptations, the nonisothermal oxygen probe developed in this study can be used for industrial applications. The only probable adjustment would be to use thicker $ZrO_2(+CaO)$ and $Mo-ZrO_2$ rods, since the probe must be fairly robust mechanically. For industrial applications, the Ni-NiO solid reference electrode oxygen probe is recommended over the air reference oxygen probe for its simplicity and ease of use.

Recently, there has been special interest in making ultra-clean steel. Continuous oxygen measurements should help in making this kind of steel by continuously monitoring the oxygen fluctuations in the liquid steel throughout the casting process. Continuous oxygen monitoring would allow control of reoxidation of the steel by oxygen in the atmosphere. The effectiveness of protection measures, such as argon shrouds, could be directly checked. As a result, oxygen measurements could help in minimizing the oxide inclusion content.

Control of deoxidation with Al, Si and Mn by oxygen activity measurements in steelmaking

Oxygen probes can be used for determining aluminum contents in steel if near-equilibrium conditions can be established in the liquid steel.⁽⁶³⁾ Measuring practice has indicated that this state of equilibrium can be approached, for example, by gas purging of liquid steel in the casting ladle. The equilibrium relationship for the reaction



was determined as in Eq. 117.

$$\log a_{[\text{O}]} = -\frac{2}{3} \log [\% \text{Al}] - \frac{1}{3} \log K(\text{Al}_2\text{O}_3)$$

within the temperature range of 1550 to 1650°C, where $a_{[\text{O}]}$ is the oxygen activity in steel, $[\% \text{Al}]$ is the weight percent of acid-soluble aluminum in steel and $K(\text{Al}_2\text{O}_3)$ is the reaction constant.

The temperature function of the reaction constant is as in Eq. 116:

$$\log K(\text{Al}_2\text{O}_3) = \frac{62680}{T} - 20.54$$

Therefore, by measuring the oxygen content in steel we can determine the concentration of dissolved aluminum in steel.

Silicon and manganese are the most widely used deoxidants. The deoxidation of pure iron with silicon was investigated by Janke⁽⁵⁸⁾. The equilibrium



was described by the following relationship:

$$\log a_{[\text{O}]} = -\frac{1}{2} \log a[\% \text{Si}] - \frac{1}{2} \log K(\text{SiO}_2) \quad (\text{Eq. 119})$$

where $a_{[\text{O}]}$ is the oxygen activity in steel, $[\% \text{Si}]$ is the weight percent of silicon in steel and $K(\text{SiO}_2)$ is the reaction constant. The temperature function of the constant is:

$$\log K(\text{SiO}_2) = 27840/T - 10.21 \quad 27.94 \text{ MILLIMETRES} \quad (\text{Eq. 120})$$

Experimental results showed a linear relationship between $\log a_{[\text{O}]}$ and $\log [\% \text{Si}]$ up to 0.3 to 0.4% Si in steel.

Similarly for manganese, there is the relationship⁽⁵⁸⁾

$$\log a_{[\text{O}]} = -0.9621[\% \text{Mn}] - 1.354 \quad (\text{Eq. 121})$$

In rimming steel, the main deoxidants used are manganese and silicon. In order to obtain close control of the deoxidants in finished rimming steel, a form of instantaneous information regarding the oxidation of metal prior to tapping is needed. This could be provided by measuring the activity of oxygen with oxygen probes. The

instantaneous readings obtained for oxygen in steel before deoxidation, in accordance with established relationships, could be used to determine the extent of deoxidation loss. On this basis, the composition of finished steel could be calculated.

Oxygen activity measurements in LD-converter processes

Oxygen activity measurements could also find useful applications in the LD-converter process. Operation guidelines could be formulated for reblowing, and also for deoxidation after tapping. Provided near-equilibrium conditions have been established it would be possible to determine the carbon content in steel by electrochemically measuring the oxygen content.⁽⁶⁴⁾

Oxygen probes in aluminum electrolysis cells

Alumina activity or concentration in $\text{Na}_3\text{AlF}_6\text{-Al}_2\text{O}_3$ melts can be measured by measuring the oxygen partial pressure associated with cryolite. This would be very helpful for the aluminum industry because the alumina content in aluminum electrolytic cells is always a very important factor in cell operation.

First of all, proper Al_2O_3 levels have to be maintained in the cell to carry out normal cell operation. Too low an alumina level is directly related to anode effects. Secondly, too much alumina will precipitate out of the electrolyte and accumulate at the bottom of industrial

cells. This will increase the electrical resistance of the cell causing cell voltage to rise, which can have adverse effects on cell operation, such as higher energy costs. By closely monitoring the alumina concentration in industrial cells, these adverse effects can be eliminated or minimized.

F. Suggestions for future work

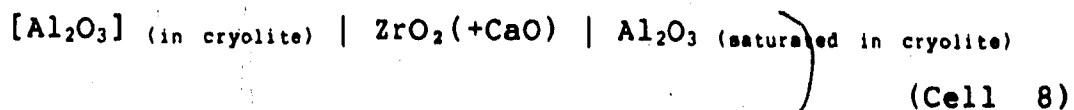
Experimental conditions for oxygen measurements in steel

To study deoxidation equilibria in steel a better protective environment has to be set up for the molten steel in the induction furnace. This will help to eliminate the reoxidation of steel by oxygen in the air so that a more stable oxygen level can be maintained. Also, it may be a help to use Al_2O_3 crucibles instead of the MgO crucibles used for containing molten steel in the induction furnace.

With the above mentioned changes, future research can use the well-studied $[\text{Al}]$ and $[\text{O}]$ equilibrium to better characterize the nonisothermal oxygen probe. Conversely, well-characterized oxygen probes can be used to study deoxidation thermodynamics or other thermodynamic reactions in steelmaking processes.

Thermodynamic study on the Na_3AlF_6 - Al_2O_3 system by using galvanic cells with $\text{ZrO}_2(+\text{CaO})$ solid electrolytes

A cell with an arrangement as follows:



can be constructed to study the activity of Al_2O_3 in the cryolite system. The experimental apparatus should have a protective environment to reduce the evaporation of the volatile components, such as aluminum fluorides.

After the above work is completed, a laboratory aluminum electrolysis cell could be set up to carry out the electrolysis process. The alumina activity in that cell can be followed by an oxygen sensor of the type constructed in this study. Furthermore, electrolysis could be carried out such that the anode effect is observed while the alumina content in the $\text{Na}_3\text{AlF}_6\text{-Al}_2\text{O}_3$ melt is followed. A relationship between the anode effect and alumina activity may thus be established.

Determination of $(S_2+Q_2^*/T)$ and $(S_3+Q_3^*/T)$ in $\text{ZrO}_2(+\text{CaO})$ solid electrolytes by Seebeck coefficient measurements

From Eq. 49 in Section E of Chapter II:

$$\alpha = \frac{t_{\text{ion}}}{2F} \left[-\frac{1}{2} S \dot{O}_2 + \frac{R}{2} \ln P O_2^* + \left(S_2 + \frac{Q_2^*}{T} \right) \right] - \frac{t_e}{F} \left[S_3 + \frac{Q_3^*}{T} \right] - \alpha^{(\text{Pt})}$$

As has been discussed in the chapter on theory, all terms in the above equation can be calculated for a given temperature and oxygen pressure except the terms:

$$\frac{t_{ion}}{2F} (\bar{S}_2 + \frac{Q_2^*}{T}) - \frac{t_e}{F} (\bar{S}_3 + \frac{Q_3^*}{T})$$

Substituting $t_e = 1 - t_{ion}$ into the above equation and regrouping gives:

$$\frac{t_{ion}}{2F} (\bar{S}_2 - 2\bar{S}_3 + \frac{Q_2^*}{T} - 2\frac{Q_3^*}{T}) + t_e \frac{1}{F} (\bar{S}_3 + \frac{Q_3^*}{T})$$

Then substituting

$$\bar{S}_2 - 2\bar{S}_3 = \bar{S}_{O_2},$$

$$\text{and } \frac{Q_2^*}{T} - 2\frac{Q_3^*}{T} = \frac{Q_{O_2}^*}{T}$$

into the above terms gives:

$$\frac{t_{ion}}{2F} (\bar{S}_{O_2} + \frac{Q_{O_2}^*}{T}) + \frac{t_e}{F} (\bar{S}_3 + \frac{Q_3^*}{T})$$

In the above terms only $(\bar{S}_3 + \frac{Q_3^*}{T})$ cannot be calculated from a given oxygen pressure and temperature. Therefore by experimentally measuring the Seebeck coefficient of $ZrO_2(+CaO)$ solid electrolyte and calculating all other terms in the Seebeck coefficient expression one may be able to estimate the the sum of \bar{S}_3 and $\frac{Q_3^*}{T}$. The results can be compared with results obtained by other methods such as the Soret effect.

Conclusions

In laboratory tests, nonisothermal oxygen probes with $ZrO_2(+CaO)$ solid electrolytes were employed to measure oxygen pressures in molten steel and molten $Na_3AlF_6-Al_2O_3$ systems. Different reference electrodes were used for the oxygen probe. As is already known, air reference electrode probes performed satisfactorily. Probes with Ni-NiO reference electrode were successful, but probes with Mo-MoO₂ reference electrode are not as promising.

The theoretical basis for nonisothermal oxygen probe measurements was fully derived. Combined with its advantages of being inert to chemical attack and having less concentration polarization, nonisothermal oxygen probes show promising potential for continuous oxygen monitoring in steelmaking processes. Though there are other ways of monitoring oxygen in steel, the simplicity of the electrochemical oxygen sensors makes them very attractive.

Initial experimental results indicate that the oxygen pressure in equilibrium with alumina in $Na_3AlF_6-Al_2O_3$ melt may be measurable with oxygen probes. Different reference electrodes were experimented. All oxygen pressures determined by different probes were in close agreement. Yet, further tests have to be performed before the oxygen probe can be applied on industrial $Na_3AlF_6-Al_2O_3$ systems.

Bibliography

- (1) W. Nernst, *Z. Electrochem.* 6, (1900) p.41.
- (2) C. Wagner, *Naturwissenschaften*, 31, (1943) pp.265-268.
- (3) K. Kiukkola and C. Wagner, *J. Electrochem. Soc.*, 104, (1957) pp.379-387.
- (4) W. D. Kingery, J. Pappis, M. E. Doty, and D. C. Hill, *J. Am. Ceram. Soc.*, 42, (1959) pp.393-98.
- (5) C. B. Alcock and T. N. Belford, *Trans. Far. Soc.* 60, (1964) pp.822-35.
- (6) T. N. Belford and C. B. Alcock, *Trans. Far. Soc.* 61, (1965) pp.443-53.
- (7) W. A. Fisher and W. Ackermann, *Arch. Eisenhüttes.* 36, (1965) pp.643-48; 37, (1966) pp.43-47.
- (8) K. Schwerdtfeger, *Trans. Metall. Soc. AIME*, 239, (1967) pp.1276-81.
- (9) K. Goto and Y. Matsushita, *Tetsu-to Hagane*, 52, (1966) pp.827-39; Engl. trans. in *Trans. Iron Steel Inst. Japan.*, 6, (1966) pp.21-28.
- (10) G. R. Fitterer, *J. of Metals*, 18, (1966) pp.961-68.
- (11) E. T. Turkdogan and R. J. Fruehan, *Can. Metall. Quart.*, 11, (1972) pp.371-84.
- (12) L. Van Bogdandy, E. Foster, W. Klappor, and H. Richter, *Stahl u. Eisen*, 89, (1969) pp.704-10.
- (13) L. Van Bogdandy, E. Foster, and H. Richter, "Kinetics of Metallurgy Processes in Steelmaking", pp.421-37, Dusseldorf, 1972.
- (14) T. H. Etsell, personal communication.
- (15) W. A. Fischer and D. Janke, *Arch. Eisenhüttes.*, 39, (1968) pp.259-63.
- (16) S. M. Shreikin and B. A. Kamaev, *Steel in the USSR*, 3, (1973) pp.905-7.
- (17) E. Foster and H. Richter, *Arch. Eisenhüttes.*, 40, (1969) pp.475-79.

- (18) E. Schurman, R. Bruder, K. Nurnberg, and H. Richter, *Arch Eisenhuttwes.*, 50 (1979) pp.139-43.
- (19) C. Gatellier, K. Torrsell, M. Olette, A. Rist, and P. Vicens, *Rev. Metallurg.*, 66, (1969) pp.673-93.
- (20) T. H. Etsell and C. B. Alcock, *Solid State Ionics*, 3/4, (1981) pp.621-26.
- (21) M. Iwase, M. Tanida, A. Mclean, and T. Mori, *Metall. Trans. B.*, 12B, (1981) pp.517-24.
- (22) R. Renz and H. Schmalzreid, *Z. Phys. Chem. (N. F.)*, 29 (1961) pp.77-82.
- (23) G. C. Charette and S. N. Flengas, *Can. Metall. Quart.*, 7, (1968) pp.191-200.
- (24) Z. Kozuka and C. S. Samis, *Metall. Trans.*, 1, (1970) pp.871-76.
- (25) V. M. Kapoor and M. G. Froberg, *Arch Eisenhuttwes.*, 42, (1971) pp.124.
- (26) R. Coombes et al., *Electrochim. Acta*, 20, (1975) pp.191-200.
- (27) Seichi Sato, T. Yokokawa, H. Kita, and K. Niwa, *J. Electrochem. Soc.*, 119, (1972) pp.1524-26.
- (28) K. H. Stern and Rm. Panayappan, *J. Electrochem. Soc.*, 124, (1977) pp.641-49.
- (29) K. H. Stern, M. L. Deanhardt, and Rm. Panayappan, *J. Electrochem. Soc.*, 83, (1979) pp.2848-54.
- (30) M. Kawakami, K. S. Goto, and M. Matsuoka, *Metall. Trans. B*, 11B, (1980) pp.463-69
- (31) Y. Wanibe, Yamauchi, K. Kawai, and H. Sakao, *Arch Eisenhuttwes.*, 44, (1973) pp.711-17.
- (32) M. Iwase, N. Yamada, H. Akizuki, and E. Ichise, *Arch Eisenhuttwes.*, 55, (1984) pp.471-76.
- (33) M. Iwase, N. Yamada, E. Ichise, and H. Akizuki, *Arch Eisenhuttwes.*, 55, (1984) pp.415-20.
- (34) M. Iwase, N. Yamada, K. Nishida, and E. Ichise, *ISS Trans.*, 4 (1984) pp.69-75.
- (35) N. E. Richards and E. R. Russell, "Paper presented at ECS meeting", New York, May 1969.

- (36) J. Thonstad, *Electrochim. Acta*, 14, (1969) pp.127-34.
- (37) J. Thonstad, *Light Metals*, Pro., 103rd AIME Annu. Meet. pp.137-49, ed. by H. Forberg, Metall. Soc. AIME, New York, (1974).
- (38) E. W. Dewing, "Proceedings of the international symposium on molten solts.", pp. 325-30, ed. by J. P. Pemsler, Washiton D. C., (1976).
- (39) J. Thonstad, *Metall. Trans. B*, 8B, (1977) pp.125-30.
- (40) H. Schmalzried, *Z. Electrochem.*, 66, (1962) p.572.
- (41) P. H. Scaife, D. A. J. Swinkels, and S. R. Richards, *High Temp. Sci.*, 8, (1976) pp.31-47.
- (42) M. Iwase, E. Ichise, M. Takeuchi, and T. Yamasaki, *Trans. Japan Inst. Metals.*, 25, (1984) pp.43-52
- (43) T. H. Etsell and S. N. Flengas, *J. Electrochem. Soc.*, 119, (1972) pp.1-7.
- (44) W. Fischer, *Z. Naturforsch.*, 22a, (1967) pp.1575-81.
- (45) R. Ruka, J. E. Bauerle, and L. Dykstra, *J. Electrochem. Soc.*, 115, (1968) pp.497-501.
- (46) S. Pizzini, C. Riccardi, V. Wagner, and C. Sinistri, *Z. Naturforsch.*, 25a, (1970) pp.559-65.
- (47) C. Wagner, *Progress in Solid State Chemistry*, vol.7, (1972) pp.1-37.
- (48) T. H. Etsell and S. N. Flengas, *Metall. Trans.*, 3, (1972) pp.27-36.
- (49) A. A. Vechev and D. V. Vechev, *Russian J. of Phy. Chem.*, 41, (1967) pp.685-88.
- (50) T. Etsell, A. S. Kucharski, and C. B. Alcock, "Seebeck coefficient measurement on stabilized ZrO_2 -applications to continuous oxygen determination in steel." *Met. Trans. B*, (in press).
- (51) J. F. Elliott, "Thermochemistry for Steelmaking", vol. II pp.566-567, Addison-Wesley Publ. Co. Inc., Reading, Mass., 1963.
- (52) K. Grjotheim, "Contribution to the theory of aluminum electrolysis", Dr. Dissertation, The Tech. Univ. of Norway, Trondheim, 1956.
- (53) K. Grjotheim, "Aluminum Electrolysis: Fundamentals of

- the Hall-Heroult Process", 2nd Ed., p.209, Aluminum W Germany, 1982.
- (54) J. L. Hölm, "Thermodynamic properties of molten cryolite and other fluorite mixtures", Dr. techn. Dissertation, The Tech. Univ. of Norway, Trondheim, 1971.
- (55) J. Thonstad and A. Hagen, *Aluminum*, 47, (1971) pp.678-81.
- (56) M. S. Beltskii, et al., *Industr. lab (Zavod. lab)*, 27, (1961) pp.711-12.
- (57) W. Pluschkell, *Stahl u. Eisen*, 199, (1979) pp.398-404.
- (58) D. Janke, "Deoxidation of liquid steel", Prepr.-Int. Conf. Adv. Chem. Metall. 1979, (suppl.), Paper 32, 36, Bombay India.
- (59) G. C. Charette and S. N. Flengas, *J. Electrochem. Soc.*, 115, (1968) pp.796-804.
- (60) I. Katayama, Z. Kozuka, *Technol. Rep. Osaka Univ.*, 23, (1973) pp.411-23.
- (61) M. Rolin and M. Bernhard, *Bull. Soc. Chim. France*, (1962) pp939-49.
- (62) H. A. Fine and Geiger, "Handbook on Material and Energy Balance Calculations in Metallurgical Processes", p.408, AIME, New York, 1979 & W. Pluschkell, *Stahl u. Eisen*, 96, (1976) pp.657-62.
- (63) G. Bauer, E. Hees, J. Koenitzer and H. Litterscheidt, *Stahl u. Eisen*, 98, (1978) pp.1138-45.

General References

- (64) C. Wagner, "The Electromotive Force of Galvanic Cells Involving Phases of Locally Variable Composition", *Advances in Electrochemistry, and Electrochemical Engineering*, vol.4, 1966, pp.1-47.
- (65) Per Kofstad, "Nonstoichiometry, Diffusion, and Electrical Conductivity in Binary Metal Oxides", Wiley-interscience, New York, 1972.

- (66) S. Chandra, "Superionic Solids (Principles and Applications)", North-Holland, New-York, 1981.

Appendix I

The program for calculating \bar{t}_{ion} by numerical integration

```
PROGRAM TION
REAL X,T,TC,TH,H,TI1,SUM,TI2,PO2C,PO2,TII
DOUBLE PRECISION PO2HMA,PO2HMI
INTEGER N,K
C THE PROGRAM IS DESIGNED
C FOR CALCULATING THE IONIC TRANSPORT
C NUMBER OF A ZrO2(+CaO) SOLID
C ELECTROLYTE UNDER NONISOTHERMAL
C AND NONISOBARIC CONDITIONS.
REAL TI
REAL A,B
A=-54500*2.303
B=14*2.303
C THE FACTORS A AND B ARE THE CONSTANTS
C IN THE EXPRESSION
C FOR THE PO2(electronic). LOG(PO2(E))=A/T+B.
C THE A AND B IN THIS EQUATION
C ARE SUBJECTED TO CHANGES DUE TO DIFERENT
C INTRINSIC PROPERTIES OF THE
C THE ELECTROLYTE UNDER INVESTIGATION
C AND ALSO THE RANGE OF TEMPERATURE.
C THE METHOD USED IS THE NUMERICAL
C INTEGRATION FOR THE CALCULATION OF THE AVERAGE
C OF THE IONIC TRANSFERENCE NUMBER OVER A RANGE OF
C TEMPERATURE AND OXYGEN PARTIAL PRESSURE.
C THE SIMPSON'S RULE IS USED HERE TO CALC.
C THE NUMERICAL INTEGRATION.
C TI1 IS THE AVERAGE OF THE  $t_{ion}$  OVER THE TEMPERATURE.
C RANGE OF TC AND TH, AND AT A SPECIFIC
C OXYGEN PRESSURE OF PO2.
C (TC,TH) IS THE TEMPERATURE RANGE UNDER WHICH
C THE ELECTROLYTE IS OPERATING.
C TI IS THE AVERAGE OF THE  $t_{ion}$  UNDER
C ISOTHERMAL CONDITIONS.
C TI2 IS THE TI AT THE STEEL TEMPERATURE.
C PO2HMIN IS THE MINIMUM OXYGEN PARTIAL
C PRESSURE TO BE MEASURED.
C AT THE HOT END OF THE ELECTRODE.
C PO2HMAX IS THE MAXIMUM OXYGEN PARTIAL
C PRESSURE TO BE MEASURED.
C PO2
C IS THE OXYGEN PARTIAL PRESSURE
C AT THE COLD END (REF. ELECTRODE).
WRITE(6,17)
WRITE(6,16)
```

PO2HMA=1.487E-9
 PO2HMA=1.487E-9 IS EQUIVALENT
 TO A OXYGEN CONTENT OF 1000 PPM.

PO2HMI=1.487E-17
 PO2HMI=1.487E-15 IS EQUIVALENT
 TO A OXYGEN CONTENT OF 1 PPM.

TC=1273
 TH=1873
 PO2C=0.210
 N=2000
 H=(TH-TC)/(2*N)
 PO2 = PO2HMA

8 SUM=0
 K=1

T=TC

TI=LOG((PO2C**0.25+EXP(A/(4*T)+B/4))/(PO2**
 *0.25+EXP(A/(4*T)+B/4)))

TI=4*TI/(LOG(PO2C/PO2))

SUM=SUM+H*TI

10 T=T+H

K=K+1

TI=LOG((PO2C**0.25+EXP(A/(4*T)+B/4))/(PO2**
 *0.25+EXP(A/(4*T)+B/4)))

TI=4*TI/(LOG(PO2C/PO2))

X=K

X=X/2.0

IF ((AINT(X))*2-K).EQ.0) THEN

C IF K IS EVEN THEN

SUM=SUM+2*H*TI

ELSE

C IF K IS ODD THEN

SUM=SUM+4*H*TI

END IF

IF (K.LT.2*N) THEN

GOTO 10

ELSE .

SUM=SUM+H*TI.

END IF

TI1=SUM/3/(TH-TC)

TI2=4*(LOG((PO2C**0.25+(7.94E-16)**0.25)
 */(PO2**0.25+(4.559E-16)**0.25)))/(LOG(PO2C/PO2))

WRITE(6,15)TC,TH,PO2,TI1,TI2

PO2 = PO2*0.01

IF (PO2.GE.PO2HMI) GOTO 8

15 FORMAT(1X,F5.0,3X,F5.0,4X,E18.4,4X,F8.4,4X,F8.4)

16 FORMAT('TC TH PO2 TI1 TI2'//)

17 FORMAT('THE OXYGEN PRESSURE AT THE
 *REFERENCE ELECTRODE IS ATM'//)

STOP

END

Appendix II

A typical input data file

1	0.0190		%[AL]
2	0.3000		%[C]
3	0.0000		%[CR]
4	0.6200		%[MO]
5	0.0000		%[N]
6	0.0000		%[O]
7	0.0000		%[P]
8	0.0000		%[S]
9	0.1300		%[SI]
10	0.0000		%[TI]
11	0.0000		%[V]
12	1.4214	1500.	720.
13	1.4206	1500.	726.
14	1.4201	1500.	737.
15	1.4196	1501.	745.
16	1.4191	1502.	754.
17	1.4201	1503.	760.
18	1.4204	1503.	764.
19	1.4210	1503.	766.
20	1.4211	1503.	769.
21	1.4198	1503.	771.
22	1.4198	1503.	773.
23	1.4215	1503.	776.
24	1.4211	1503.	769.
25	1.4211	1503.	779.
26	1.4216	1505	780.
27	1.4222	1505.	780.
28	1.4216	1505.	782.
29	1.4209	1506.	784.
30	1.4207	1506.	785.
31	1.4203	1506.	786.
32	1.4195	1506.	787.
33	1.4191	1506.	788.
34	1.4190	1506.	789.
35	1.4187	1506.	790.
36	1.4191	1505.	791.
37	1.4205	1505.	790.
38	1.4195	1506.	792.
39	1.4201	1506.	792.
40	1.4208	1506.	792.
41	1.4194	1507.	793.
42	1.4190	1507.	794.
43	1.4184	1507.	795.
44	1.4176	1507.	796.
45	1.4169	1508.	796.
46	1.4165	1508.	797.
47	1.4158	1508.	797.

Appendix III

A typical output data file

E(V)	TH(K)	TC(K)	P1(ATM)	C(PPM)
1.3469	1772.	1135.	0.239E-12	19.63
1.3502	1772.	1137.	0.211E-12	18.47
1.3504	1773.	1139.	0.210E-12	18.32
1.3484	1773.	1141.	0.216E-12	18.59
1.3569	1773.	1143.	0.164E-12	16.22
1.3594	1774.	1144.	0.155E-12	15.68
1.3634	1774.	1145.	0.136E-12	14.69
1.3651	1773.	1146.	0.124E-12	14.10
1.3667	1773.	1147.	0.117E-12	13.68
1.3677	1773.	1148.	0.112E-12	13.39
1.3689	1772.	1148.	0.105E-12	13.04
1.3700	1772.	1149.	0.100E-12	12.74
1.3710	1772.	1148.	0.990E-13	12.65
1.3719	1771.	1149.	0.925E-13	12.28
1.3722	1772.	1149.	0.942E-13	12.34
1.3727	1772.	1149.	0.928E-13	12.25
1.3515	1773.	1128.	0.237E-12	19.47
1.3527	1772.	1130.	0.217E-12	18.71
1.3541	1773.	1133.	0.205E-12	18.12
1.3589	1773.	1135.	0.174E-12	16.67
1.3635	1773.	1138.	0.146E-12	15.27
1.3663	1773.	1140.	0.131E-12	14.46
1.3686	1773.	1141.	0.120E-12	13.89
1.3705	1773.	1142.	0.112E-12	13.41
1.3707	1773.	1144.	0.109E-12	13.19
1.3710	1774.	1146.	0.107E-12	13.06
1.3706	1774.	1147.	0.107E-12	13.04
1.3696	1774.	1147.	0.110E-12	13.23
1.3703	1774.	1147.	0.108E-12	13.10
1.3719	1774.	1148.	0.102E-12	12.71
1.3717	1775.	1148.	0.105E-12	12.86
1.3709	1775.	1149.	0.106E-12	12.92
1.3703	1775.	1149.	0.108E-12	13.03
1.3703	1775.	1150.	0.106E-12	12.94
1.3701	1776.	1150.	0.110E-12	13.09
1.3698	1776.	1150.	0.111E-12	13.15
1.3696	1776.	1151.	0.110E-12	13.10
1.3697	1776.	1151.	0.110E-12	13.08
1.3703	1776.	1152.	0.106E-12	12.87
1.3697	1776.	1152.	0.108E-12	12.98
1.3696	1776.	1152.	0.108E-12	13.00
1.3694	1777.	1153.	0.110E-12	13.07
1.3692	1777.	1153.	0.111E-12	13.10
1.3694	1777.	1153.	0.110E-12	13.07

Appendix IV

The program for processing the experimental data

C THIS PROGRAM HAS THE PURPOSE OF CALCULATING
C THE OXYGEN CONTENT IN STEEL FROM THE PROBE
C VOLTAGE MEASURED. THE PROBE IS AN ISOOTHERMAL
C AND ISOBARIC OXYGEN CONCENTRATION CELL WITH
C $ZrO_2(+CaO)$ SOLID ELECTROLYTE.

C THE FOLLOWING FUNCTION IS DEFINED TO CALC THE
C OXYGEN PRESSURE AT WHICH THE ELECTRONIC
C TRANSFERENCE NUMBER IS EQUAL TO 0.5.

```
FUNCTION PO2E(TH)
REAL A,B, PO2E
A=-54500
B=14
PO2E=EXP((2.303*A/TH)+(2.303*B))
END
```

PROGRAM EMF

C THIS PROGRAM IS GOING TO BE APPLIED
C TO THE DATA OBTAINED IN THE EXPERIMENT WHERE THE
C REFERENCE ELECTRODE IS THE AIR($P_2=0.21$).

C P_1 IS THE UNKNOWN OXYGEN PRESSURE IN
C THE MOLTEN STEEL.
C P_2 IS THE REFERENCE ELECTRODE OXYGEN PRESSURE.
C T_C IS THE COLD END TEMPERATURE.
C T_H IS THE HOT END TEMPERATURE .
C E IS THE MEASURED CELL (PROBE) VOLTAGE.
C G IS THE FREE ENERGY CONTRIBUTED SOLELY BY THE
C OXYGEN GRADIENT.

```
REAL P2, TC, TH, G, E, ETH, ESUM, EAVE, AO, DELTAT, EP
REAL CAL, CC, CCR, CMO, CN, CO, CP, CS, CSI, CTI, CV, LNFO, FO
```

C THE ABOVE LINE LISTS ALL ELEVEN ELEMENTS WHICH
C AFFECT THE ACTIVITY COEFFICIENT OF OXYGEN.
C THE %WT OF THE ELEMENTS IS READ IN AND
C OXYGEN ACTIVITY COEFFICIENT CALCULATED
C ACCORDINGLY.

```
DOUBLE PRECISION P1, P1SUM, P1AVE, C, CSUM, CAVE
DOUBLE PRECISION C1, C1SUM, C1AVE
INTEGER N
ESUM=0
P1SUM=0
CSUM =0
N=0
READ(5, 10) CAL, CC, CCR, CMO, CN, CO, CP, CS, CSI, CTI, CV,
```

10 . . FORMAT(F7.4)

LNFO=-0.94*CAL-0.13*CC-0.041*CCR+0.0035*CMO+0.057*N
 *-0.20*CO+0.091*CS-0.14*CSI-0.19*CTI-0.27*CV
 FO=EXP(LNFO)

C FO IS THE OXYGEN ACTIVITY COEFF. DETERMINED
 C BY THE ALLOYING ELEMENTS IN STEEL.

WRITE(6,95)
 95 FORMAT(1X,'E(V) TH(K) TC(K) P1(ATM) C(PPM)

C ETH IS THE THERMAL CONTRIBUTION OF THE TWO
 C DIFFERENT LEADS.

TC=TC+273.15
 TH=TH+273.15
 DELTAT=TH-TC
 EP=E-ETH

C THE THERMAL CONTRIBUTION 'ETH' IS SUBTRACTED
 C THE CELL VOLTAGES.

ESUM=ESUM+E

C THE FOLLOWING PART OF THE PROGRAM IS INTENDED
 C TO CALCULATE THE OXYGEN PRESSURE IN THE MOLTEN
 C STEEL FROM THE MEASURED CELL VOLTAGES.

P2=0.21

C THE FREE ENERGY CONTRIBUTION BY THE
 C NONISOTHERMAL PART IS CONSIDERED BY THE
 C SEEBECK COEFFICIENT.

EP=EP-(0.505*DELTAT*0.001)

C NOW THE 'EP' IS CONTRIBUTED BY
 C THE OXYGEN PRESSURE ONLY.

G=EP*4*23060.95

P1=((P2**0.25+PO2E(TH)**0.25)/EXP(G/(4*1.987*TH)))
 *-PO2E(TH)**0.25
 P1=P1**4

C P1 IS THE UNKNOWN OXYGEN
 C PRESSURE IN THE STEEL MELT WE ARE TRYING
 C TO MEASURE. CALCULATING THIS WAY WE HAVE TAKEN
 C THE IONIC TRANSFERENC NUMBER INTO CONSIDERATION.

AO=(P1**0.5)*EXP((28000+0.69*TH)/(1.987*TH))

C TAKING THE DISSOLUTION FREE ENERGY OF OXYGEN
 C INTO STEEL INTO CONSIDERATION , WE CAN CALC THE
 C OXYGEN ACTIVITY FROM ITS PRESSURE NOW.

C1=AO*(1E+4)/FO
 C=AO*(1E+4)

C C IS THE CONCENTRATION OF OXYGEN IN STEEL IN PPM.
 C C1 IS THE CONC. OF OXYGEN IN STEEL AFTER
 C THE ACTIVITY COEFFICIENT IS CONSIDERED.

CSUM=CSUM+C
 C1SUM=C1SUM+C1
 P1SUM=P1SUM+P1
 N=N+1.

WRITE(6,100)E,TH,TC,P1,C,C1
 100 FORMAT(F8.4,1X,F5.0,1X,F5.0,2X,E13.3,4X,F7.2,4X,F8.2)
 GOTO 90

C AFTER FINISHING WITH ONE GROUP OF E,TC,AND TH
 C DATA, IT GOES BACK FOR ANOTHER LOOPING.

190 EAVE=ESUM/N
 CAVE=CSUM/N
 C1AVE=C1SUM/N
 P1AVE=P1SUM/N

WRITE(6,199)
 WRITE(6,199)
 WRITE(6,199)
 199 FORMAT(' ')
 WRITE (6,200)
 WRITE (6,210)
 WRITE (6,220) EAVE, P1,CAVE ,C1AVE
 WRITE (6,199)
 WRITE (6,199)
 WRITE (6,199)
 WRITE (6,199)

200 FORMAT('MEASURED CELL CALCED OXYGEN CALCULATED(ppm)')
 210 FORMAT(2X,'VOLTAGE(V) PRESSURE(atm) CONCENTRATION')
 220 FORMAT(F7.3,6X,E16.3,4X,F8.2,4X,F8.2)

STOP